

Effect of light-absorbing impurities on the albedo of the Alpine glacier Plaine Morte

Inauguraldissertation

Der Philosophisch-naturwissenschaftlichen Fakultät

Der Universität Bern

Vorgelegt von

Anna Dal Farra

Aus Italien

Leiterin der Arbeit:

Prof. Dr. Margit Schwikowski

Departement für Chemie und Biochemie der Universität Bern

Effect of light-absorbing impurities on the albedo of the Alpine glacier Plaine Morte

Inauguraldissertation

Der Philosophisch-naturwissenschaftlichen Fakultät

Der Universität Bern

Vorgelegt von

Anna Dal Farra

Aus Italien

Leiterin der Arbeit:

Prof. Dr. Margit Schwikowski

Departement für Chemie und Biochemie der Universität Bern

Von der Philosophisch-naturwissenschaftlichen Fakultät angenommen.

Bern, (05/12/2017)

Der Dekan

Prof. Dr. Gilberto Colangelo

*“A painter should begin every canvas with a wash of black,
because all things in nature are dark except where exposed
by the light.”*

– Leonardo da Vinci

Summary

The incoming solar radiation is a crucial component of the Earth's energy balance. As the Sun's emissions reach the Earth's surface, a certain percentage of that energy is absorbed by Earth. Albedo is defined as the ratio of the radiant flux reflected from a unit surface area into the whole hemisphere to the incident radiant flux of hemispherical angular extent. It is a dimensionless value that ranges from 0 to 1. The total Earth albedo is currently estimated around 0.3. Each type of surface present on Earth contributes differently to its total albedo, however no natural occurring surface has a higher albedo than fresh snow, which can be as high as 0.90. Snow-covered areas therefore play a key role in the Earth's energy balance. The duration and extension of a snowpack can influence the amount of radiation absorbed by the Earth surface, hence the global temperature. Albedo is relevant both at a large global scale and at a smaller scale, when considering systems like glaciers. For glaciers, albedo is influenced by the ageing of the snow, which affects snow grain size. The older it is the larger are the snow crystals and consequently the lower the albedo. Also the presence of liquid water lowers albedo by increasing the snow crystal size and the penetration depth of the radiation. Further decrease of albedo is caused by the exposure of underlying bare ice on glaciers, and by the presence of light-absorbing impurities (LAI). LAI darken the snow/ice surface, resulting in greater absorption of solar energy, consequently increasing surface temperature. In glaciers with high LAI deposition and enrichment, LAI can be a larger driver of snow/ice melt than temperature. The types of LAI present on a glacier depend on the local conditions. Principally they can be divided into three categories: black carbon (BC), organic matter and mineral dust. BC is a product of incompletely combusted gas phase condensates of biomass or fossil fuels; with natural and anthropogenic sources, in the case of biomass. The organic matter can be the living biota whose habitat is the glacier itself or humic substances, which are formed by the decomposition of algae and bacteria, and possess very dark colouring. Mineral dust sources can be natural, like desert regions and local outcrops or anthropogenic as construction areas and agricultural sites. Most studies have focused on one or two of these types of LAI, with a special emphasis on anthropogenic BC. The majority of these studies have considered the LAI's influence on snow and not on ice. Therefore a knowledge gap exists for LAI identification and quantification on a snow free glacier surface considering all involved LAI.

The aim of this research project was therefore to characterize the LAI present on a glacier, to identify their main classes and their optical properties and finally to quantify their contribution to the albedo lowering. The final task was to upscale the quantification of the LAI effect by using high spatially resolved reflectance data collected remotely with the Airborne Prism Experiment (APEX) sensing flight. A number of techniques were applied in the effort to characterize the complex mixture that comprises LAI on the glacier surface. Scanning electron microscopy, Raman micro-spectroscopy, inductively coupled plasma atomic emission spectroscopy, single particle soot photometry and X-Ray diffractometry all contributed to understanding the nature and composition of the LAI. Glacier de la Plaine Morte was chosen as study site because it is both easily accessible and its mass balance is strongly negative; resulting in a strong ice-albedo feedback as all the various melting events enrich the surface with increasing amount of impurities. To characterize the optical properties of the different LAI classes mineral dust, organic matter and BC, a new method was developed by modifying a Hyperspectral Imaging Microscope Spectrometer (HIMS). The use of the HIMS for this particular research question represented a new application for this instrument. Both the hardware and the method approach needed to be adapted to the requirements of the analysis. The HIMS method was validated through the comparison with a field spectroradiometer by measuring different standard materials. The measurement of the bulk standard materials with the field spectroradiometer agreed well with the measurements of the same materials with the HIMS, with an average deviation between the spectra of 3.2% for the 400 to 1000 nm wavelength range. To be able to define the LAI condition at Glacier de la Plaine Morte and its link to albedo decrease the relative abundance of each LAI class present on the glacier was determined with a thermo-optical OC-EC analyser. This measurement was done on 110 surface samples collected in a grid-like manner in a campaign that occurred in August 2015. On average a relative abundance of 91.1 ± 3.7 , 8 ± 3.5 and 0.9 ± 0.4 % was found for mineral dust, organic matter and black carbon, respectively. Interpolating the 110 measured points the distribution of the relative abundance of the three LAI classes was obtained. From this distribution map it was revealed that both mineral dust and organic matter are mostly of local origin. This was confirmed for the mineral also by the composition found with X-ray diffractometry, which is compatible with the local geology, primarily made up of limestone with marl beds, calcareous phyllite and marly shale. Using the HIMS the reflectance spectrum of each LAI class was determined, averaging 10 to 15 reflectance measurements for each LAI class. The characteristic reflectance spectrum of each LAI class was used as endmember, along with the one of bare ice, for the spectral unmixing of five reflectance spectra measured on the glacier with a field spectroradiometer. The relative abundance determined by spectral unmixing matched well, with a 0.4% average standard deviation, with the values measured for the five surface sample collected where surface spectral

reflectance was measured. The spectral unmixing method was also used on the APEX hyperspectral dataset, determining the distribution on the LAI of the glacier, which was compared with the interpolation of the measured samples and the average relative abundance values 91.6, 4.9 and 3.3% for minerals, organic matter and BC respectively; both results provided a good match with the measured data. The same spectral unmixing was applied on a highly spatially resolved airborne hyperspectral dataset, covering the entire glacier surface. The resulting distribution of the LAI on the glacier and the average relative abundance values agreed well with the measured data. Relatively high abundance of organic matter in the areas with particularly low albedo suggests that the latter plays an important role in glacier darkening. The study executed on Glacier de la Plaine Morte revealed plenty of valuable information on sources, effect and distribution on LAI, such approach could be explored for other glacier as well as considering reflectance spectra collected by satellite remote sensing.

Contents

Summary	5
Contents	8
List of abbreviations	11
1 Introduction	13
1.1 Albedo.....	18
1.2 Light-absorbing impurities.....	20
1.2.1 Black Carbon.....	20
1.2.2 Mineral dust.....	21
1.2.3 Organic matter.....	22
1.3 Motivation of the study.....	23
2 Methods	25
2.1 Glacier de la Plaine Morte site.....	25
2.2 Field campaign 2014.....	27
2.3 Field campaign 2015.....	29
2.4 Scanning Electron Microscope (SEM).....	31
2.5 Raman Micro-spectroscopy.....	34
2.6 Inductively coupled plasma atomic emission spectroscopy.....	35
2.7 Thermal Optical OC-EC Analyser.....	36
2.8 Single Particle soot photometer (SP2).....	37
2.9 Optical Microscopy.....	38

Spectral signatures of submicron scale light-absorbing impurities in snow and ice using hyperspectral microscopy.....41

1 Introduction.....42

2 Methods45

 2.1 Modification of the HIMS.....45

 2.2 Validation of the HIMS.....47

 2.3 The environmental sample.....48

3 Results.....49

 3.1. Internal calibration of the HIMS.....49

 3.2 Measurement substrate.....49

 3.3 Reflectance standards.....50

 3.4 Influence of particle orientation on the reflectance.....52

 3.4. Diesel soot, mineral, and organic standards.....53

 3.5 Environmental sample.....54

4 Conclusion.....57

Glacier de la Plaine Morte: a study on the location and effect of light-absorbing impurities.....58

1 Introduction.....59

2 Method.....61

3 Results.....66

 3.1 Relative abundances of mineral, BC and OC.....66

 3.2 Mineral composition.....67

 3.3 Characteristic reflectance spectra of different LAI classes.....68

3.4 Contribution of each LAI class to the glacier surface reflectance.....	69
4 Conclusions.....	74
5 Conclusions and outlook.....	76
5.1 Conclusion.....	76
5.2 Outlook.....	77
References.....	80
Appendix.....	87

Abbreviations

a.g.l	Above Ground Level
APEX	Airborne Prism EXperiment
ASD	Analytical Spectral Devices
a.s.l.	Above sea level
BSE	Back-Scattered Electrons
BC	Black Carbon
BP	Before Present
CL	Cathodo-Luminescence
EC	Elemental Carbon
EDS	Energy-Dispersive X-ray Spectroscopy
ELA	Equilibrium-Line Altitude (ELA)
ESA	European Space Station
HIMS	Hyperspectral Imaging Microscope Spectrometer
HCRF	Hemispherical Conical Reflectance Factors
IPCC	Intergovernmental Panel on Climate Change
ICP-OES	Inductively Coupled Plasma - Optical Emission Spectroscopy
LAI	Light-absorbing Impurities
MAC	Mass Absorption Cross-section
MCWS	Multi-Component Wavelength Standard
OC	Organic Carbon
PET	PolyEthylene Terephthalate

PGP	Prism-Grating-Prism
p-LMM	p-Linear Mixture Model
POD	POLytope Decomposition
RF	Radiative Forcing
ROI	Region of Interest
SE	Secondary Electrons
SEM	Scanning Electron Microscope
SP2	Single Particle Soot Photometer
SWIR	ShortWave InfraRed
VNIR	Visible and Near-InfraRed
XRD	X-Ray Diffractometry

1 Introduction

It is universally acknowledged that the earth's climate is changing. The effects of these changes strongly impact all aspects of life on Earth. It has been shown that these changes are induced by mankind, by the pressure that we exert on the climate system through the emission of greenhouse gases, which highly affect the Earth's radiation balance (Myhre et al., 2013). The relationship between temperature and greenhouse gases such as carbon dioxide (CO₂), methane (CH₄) and nitrous oxide (N₂O) is well established and their temporal evolution has been documented for the last 800 kyr (Figure 1) (Schilt et al., 2010) thanks to the advances in ice core research. What is not yet as clear is how each aspect of Earth's climate will be affected. The complexity and interconnectivity of biosphere, atmosphere, hydrosphere and cryosphere pushes the scientific community, with an unprecedented sense of urgency, to understand, model and project the fate of the climate.

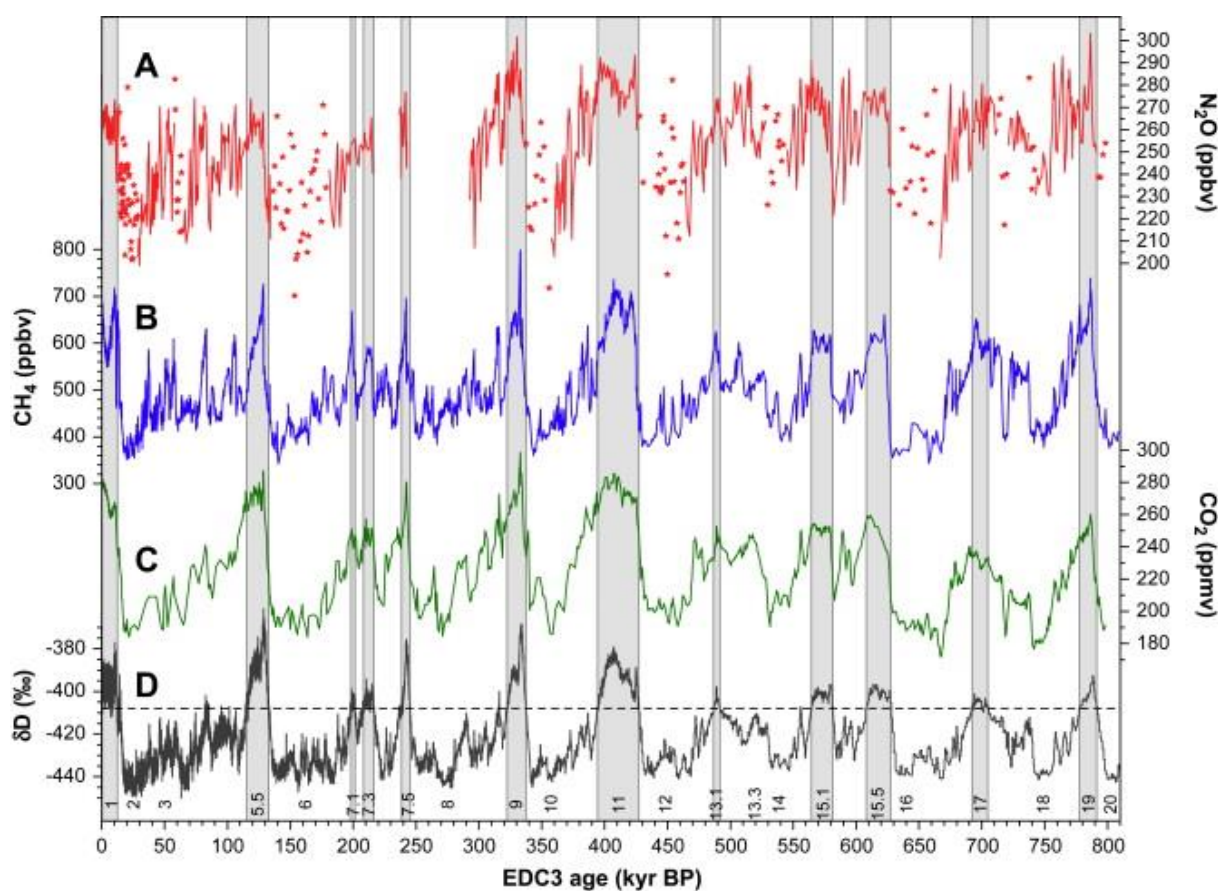


Figure 1 Reconstructed greenhouse gas concentrations from Antarctic ice cores (Schilt et al., 2010). A: N₂O from EDC; B: CH₄ from EDC; C: CO₂ from Vostok between 20 and 390 kyr BP, EDC elsewhere; D: δD EDC; grey shade area mark interglacials.

An important part of the Earth’s climate is the cryosphere. The cryosphere, from the Greek *kryos* meaning cold, constitutes the frozen water part of the Earth system. It comprises mountain glaciers, ice sheets, ice caps, ice shelves, sea ice, seasonal snow, permafrost and frozen rivers and lakes; permanently covering up to 10% of Earth surface (Figure 2).

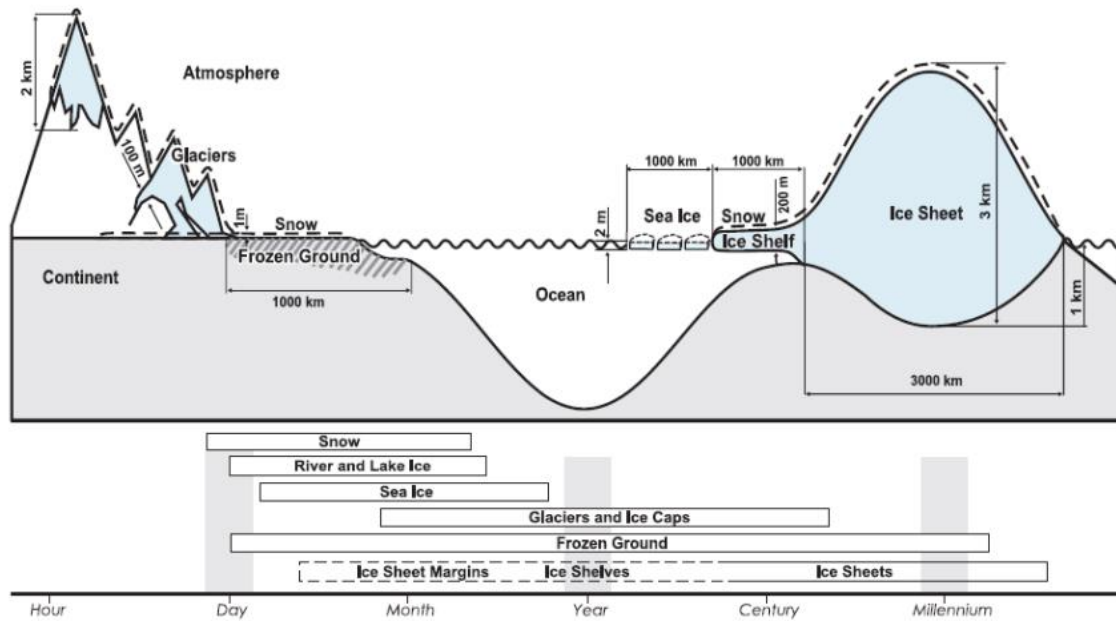


Figure 2 Components of the cryosphere and their relative time-scales (IPCC, 2013).

The subject of this thesis is the cryosphere, in particular alpine glaciers. The IPCC (IPCC, 2013) reported that, even taking in consideration the great variability given by the different response times and the local environments, the annually measured glacier terminus fluctuations from about 500 glaciers worldwide reveal a largely homogeneous trend of retreat. Glaciers in Europe are also following this trend (Figure 3), and Switzerland, with its many glaciers, is particularly affected. Switzerland is known as the “water tower” of Europe due to its numerous glaciers and rivers (Agrawala, 2007); much of its agriculture and hydropower depend on them. The current glacier retreat threatens the survival of many species of flora and fauna as well as the Swiss economy (Walther et al., 2002). Although to a large degree the increase of temperature caused by greenhouse gases may be responsible for accelerating glacier melt, a number of mechanisms contribute to influence radiative forcing as well (Bony et al., 2006). Some of the mechanisms in question are called feedback mechanisms as they are caused by the temperature increase and in case of a positive feedback mechanism contribute to further enhancing the temperature. Positive feedbacks are e.g. methane release from melting of permafrost, methane is also a

greenhouse gas (Anisimov, 2007), ocean warming, which reduces the uptake of CO₂ by oceans (Soden and Held, 2006) etc. Many types of aerosol particles, like BC (Black Carbon) or mineral dust, when released in the atmosphere generate climate feedback. These particles scatter the sunlight in the atmosphere, thus preventing it from reaching the Earth's surface. A positive feedback can be given when these aerosol particles are deposited on snow and ice influencing radiative forcing as much as by -1.2 Wm⁻² (Figure 5)(CHARLSON et al., 1992). This phenomenon causes the reduction of glacier albedo.

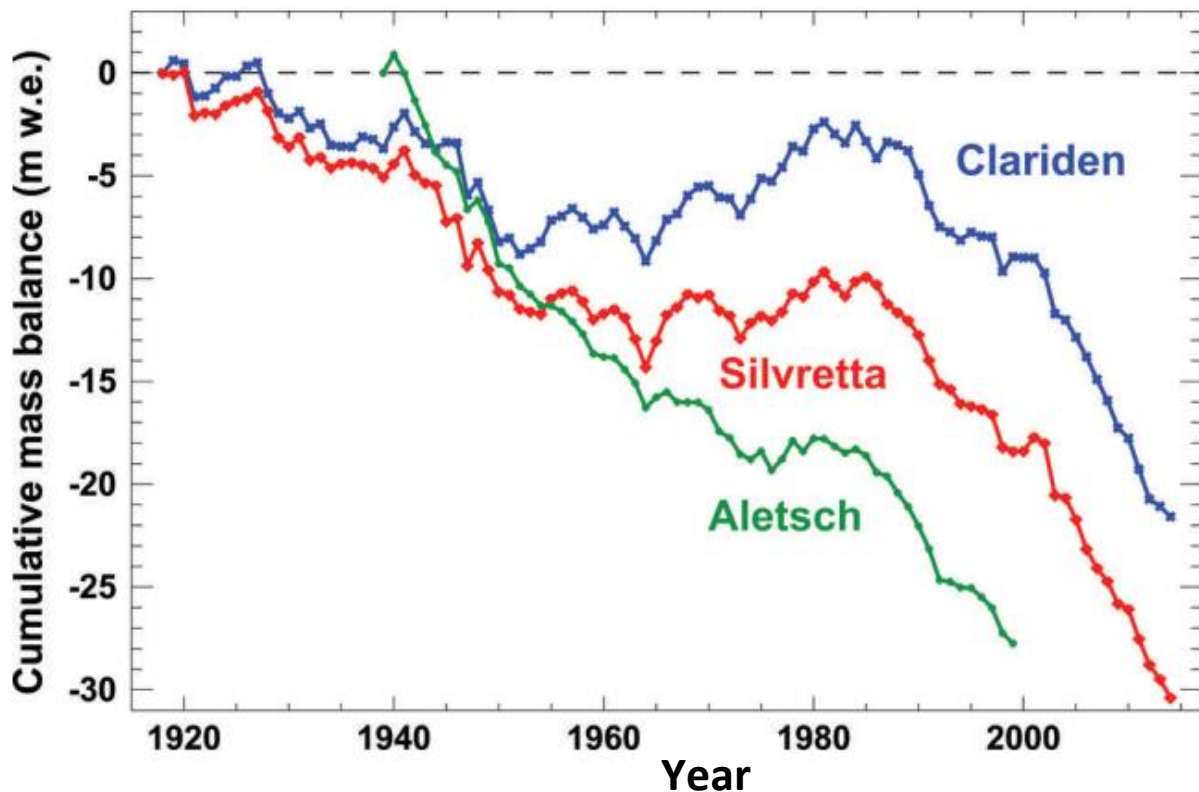


Figure 3 Cumulative mass balance for Clariden and Silvretta (1918–2014) and Aletsch glacier (1939–1999) (Huss et al., 2017).

The first mentions of the effect of albedo-reducing materials and their effect on snow go back to 1968 (Megahan and Meiman, 1968). Many studies have been published since then. Several techniques have been developed and remote sensing has certainly played a part in describing and quantifying the phenomenon (Oerlemans and Hoogendoorn, 1989;Konig et al., 2001;Corripio, 2004;Painter et al., 2016) with much attention focused on the variation in grain size. The snow grain size can vary up to 50%, (Wiscombe and Warren, 1980), this variation is part of the snow aging processes, effecting albedo in the infrared range; it was reported to lower albedo by 0.12 in the course of 14 days (Flanner et al., 2007a). The effect of the reduction of snow albedo is visible in Figure 5 under the label "black carbon (BC) on snow", listed and

estimated along with all other known radiative forcing (Ramanathan et al., 2007). The radiative forcing given by “soot in snow” corresponds to 0.65 Wm^{-2} , which is one third of the radiative forcing of CO_2 but with a much larger uncertainty. In Figure 6 albedo is shown for different concentration of BC in snow and for different snow grain sizes. McConnell, 2007 #55 reported that, in Greenland, for the period of maximum emission of BC (1906 – 1910) the estimated surface climate forcing in early summer from BC in Arctic snow was ca. 3 Wm^{-2} , which is eight times the typical preindustrial forcing value. Most of the focus has been the effect of light-absorbing impurities (LAI, all matter absorbing light in the visible range), especially BC, in snow, and the effect that these have on snow melt. The phenomenon can be described this way: when LAI are present in snow they cause direct surface warming due the additional absorption of solar radiation (Hansen and Nazarenko, 2004; Jacobson, 2004; Gardner and Sharp, 2010; Yasunari et al.; Aoki et al., 2011). The sun’s spectral irradiance (Figure 4) is highest in its intensity in the visible range (400-700 nm) of the light spectrum, coloured LAI that are present on a glacier’s surface receive this powerful radiation in its entirety when sunlight is not obstructed by clouds and the darker the LAI are the more radiation they will receive, translating into higher temperatures (Hall et al., 1990; Cutler and Scott Munro, 2017).

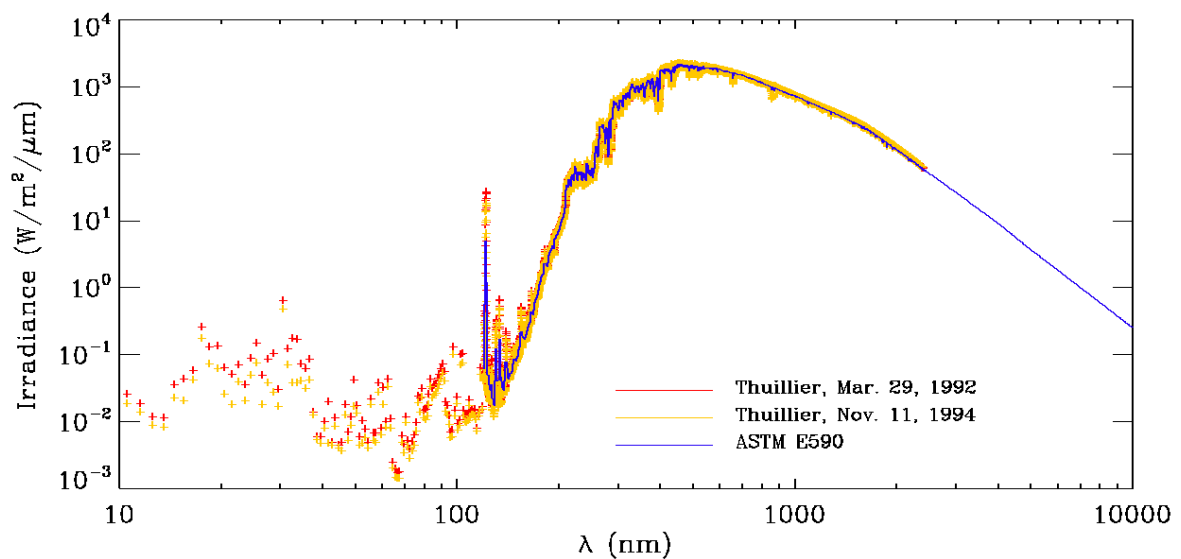


Figure 4 Three models of spectral irradiance for the top of the atmosphere, intensity in logarithmic scale (Thuillier et al., 2004)

The absorbed solar radiation causes a rise in temperature of the surface ultimately contributing to higher melt rates. Among the various approaches a widely used model has been developed to calculate the albedo of snow, considering several variables like snow grain size, BC and mineral dust concentration (Flanner et al., 2007b).

Snow albedo has received more attention from the scientific community (Nolin and Dozier, 2000;Dozier and Painter, 2004); less visibility however has been given to the impact of LAI on glacier ice on the ablation zone. Glaciers have typically two distinct areas: an accumulation zone and an ablation zone; the first maintains snow cover throughout the year and gains mass while in the latter the snow melts away in the warmest months exposing the ice underneath consequently losing mass (Boggild et al., 2010;Gabbi et al., 2015). These two zones are separated by the equilibrium-line which, depending on the condition of the glacier, may be at higher or lower elevations.

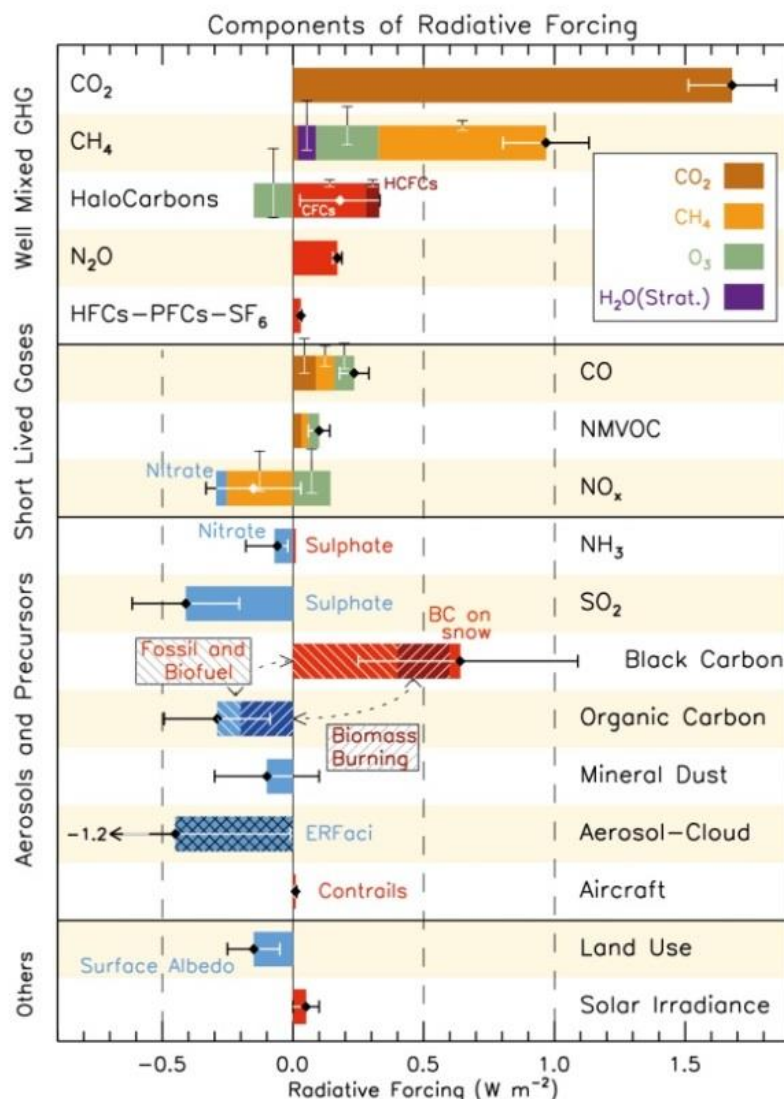


Figure 5 Change of Radiative Forcing (RF) between 1750 and 2011 for the different components based on emitted compounds or other changes (IPCC, 2013).

The LAI that are located on the bare ice surface of the ablation zone are consequently enriched by the different layers that each year deposits on the fresh snow (Moustafa et al., 2015). The lack of scientific studies on albedo effect on bare ice surfaces can be attributed to the fact a

glacier reveals its surface partially and only for a limited amount of time in the warmer months. Furthermore bare ice has a lower albedo than snow (0.4 and 0.8 respectively) (Gabbi et al., 2015). The exposure of the ice surface is however bound to increase both in width and in time, having a greater effect on the radiative balance on a glacier.

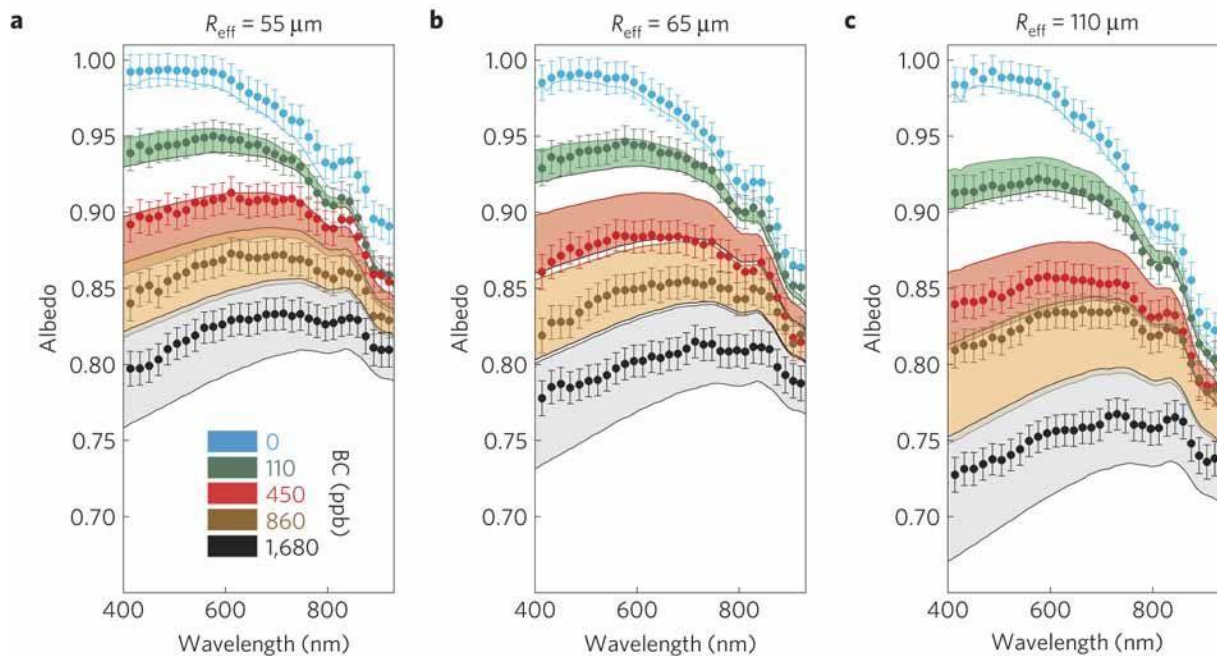


Figure 6 a, 55 μm R_{eff} , b, 65 μm R_{eff} and c, 110 μm R_{eff} . Error bars show the standard deviation of the measurements. Upper and lower boundaries of the shaded bands correspond to modelled albedo assuming BC mass absorption cross-sections, at $\lambda=550$ nm, of 7.5 and

1.1 Albedo

The origin of the word albedo is Latin and its meaning is whiteness. In more scientific terms, the albedo of a surface is the ratio of the radiant flux reflected from a unit surface area into the whole hemisphere to the incident radiant flux of hemispherical angular extent (Schaepman-Strub et al., 2006)(Figure 7). To demonstrate the role of albedo on the earth's energy balance a computer simulation named Daisyworld was introduced in 1983 (Wood et al., 2008). Daisyworld considers a hypothetical world orbiting a star whose radiant energy is slowly increasing or decreasing. It is meant to mimic important elements of the Earth-Sun system and its final purpose is to illustrate the plausibility of the Gaia hypothesis (Lenton, 1998). Daisyworld is seeded with two varieties of daisy as its only life forms: black daisies and white daisies. White daisies reflect light, while black daisies absorb light. The simulation tracks the two daisy populations and the surface temperature of Daisyworld as the sun's rays grow more powerful. The surface temperature of Daisyworld remains almost constant over a broad range

of solar output. The temperature that is most comfortable for the two life forms is achieved; the daisies act as a buffer for temperature. When the solar radiation reaches high enough levels the white daisies proliferate up to a point in which the temperature is too high to support their own growth and ultimately they die out; leaving the world with a lower albedo and therefore an even higher temperature. The Daisyworld simulation can be loosely applied to the case of the Earth albedo and what is currently happening to the albedo for the Earth, now that we are pushing its boundaries.

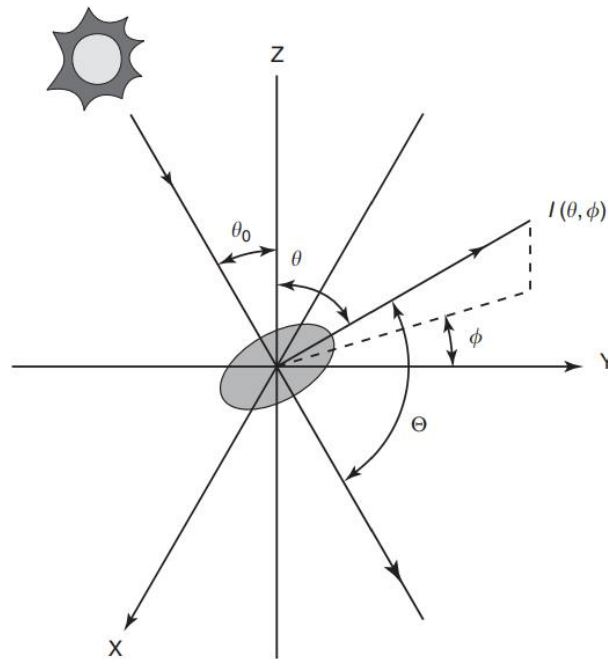


Figure 7 Orientation of incident sunlight (incident on the surface XY) and reflected light. θ_0 is the solar zenith angle, θ is the view zenith angle, ϕ is the relative azimuth angle, and Θ the scattering angle. The incident sunlight is taken to be in the YZ plane.

The spectral albedo α_λ is the albedo of monochromatic radiation at wavelength λ . This value is given by

$$\frac{F_\lambda^+}{F_\lambda^-} = \alpha_\lambda \quad F_\lambda^- : \text{flux of incident light on the surface, } F_\lambda^+ : \text{flux of reflected light on the surface}$$

Radiative flux is therefore the energy in Wm^{-2} per unit area per unit wavelength interval which is incident on or reflected by the surface. Irradiance is a common term for radiative flux. The broadband albedo, which is often referred as just albedo, is given by the ratio of the total radiative fluxes,

$$\frac{F_i^+}{F_i^-} = \alpha_i \quad F_i^- : \text{flux of incident light on the surface, } F_i^+ : \text{flux of reflected light on the surface}$$

Where the integration over wavelength is performed separately for the incident and reflected radiative fluxes prior to taking the ratio. Each surface found on Earth has a certain albedo, lower for water and evergreen forests and higher for deserts and snow covered areas (Coakley, 2003 (Coakley, 2003 #303). It is not however an intrinsic property of a surface but rather it depends on the spectral and angular distribution of the incident light; in case of solar energy this varies depending on the atmospheric composition and the direction of the beam of light coming from the sun.

1.2 Light-absorbing impurities

LAI are materials that present a certain absorption in the visible range of the solar spectrum (390 - 700 nm, Figure 4). The different altitude, location and topography of a glacier influences the types of LAI encountered on its surface, a certain variance between glaciers is therefore to be expected (Nagatsuka et al., 2014). Varying concentration of impurities is also observed within the same glacier (Takeuchi et al., 2014).

1.2.1 Black Carbon

BC has both natural and anthropogenic sources and is a product of incompletely combusted gas phase condensates of fossil fuels or biomass, it is refractory, with vaporization temperature near 4000K and exists as an aggregate of small spheres. The emission sources of BC can be defined by a few categories; diesel engines, industrial BC, residential solid fuel, and open burning (all main sources and climate effects are visible in Figure 8). Due to the strong light absorption properties (mass absorption cross section (MAC) $>7.5 \pm 1.2 \text{ m}^2/\text{g}$ at 550 nm (Bond et al., 2013)) BC has long been investigated in the climate science community. It is a major contributor to positive climate forcing by causing atmospheric warming and reducing snow and ice albedo (Bond et al., 2013; IPCC, 2013). Hansen et al, 2005 estimated that fossil fuel BC has an efficacy of about 78% (efficiency being the effectiveness in causing climate change) and found that considering indirect effects (snow albedo and cloud changes) fossil fuel soot constitutes an overall net positive forcing. Considering specifically the effect of BC in snow it has been found to lower albedo by 5% ca. depending on the snow crystal size (Grenfell et al., 2002; Ming et al., 2009; Yasunari et al., 2010) and the BC concentration.

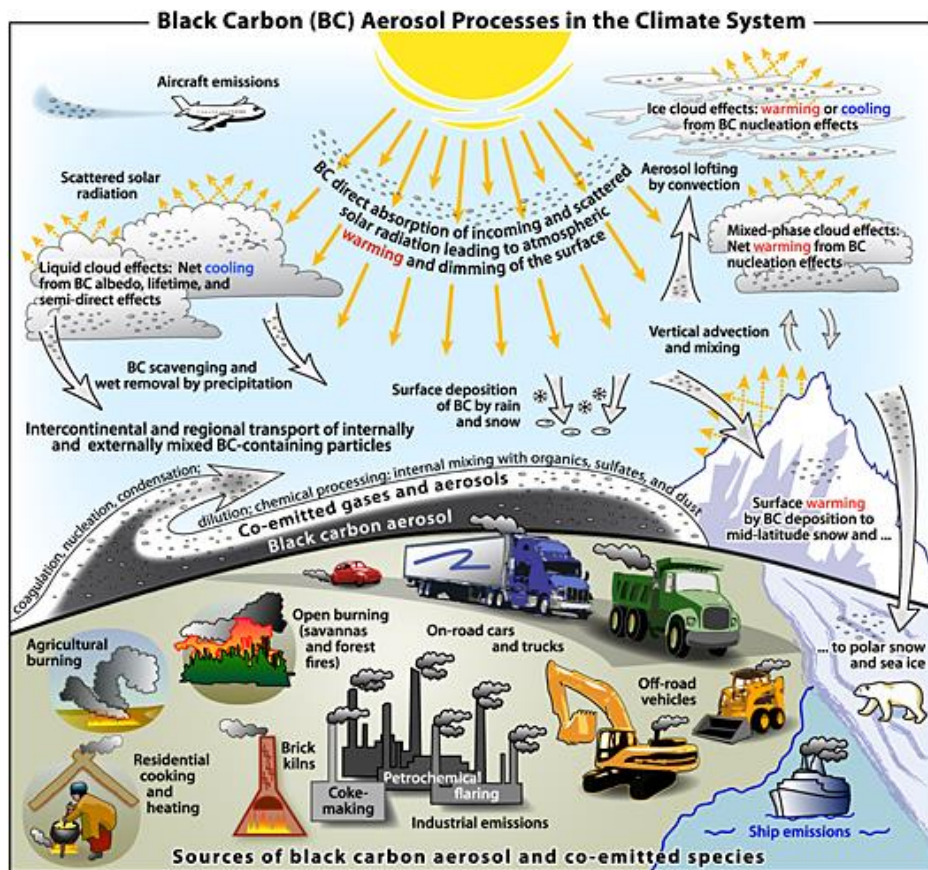


Figure 8 Schematic overview of the primary black-carbon emission sources and the processes that control the distribution of black carbon in the atmosphere and determine its role in the climate system (Bond et al., 2013)

1.2.2 Mineral dust

Sources of mineral dust found on glacier can be very diverse. Mineral dust can be mobilized in the large desert regions and transported over long distances in the atmosphere (Schwikowski et al., 1995). Additionally local outcrops or land use (construction and agriculture) can also be important sources of mineral dust (Tegen and Fung, 1994; Xuan and Sokolik, 2002). The variability in origin translates in a large variability of the mineral composition. Light absorption by mineral dust depends on the dust composition (Tedesco et al., 2013; Nagatsuka et al., 2014; Nagatsuka et al., 2016). Iron oxides are the most light-absorbing compounds in the visible range of the spectrum which can be found in mineral dust (Alfaro et al., 2004; Lafon et al., 2006). Due to the high MAC of BC, the majority of LAI in snow research has focused on BC; the MAC of hematite ($0.97 \pm 0.02 \text{ m}^2/\text{g}$ at 550 nm) is lower than BC. However, recent research suggests that because dust is present in much larger concentrations than BC in some regions, dust can dominate LAI albedo reductions and melt (Clarke et al., 2004; Kaspari et al., 2014). However hematite is not necessarily present in the mineral dust located on a glacier, which can be

composed of a broad range of minerals, some of which absorb in the visible wavelength range. More information needs to be collected on the optical properties of mineral dust and their role on decreasing glacier albedo.

1.2.3 Organic matter

When talking about the influence of organic matter on albedo one must also take into consideration the different sources that the organic matter may have. Organic matter can originate from biota autochthone to the glacier or from windblown matter originating from flora more or less removed from the glacier. As for the biota that naturally grows on the glacier a primary and a secondary effect can be identified that lower albedo in different ways. The primary effect is the direct absorption of light from certain snow algal species, e.g. *Chlamidomonas nivalis*, which reduces spectral reflectance in the range of carotenoid (400-600 nm) and chlorophyll (670-680 nm) absorption bands (Thomas and Duval, 1995). (Lutz et al., 2016) found that in the Arctic red algal bloom might be responsible for 13% decrease in snow broadband albedo over the course of one melt season. The summer months provide the necessary melting condition so that the presence of liquid water promotes algal growth. Minerals necessary for the algae's growth is supplied by windblown dust. The algae produce an anti-freeze that keeps the bodies liquid well below 0°C. In the winter months, the small cells of the red algae are covered under layers of snow, however with summer, the algae move up towards the surface where light and the higher temperatures are available (Attenborough, 1995). The secondary effect that concerns organic matter has to do with the product of decomposition of the algae and bacteria that inhabit the glacier. Humic substances are formed by the decay of microorganisms and exhibit dark coloration due to a large amount of conjugated double bonds related mainly to phenolic and carboxylic functional groups (Kumada and Kumada, 1987). The latter effect is expected to be predominant in the ablation zones of a glacier, where an accumulation of the various years of biological activity is present. Organic matter in glaciers is mainly present in the form of cryoconite granules; these granules, whose schematic is shown in Figure 9, are composed of bacteria, algae, mineral particles and black carbon particles in a humic substance matrix, and can vary greatly in content both among different glaciers but also within one glacier. The variation can be in the mineralogy, in the biology or in the chemistry of the granule (Uetake et al., 2016); all of the above can determine a higher or lower effect on a glacier albedo (Musilova et al., 2016). Furthermore cryoconite granules can occur both in holes or as superficial impurities, both of which affect albedo.

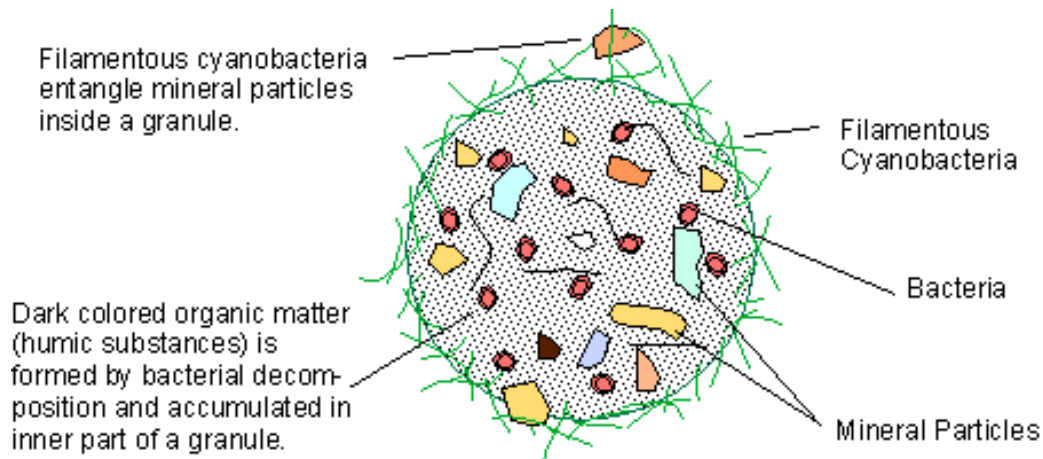


Figure 9 Cross section of a cryoconite granule (www-es.s.chiba-u.ac.jp/~takeuchi/crygranule.html).

1.3 Motivation of the study

For the last forty years studies have been carried out on snow albedo; but a lack of knowledge remains for the bare ice albedo of ablation zones. Climate change is affecting snow coverage; in glaciers this translates into a progressively upward movement of the equilibrium line altitude (ELA); a larger exposure of bare ice in the warmest months with progressively larger ablation zones. For this reason it is now necessary to further our understanding of the albedo of bare ice. The approaches with which bare ice albedo has been studied have mostly been the same techniques and methods used to look at albedo of snow. These approaches ignore the relevant differences between the two surfaces (reflectance spectra in the visible and IR), their optical properties and interaction with LAI. To obtain the maximum information and draw robust conclusions a step back must be taken and new and more suitable ways to analyse the phenomenon must be outlined. One of the motivations for this project is the fact that most studies have focused on BC, on BC and mineral dust or only on organic matter. We propose a method that allows the measurement of most LAI present on a sample, LAI belonging to different classes, thus allowing all to be measured with the same technique. As study site Glacier de la Plaine Morte was chosen; this glacier was selected since it has a large ablation zone, it is easily accessible and was subject to albedo remote sensing studies. On Glacier de la Plaine Morte we outlined a method to understand the role of LAI on bare ice, with the application being of use also in other glaciers. Glacier de la Plaine Morte presents an enriched layer of LAI on its surface and different questions emerged:

- What composes these LAI, can we quantify the different classes?
- How are the LAI distributed on the glacier, what is their gradient?

- To what extent does each class contribute to lowering the surface albedo?
- Is it possible to develop a method to determine the abundances of classes through the analysis of surface spectral reflectance?
- Is it possible to upscale the previous point to reflectance spectra collected with the APEX flight over the glacier, what about satellite remote sensing?

To answer these points we developed a method to determine optical properties of individual LAI classes within a sample. Such method, whose development, validation and use is described in this thesis, collects the characteristic reflectance spectra of particles under a microscope so as to determine what is the contribution of each class to a total spectrum of the glacier surface; may it be a portable spectrometer or remote sensing data.

This thesis is divided into 7 parts. In chapter 1 the current knowledge on glacier LAI and their effect on albedo are summarized and the motivation for the study is stated. The doctoral project started with an open research question and required method development, therefore different methods were tested; in chapter 2 the results from different techniques are shown. The techniques reveal valuable information on the research subject but are not part of published works. In chapter 3 the first paper (in the revision process in the Journal of Glaciology) is reported; the method developed for the identification of characteristic reflectance spectra for each LAI classes is described and validated. The developed method is applied in chapter 4 as part of a broader study of Glacier de la Plaine Morte (on a paper to be submitted). In chapter 5 an outlook is given for the further development of the method shown in the previous chapters and an outline is given to apply the same methods described to other glaciers. A conclusion is given in chapter 6 while in the appendix all measurements with the HIMS reported.

2 Methods

The project developed in the course of the PhD stemmed from the interest in the LAI that are present on Glacier de la Plaine Morte and more generally on the bare ice surfaces of glaciers. In order to obtain this information a number of techniques were used as first approach to understand the studied subject (SEM-EDX, Raman Spectroscopy, ICP-OES, SP2, optical microscopy). A principal challenge is the nature of LAI themselves; LAI on glaciers are typically very finely mixed heterogeneous material, can vary greatly from glacier to glacier and not much is known about their composition (Pautler et al., 2013; Nagatsuka et al., 2014; Liu et al., 2017). Being the scope of the thesis to explore the suitability of techniques and methods to investigate LAI, a large part of the research project was spent on testing out different methods before arriving at the most suitable one. In this chapter the various techniques will be described and the results obtained from them will be shown as they contain valuable information on the nature and behaviour of the LAI of Glacier de la Plaine Morte. Overall two field campaigns were conducted to collect LAI. During the first campaign in August 2014 sufficient samples of LAI were collected to test various techniques. The second campaign in August 2015 was structured to obtain good sample coverage from the entire glacier.

2.1 Glacier de la Plaine Morte

As study site the Glacier de la Plaine Morte (latitude 4637988 – 4638454, longitude 750895 – 751231) was chosen; this glacier has an easy access and has been one of the subjects of the Swiss Earth Observatory Network (SEON) projects, looking at hyperspectral imaging from an aircraft. Glacier de la Plaine Morte is located in the western Swiss Alps, where it forms the water divide between the cantons of Valais and Bern. The glacier forms a large plateau, having an area of 7.52 km² in 2013 (Naegeli et al., 2015), a mean altitude of 2750 a.s.l and a small outlet tongue towards the north side (Rezgligletscher). The region has a long history of tourism and winter sports, with the first alpine ski competition of 1911 taking place at the Plaine-Morte glacier. Plaine Morte is still strongly influenced by human activity and is currently accessible with a cable car running from Crans Montana to the glacier's edge. The equilibrium line altitude has lain above the glacier since 2002, leaving the glacier entirely snow free by mid-August, as shown in Figure 10. The mass balance is strongly negative (Figure 11); this results in a strong ice-albedo feedback as all the various melting layers enrich the surface with increasing amount of

impurities. Several studies on albedo have had Glacier de la Plaine Morte as their subject; (Paul, 2005) and (Naegeli et al., 2015) looking at albedo and remote sensing, (Bühlmann, 2011) characterizing the impurities on Plaine Morte and Huss, 2013 #108 determining the effect of climate change on this particular glacier.

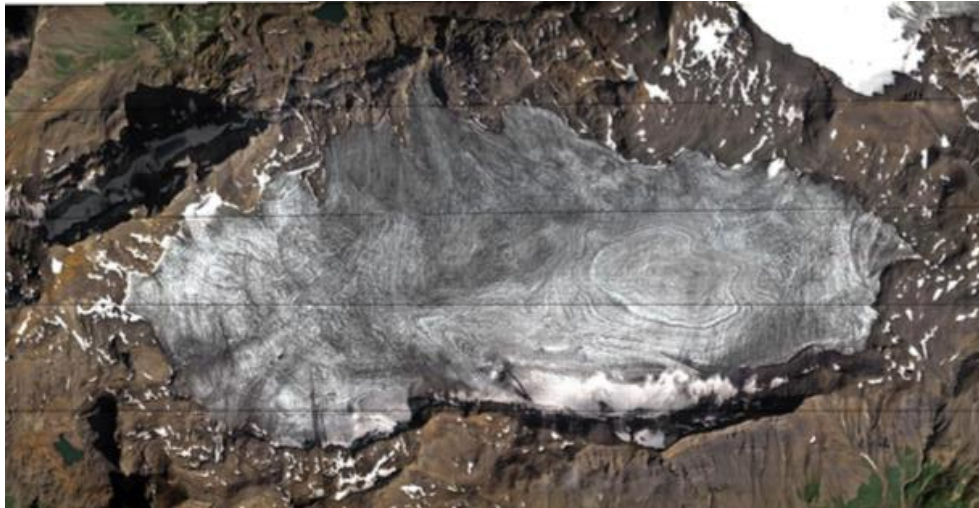


Figure 10 Glacier Plaine Morte hyper spectral image taken on August 2013 with the APEX imaging spectrometer (Naegeli et al., 2015).

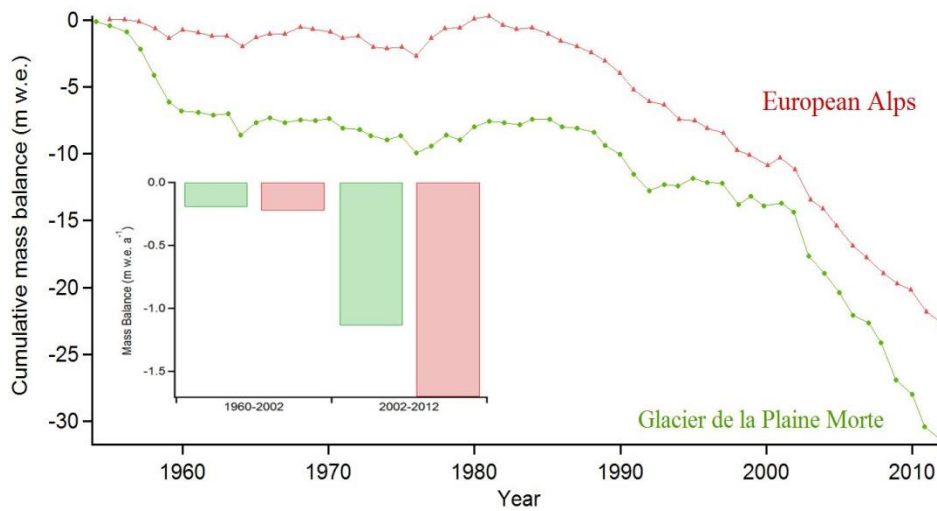


Figure 11 Cumulative mass balance of Glacier de la Plaine Morte since 1954 compared to the average of the European Alps. The inset shows mean mass balance in two periods (Huss et al., 2013).

2.2 Field campaign 2014

The LAI samples used to carry out the series of preliminary test discussed in this chapter were collected during a field campaign which was conducted on Glacier de la Plaine Morte on August 29th 2014. The collection of the samples consisted of extracting fourteen blocks of surface ice with dimensions of about 30 x 30 x 8 cm using a battery driven electrical chainsaw (Figure 12) and stored in pre-cleaned sealed plastic containers. The blocks (one of which is shown in Figure 13) were kept frozen during the transport to Paul Scherrer Institute, weighted (Table 1) and stored until analysis. The blocks were cut into ca. 2 x 2 x 8 cm sections and stored in 50 ml polypropylene vials, resulting in a total of 396 samples (Table 1), which were stored frozen until analysis. Before the extraction of the block the reflectance spectrum of each surface was collected with a Field Spectroradiometer (FieldSpec 3, ASD Inc., PANalytical) (the location of the measurements are shown in Figure 14). All measurements (Figure 15) display reflectance in % as each measurement was light corrected with a white reference (Spectralon, Labsphere) accounting for the variations of the sky condition. For each surface area measured 30 spectra were measured and averaged. The field spectroradiometer used measures the 350–2500 nm spectral range, has a spectral sampling interval of 1.4 nm (350–1000 nm) and 2 nm (1000–2500 nm), and a full width half maximum of 3 nm at 700 nm and 10 nm at 1400 nm (Analytical Spectral Devices, I., 2014). Approximately a 30 cm² area was measured (the height from the ground of the fibre optic pistol determines the area measured); unfortunately because of a malfunctioning of the field spectroradiometer 8 out of the 14 measurements had to be discarded (in Figure 16 are the 6 spectra not effected by the malfunctioning).

Table 1 Samples collected on Plaine Morte during the 2014 expedition.

Sample	Weight (g)	Vials number	Degrees lat, long (32T)	Malfunction
1	2311.5	1-76	46.3756431, 007.4887960	
2	945.2	77-99	46.3762898, 007.4887002	
3	1029.1	100-123	46.3762984 007.4886739	
4	795.4	124-149	46.3767424 007.4882196	X
5	790.7	150-179	46.3769302 007.4881234	X
6	1117.8	180-192	46.3789519 007.4871963	X
7	1572.0	193-215	46.3786256 007.4883886	

8	965.6	216-249	46.3782089 007.4895445	X
9	1753.9	250-283	46.3782309 007.4898429	
10	1850.5	284-311	46.3779966 007.4898234	X
11	2472.2	312-334	46.3778805 007.4898916	X
12	761.1	335-352	46.3776086 007.4897431	
13	1304.9	353-380	46.3775364 007.4897321	X
14	1169.1	381-396	46.3768198 007.4893097	X



Figure 12 Cutting of the ice blocks samples using an electrical chainsaw.



Figure 13 Sample block 11 before being cut into smaller sections the size is ca. 30 x 30 x 8 cm.

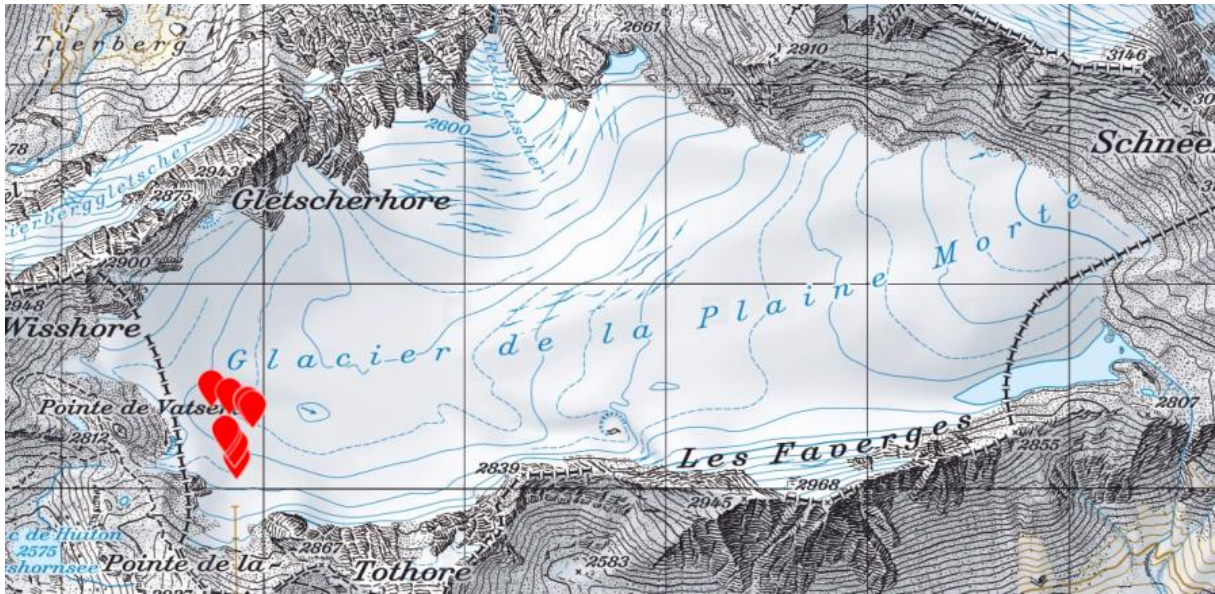


Figure 14 Sampling points of the 14 samples shown in more detail in Figure 13 (Swiss Federal office of Topography).

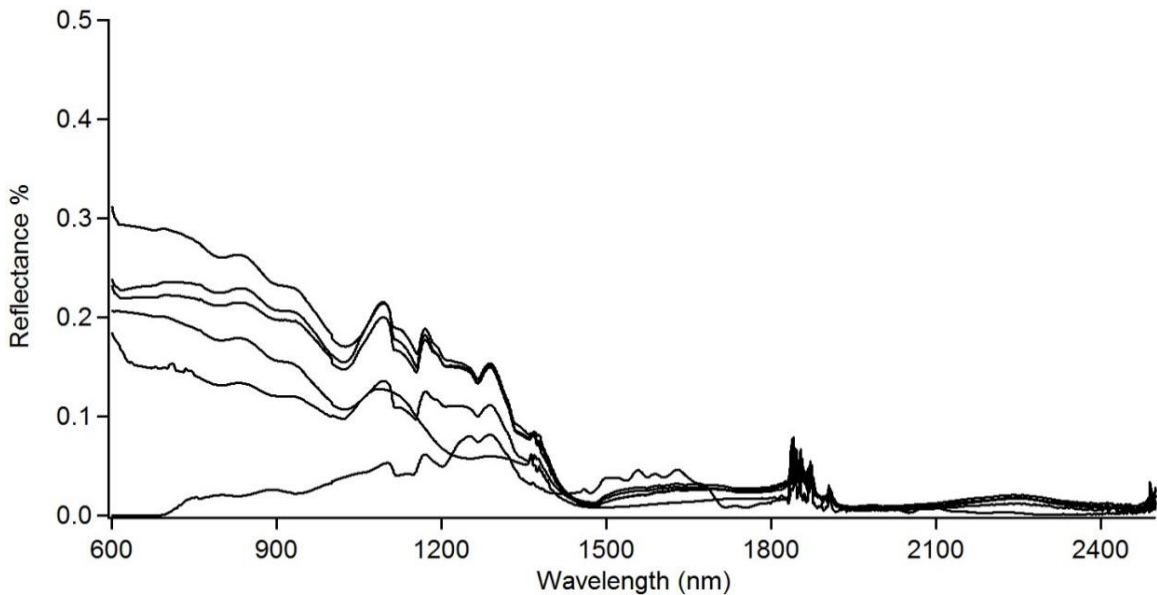


Figure 15 Reflectance spectra of 2014 sampled areas, showing only the spectra unaffected by the noise for the 600 – 1000 nm range.

2.3 Field Campaign 2015

On 20th and 21st of August 2015 a fieldwork was carried out on Glacier de la Plaine Morte. On the first day a total of 90 surface samples were collected. On the second day 20 surface reflectance spectra were measured and the measured area was then sampled, with the same procedure adopted for the sampling on the previous day. The collection of the first 90 samples went as follows: five members of the fieldwork team were each given 18 PET containers (500 ml) a plastic spatula and a plastic shovel; the spatula was used to lightly break apart the surface

and the shovel to collect the ice and LAI in the containers. The 18 samples were collected by each member along the length of the glacier keeping equal distance with each other. This collection resulted in a grid-like sampling (Figure 16). GPS positions were determined for the starting point of the travellers and ending point as well as for each collection site by one of the members as shown in Figure 16. To ensure an equally spaced grid the members maintained an equal distance and kept as much as possible a linear trajectory (with Glacier de la Plaine Morte being very flat, the members were able to observe the positions of their adjacent members). The estimated uncertainty in the sampling point is ± 25 m, and is given by the standard deviation of the distances between GPS points (green points of Figure 16). All the samples were kept frozen until analysis. The second day of fieldwork a field spectroradiometer (FieldSpec 3, ASD Inc., PANanalytical) was used to collect reflectance spectra of the surface; the measurements were obtained in cloud free conditions between 11:00 and 13:00. The field spectroradiometer used measures the 350–2500 nm spectral range, has a spectral sampling interval of 1.4 nm (350–1000 nm) and 2 nm (1000–2500 nm), and a full width half maximum of 3 nm at 700 nm and 10 nm at 1400 nm (Analytical Spectral Devices, I., 2014). Approximately a 20 cm² area was measured (the height from the ground of the fibre optic pistol determines the area measured). Unfortunately because of a malfunction of the field spectroradiometer 15 out of the 20 measurements were discarded, in Figure 17 the valid spectra are reported.

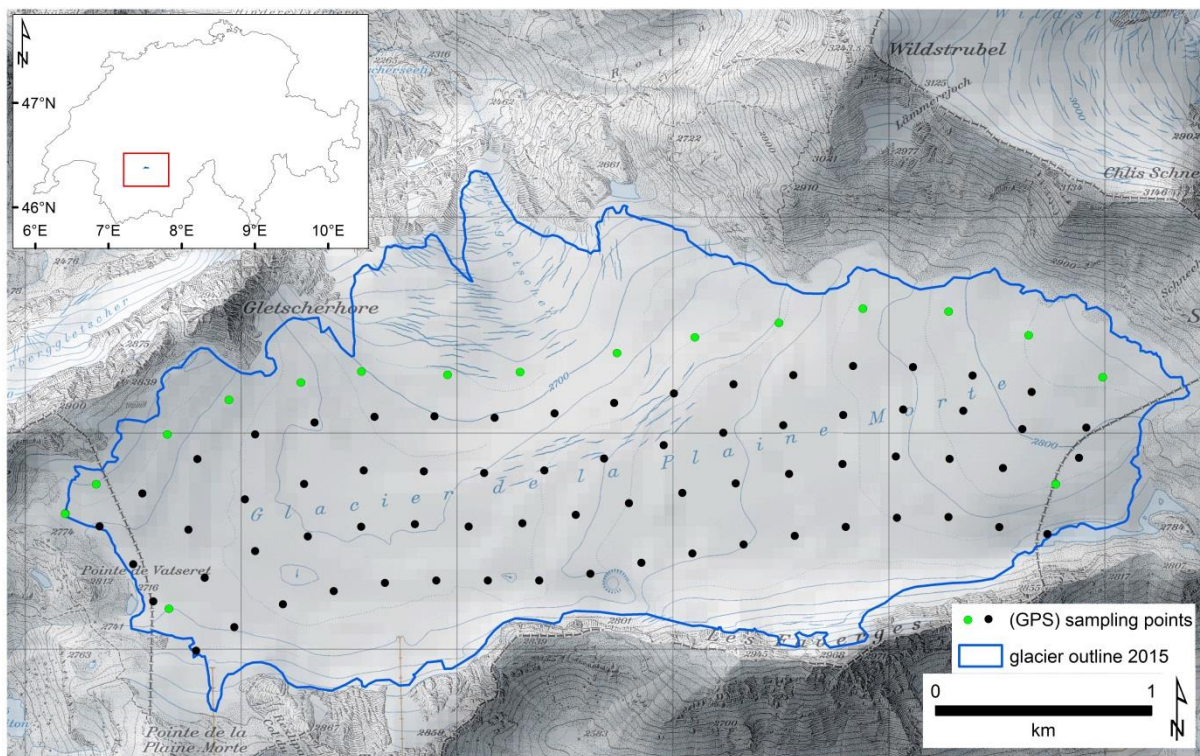


Figure 16 Glacier de la Plaine Morte and its location within Switzerland (inset). The grid-like dotted pattern represents the sampling locations; the green points indicate GPS position and the black points the estimated position of sampling (Swiss Federal office of Topography).

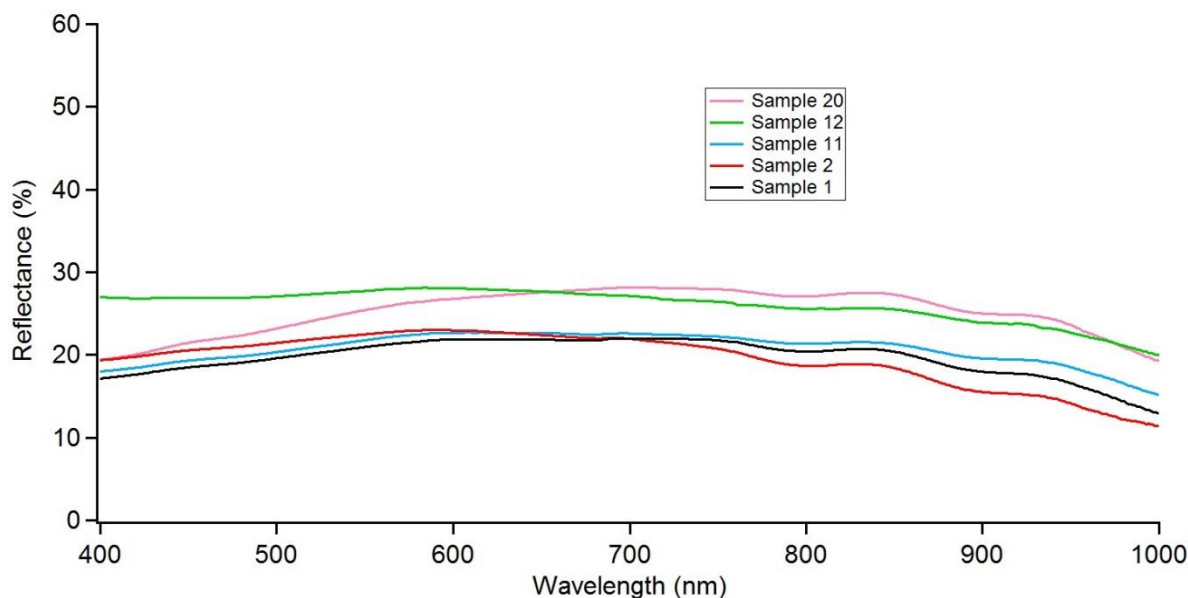


Figure 17 Reflectance spectra collected with the field spectroradiometer on the surface of Plaine Morte.

All measurements display reflectance in % as each measurement was light corrected with a white reference (Spectralon, Labsphere) accounting for the variations of the sky condition. For each surface area measured 30 spectra were averaged. The 20 cm² area measured with the field spectroradiometer was sampled according to the sampling practice adopted the previous day; the depth of the sampling ranged from 1 to 2 cm. The samples were all kept frozen until they were stored in freezers at -20° C in Paul Scherrer Institute. Each of the 110 samples were melted at room temperature and filtered with a vacuum pump on glass fibre filters (Whatman GF/B, 4 cm diameter). The filtrate was dried overnight in an oven at 80° C and the weight of each was recorded after cooling, in Table 1 of the Appendix each dried sample weight is reported.

2.4 Scanning Electron Microscope Energy dispersive X-ray spectroscopy (SEM-EDX)

SEM is an electron microscope type which produces images from a sample by scanning its surface with a focused electron beam. It uses a focused high energy electron beam to generate a number of signals at the surface of a solid specimen; secondary electrons (SE), back-scattered electrons (BSE)(used to generate the image), characteristic X-rays (used for the detection of the elemental composition), light (cathodoluminescence, CL), absorbed current (specimen current) and transmitted electrons. The various processes that occur are shown in Figure 18. The signals produced by the electron-sample interaction disclose information about the sample; revealing

the elemental composition of any specific point selected in the image as well a detailed morphology. SEM has been used in studies concerning cryoconite mainly for the purpose of studying size and morphology of the particles of the sample (Hoover and Gilichinsky, 2001; Suzuki, 2006; Dong et al., 2016). The SEM (NVision 40, Zeiss) used to conduct the measurements of the LAI belongs to the Electron Microscopy Facility (EMF) at the Paul Scherrer Institute; it was used for all measurements at 10kV. The sample's surface must be conductive in order to provide a measurement; being that the LAI is mostly not conductive it was treated with a carbon coating, providing a conductive surface. A total of 32 Energy-dispersive X-ray spectroscopy (EDX) measurements were completed; 14 of which were identified as quartz and one as an iron oxide, whereas all remaining minerals were not easily identifiable but comprised nonetheless a variety of mixtures of the following elements: Si, Al, K, Fe, Na, C and O (see two EDX spectra in Figure 19). This elemental composition is compatible with silicate type minerals.

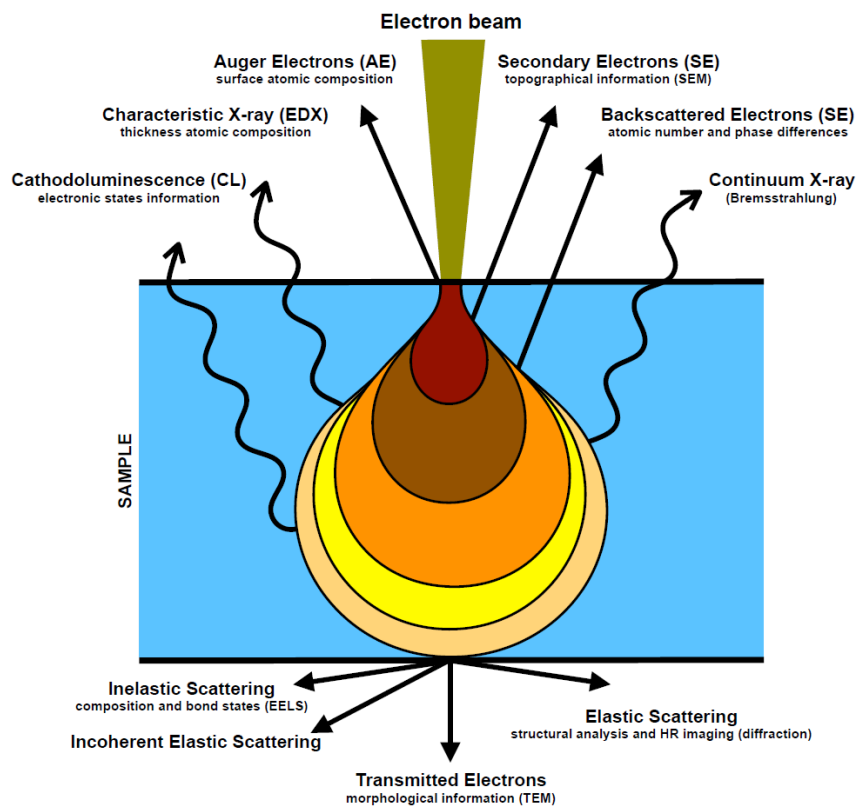
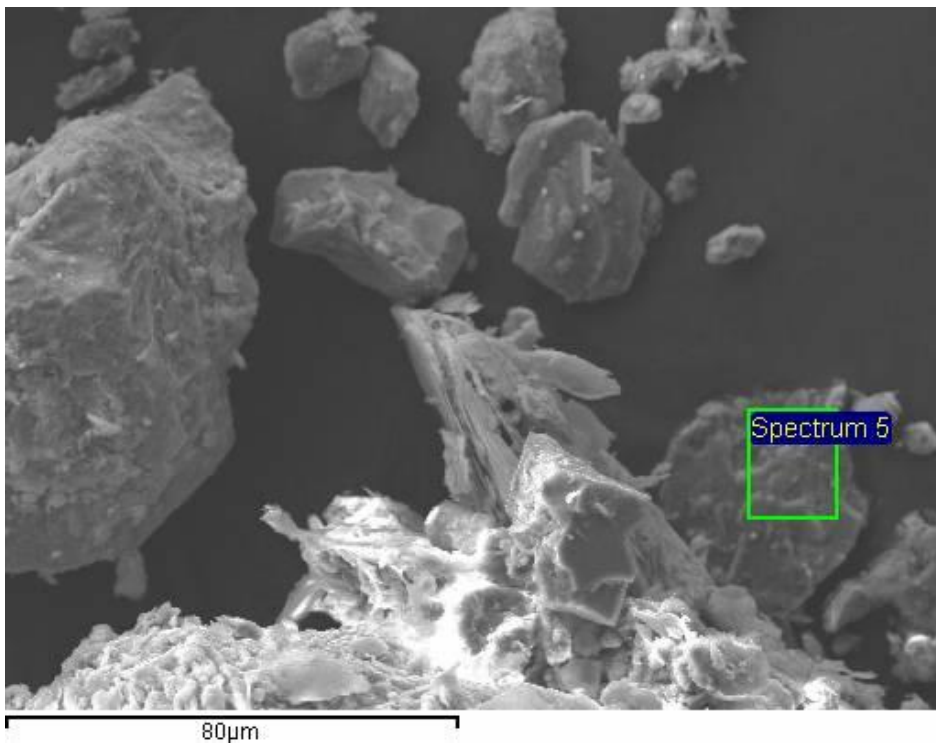
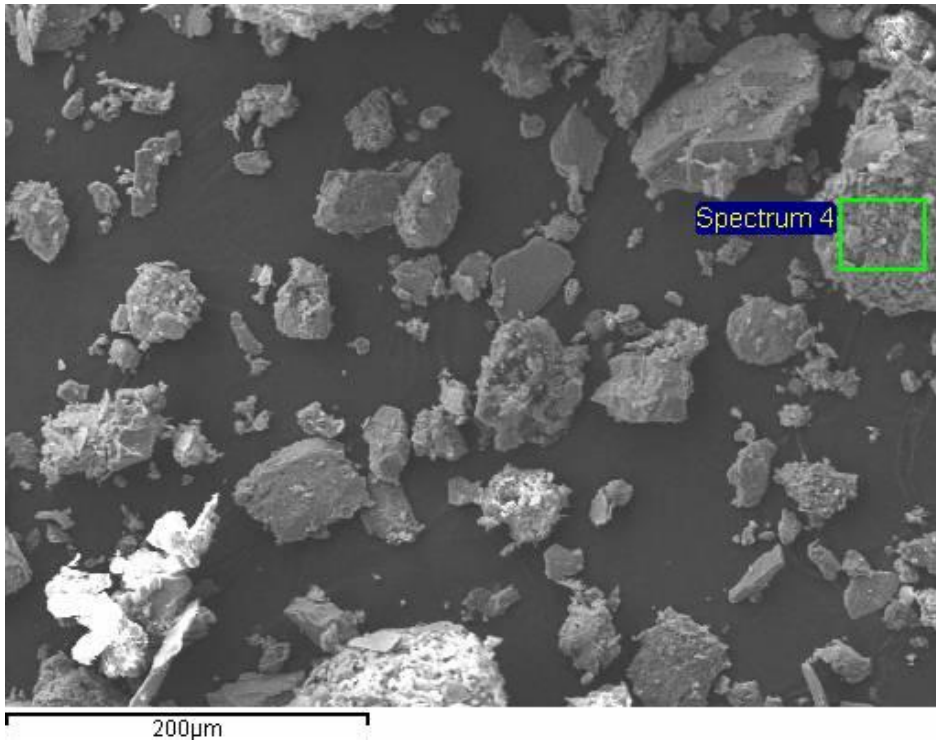


Figure 18 Phenomena that occur from the interaction of highly energetic electrons with matter.



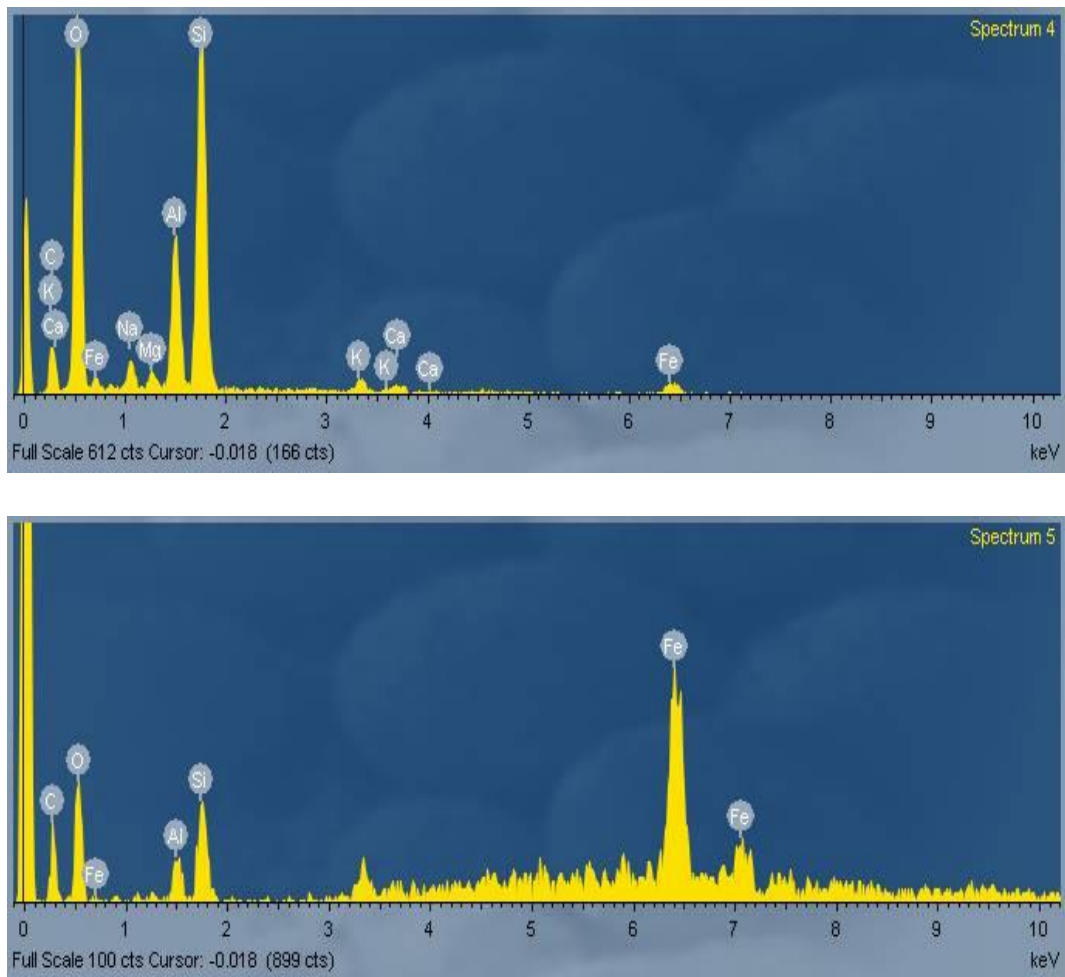


Figure 19 SEM image of measured areas for Spectrum 4 (a) and Spectrum 5 (b) (measured area in the green box) along with their respective EDS spectra (c)(d).

2.5 Raman Micro-spectroscopy

Raman Micro-spectroscopy is a technique that observes the vibrational, rotational, and other low-frequency modes in molecules, and is commonly used in chemistry to provide a structural fingerprint by which molecules can be identified. Raman Micro spectroscopy measures samples at the microscopic scale. The optical image is displayed on a monitor and on this image the laser beam can be pointed to obtain a measurement of the correspondent area. One of the advantages of this technique is the little sample preparation; it requires minimal quantity of material (<15 mg) and no sample treatment. The instrument used is a Jobin-Yvon LabRam HR-800 laser Raman spectrometer located at the University of Bern in the Geology department within the rock-water interaction group. Minerals can be identified with the help of a spectral library that is able to provide a match with a known material. Through the use of this technique a relation was found between the morphology of the various particles observed in the Glacier de la Plaine

Morte samples and their chemical and mineralogical composition. The minerals identified were silicate minerals: albite, feldspar, mica, muscovite, quartz and talc or iron oxide minerals: hematite and goethite, or chalcocite, a sulphide mineral. Visually correlating minerals in a sample with their composition proved valuable when, with the hyperspectral imaging spectrometer microscope (HIMS), a microscopic visual inspection of the samples was done. The Raman Micro-spectrometer used did not offer the possibility to collect the images of the area measured, but offered in turn a precise and quick detection of the sample's main mineralogical types.

2.6 Inductively coupled plasma optical emission spectroscopy (ICP-OES)

Inductively coupled plasma optical emission spectroscopy is a technique which uses an inductively coupled plasma to excite atoms and ions to emit electromagnetic radiation at wavelengths characteristic of a particular element. The plasma temperature in the ICP ranges between 6000 and 10000 K. The emission's intensity depends on the concentration of the element in the sample. The instrument used in this study is an ICP-OES (Vista Pro AX, Varian) operated by Silvia Köchli at Paul Scherrer Institute. The dissolution of the sample was carried out with acid digestion on a microwave oven (turboWAVE Terminal 660, MWS). The silicon however cannot be determined with this method due to the high background. The elemental concentrations detected in sample 89 (2015 Plaine Morte campaign) are reported in Table 1 all values are above the limit of quantification. The abundant iron content suggests that the minerals present on this sample might be light-absorbing as iron rich minerals are correlated with light absorbency (Alfaro et al., 2004; Linke et al., 2006).

Table 1 Elemental composition of Sample 89 from the 2015 Glacier de la Plaine Morte campaign.

Element	Plaine Morte (mg/g)	%
Al	29.20	36.16
Fe	17.51	21.68
Ca	11.62	14.38

K	7.29	9.03
Mg	5.02	6.22
Na	4.32	5.35
Ti	1.20	2.47
S	1.14	1.41
P	1.09	1.35
Cu	0.47	0.58
Mn	0.34	0.42
As	0.26	0.33
Zn	0.17	0.21
Ba	0.13	0.16
Zr	0.10	0.13
Ce	0.10	0.12
Total ppm	320.66	
Total %	32.1	

2.7 Thermal Optical OC-EC Analyser

A Thermal Optical OC-EC Analyser (Model4L, Sunset Laboratory Inc, USA) was used, applying the Swiss 4S protocol (Zhang et al., 2012), to determine the amount of OC (organic carbon) and EC (elemental carbon) present in the surface samples from Glacier de la Plaine Morte. To obtain the mass of organic matter, the mass of OC was multiplied by a factor of two (Pribyl, 2010). EC is considered as an upper limit of the amount of BC is equated to organic matter. The basic principle of the instrument is the following: the sample, deposited on a quartz filter, is introduced in a chamber where it is subjected to stepwise increasing temperature and changing carrier gasses to oxidize separately the OC (first) and EC (second). The carrier gasses used are pure O₂ for steps 1, 2 and 4 and He (pre-cleaned with a moisture/O₂/hydrocarbon trap) for step 3. With a 660-nm tuned-diode laser the transmittance of the filter is monitored. The CO₂ fractions are detected and quantified with a non-dispersive infrared (NDIR) detector.

The sample preparation occurred as follows: 18 samples (from the Plaine Morte campaign of 2015) were melted at room temperature and filtered with a vacuum pump on glass fibre paper filters (Whatman GF/B, 4 cm diameter). The filtrate was dried overnight in an oven at 80° C and the weight of each was recorded after cooling. The filtrate was grinded and mixed in an agate mortar; a small amount of the sample (4 mg ca.) was weighted and placed in a plastic vial. The vial containing the sample was then filled with 30 ml of Milli-Q water and sonicated for 30 minutes, with the purpose of braking apart large aggregates. The suspension was then filtered onto preheated quartz fibre filters (Pallflex Tissuquartz, 2500QA0UP, filtration efficiency of $91 \pm 7 \%$ (Liechti, 2015)).

2.8 Single Particle soot photometer (SP2)

The SP2 (Schwarz et al., 2006, Droplet Measurement Technologies, Boulder, CO) uses a 1064 nm Nd:YAG intra-cavity laser which induces the incandescence and scattering signals of refractive BC-containing particles. The refractive BC mass is proportional to the intensity of the incandescence signal. For application to liquids, the sample needs to be aerosolized, because the instrument only analyses airborne particles (Laborde et al., 2012). The SP2 has been used in many studies to determine BC concentrations in snow and ice (Kaspari et al., 2011; Lim et al., 2014; Wendl et al., 2014; Jacobi et al., 2015). The advantages are that no filtration step is required, making it less time consuming than other methods and allowing it to be used in a continuous flow system. Here we applied the SP2 to determine the efficiency of the filter used to collect the LAI. The BC concentration was analysed in the filtrate liquid and related to the EC amount on the solid LAI sample obtained with the thermal optical method. The amount of BC in the filtered liquid represents in average 0.005% of the total amount of EC in the investigated samples.

This results confirms the efficiency of the filtration method.

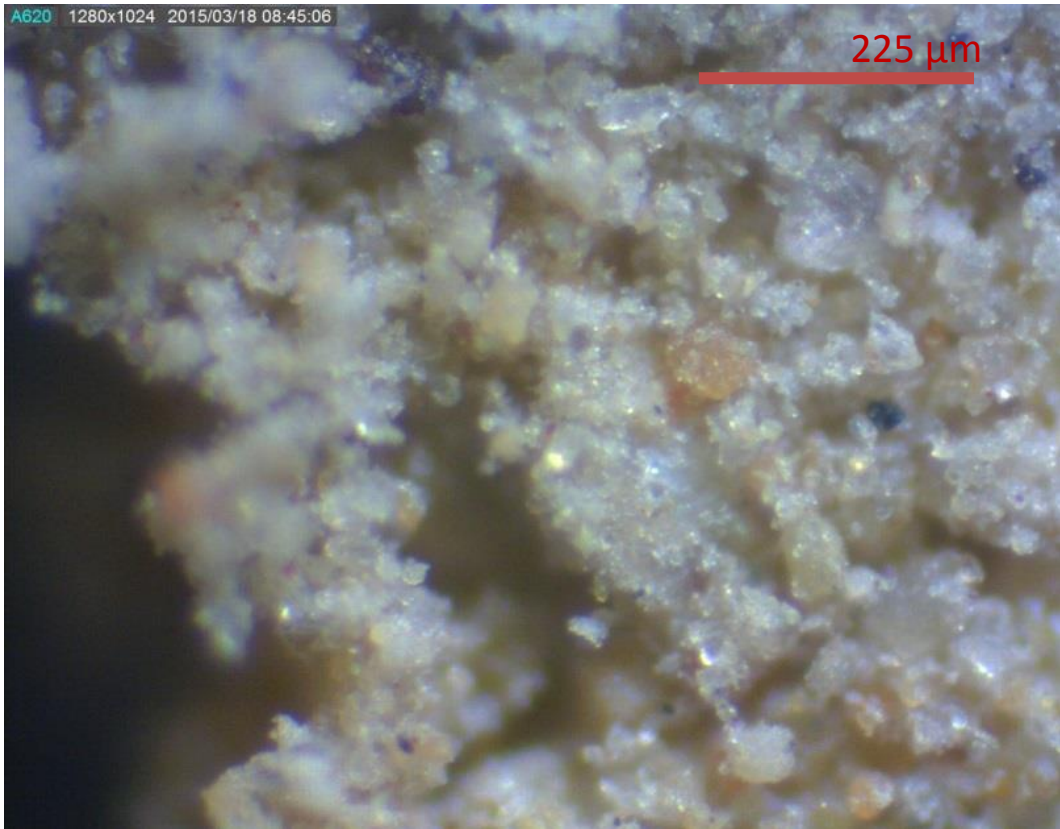
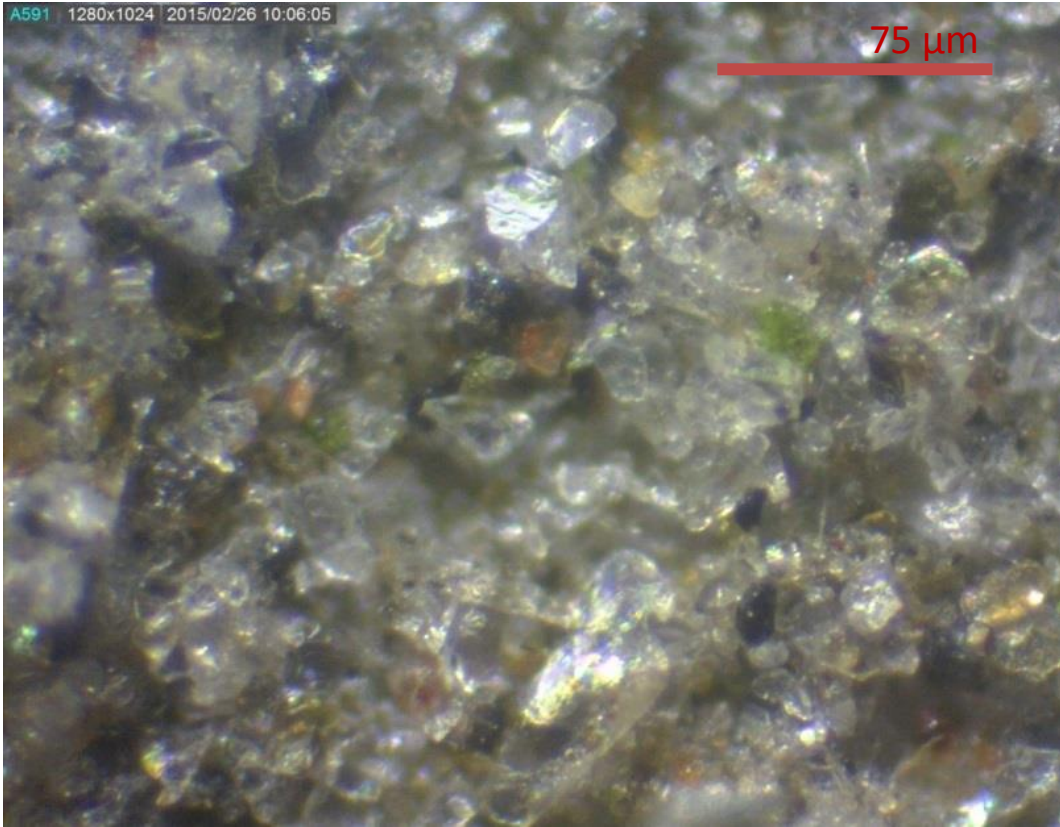
Table 2 Amount of BC in filtered liquid compared to the total amount of EC in the sample

Sample	BC (μg)	EC (mg)
PM1	0.77	13.31
PM2	0.42	19.53
PM3	4.82	75.55
PM4	0.86	71.88
PM5	1.41	42.44

PM6	1.00	68.16
PM7	1.12	33.54
PM8	1.46	39.44
PM9	2.46	45.75
PM10	8.00	41.72
PM11	4.83	42.90
PM12	1.41	19.07
PM13	2.60	28.88
PM14	2.00	30.37
PM15	8.64	386.00
PM16	10.25	40.66
PM17	8.22	218.35
PM18	1.39	91.43
Average	3.43	72.72

2.9 Optical Microscopy

The first approach to understand any given material is a close up observation. With the use of an optical microscope with a 60x magnification objective (Figure 20 a, c) and with a 20 x objective (Figure 20 b) (Bresser Erudit, 20X-1536X) both equipped with an eyepiece camera (Dino-Eye, AM4023CT USB) the dried LAI was observed. In Figure 20a a dense group of particles are present; lighter bright semi-transparent minerals are observed alongside with yellow, red and green coloured ones. Darker particles are also present, but for this area they are in relatively small number. A large light yellow aggregate is shown in Figure 20b. In Figure 20c looser particles, detached from larger aggregates, are shown; a transparent mineral with yellow hues, one bright white and a small red particle in the centre.



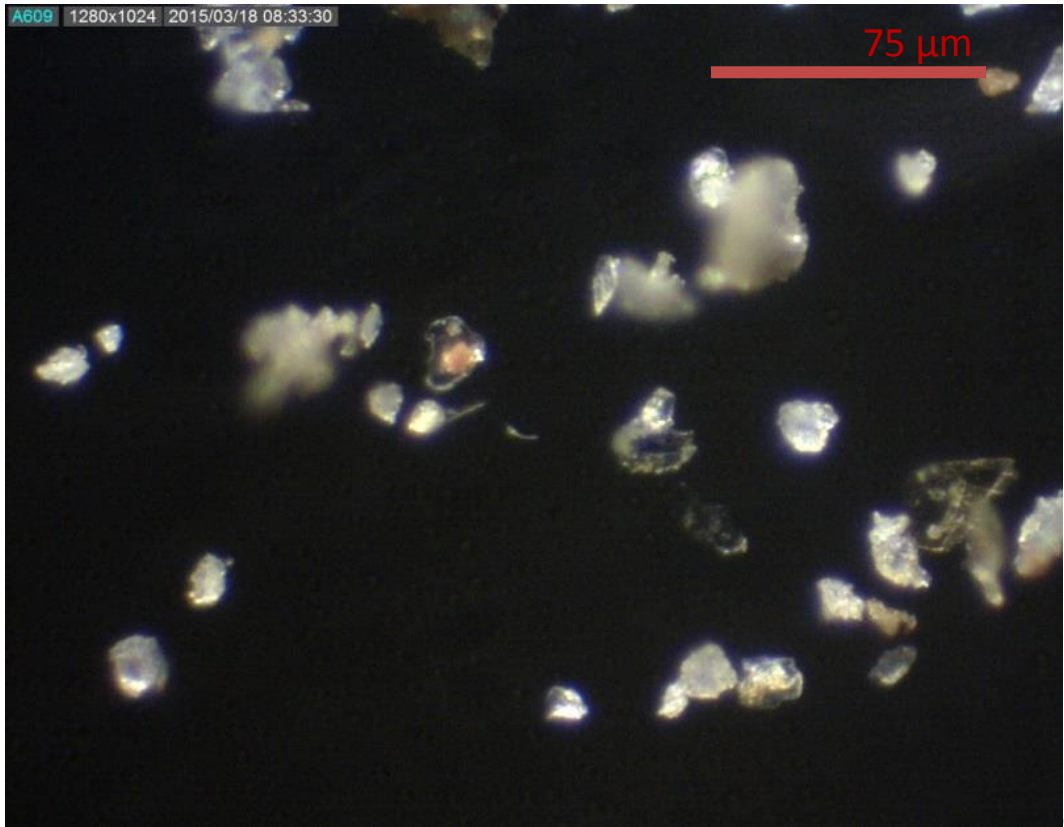


Figure 20 Optical microscope images of impurities collected on Glacier de la Plaine Morte with 60x (a, c) and 20x (b) magnification.

Spectral signatures of submicron scale light-absorbing impurities in snow and ice using hyperspectral microscopy

Anna Dal Farra^{1,2,3}, Susan Kaspari⁴, James Beach⁵, Thomas D. Bucheli⁶, Michael Schaepman⁷, Margit Schwikowski^{1,2,3}

¹Laboratory of Environmental Chemistry, Paul Scherrer Institute, 5232 Villigen PSI, Switzerland

²Department of Chemistry and Biochemistry, University of Bern, 3012 Bern, Switzerland

³Oeschger Centre for Climate Change Research, University of Bern, 3012 Bern, Switzerland

⁴Department of Geological Sciences, Central Washington University, Ellensburg, WA 98926, USA

⁵CytoViva, Inc., 570 Devall Drive, Suite 301, Auburn, Alabama 36832, USA

⁶Environmental Analytics, Agroscope, 8046 Zürich, Switzerland

⁷Remote Sensing Laboratories, Department of Geography, University of Zurich, Winterthurerstrasse. 190, 8057 Zurich, Switzerland,

Correspondence to: Anna Dal Farra (anna.dal-farra@psi.ch), Margit Schwikowski (margit.schwikowski@psi.ch)

Submitted to Journal of Glaciology on the 24th of July 2017, under review.

Abstract. Light-absorbing impurities (LAI) can darken snow and ice surfaces, reduce snow/ice albedo, and accelerate melt. Efforts to allocate the relative contribution of different LAI to snow/ice albedo reductions have been limited by uncertainties in the optical properties of LAI. We developed a new method to measure LAI spectral reflectance at the submicron scale by modifying a Hyperspectral Imaging Microscope Spectrometer (HIMS). We present the instrument's internal calibration, and the overall small influence of a particle's orientation on its measured reflectance spectrum. We validated this new method through the comparison with a field spectroradiometer by measuring different standard materials. Measurements with HIMS at the submicron scale and the bulk measurements of the same standard materials with the field spectroradiometer are in good agreement with an average deviation between the spectra of 3.2% for the 400 to 1000 nm wavelength range. The new method was used 1) to identify BC (black carbon), mineral dust, hematite, and the humic substances present in an environmental sample from Plaine Morte glacier and 2) to collect the individual reflectance spectra of each of

these types of impurity. The results indicate that this method is applicable to heterogeneous samples such as the LAI found in snow and ice.

1. Introduction

Glaciers and the seasonal snowpack are important sources of water in many regions (Jansson et al., 2003; Barnett et al., 2005), and are essential components of the Earth's climate system. Widespread decline in glacier size and snowpack depth as well as extent has occurred in recent decades (IPCC, 2013). Previous studies have suggested that along with rising temperatures, a decrease in surface albedo plays a role in their decline (Hock, 2005; Flanner et al., 2007b). Albedo is defined as the ratio of the radiant flux reflected from a unit surface area into the whole hemisphere to the incident radiant flux of hemispherical angular extent (Schaepman-Strub et al., 2006). For snow and ice, albedo is influenced by the ageing of snow, which affects snow grain size (Dozier and Painter, 2004); the presence of liquid water (Colbeck, 1979; Gardner and Sharp, 2010; Brun, 2017); the exposure of underlying bare ice on glaciers; and the presence of light-absorbing impurities (LAI) (Wiscombe and Warren, 1980; Gardner and Sharp, 2010). LAI cause darkening of the snow/ice surface (i.e., reduce the albedo), resulting in greater absorption of solar energy, heating of the snow/ice, and accelerated snow and glacier melt. In regions with high LAI deposition, LAI can be a larger driver of snow/ice melt than temperature (Hansen and Nazarenko, 2004)

LAI include BC, and certain types of mineral dust and organic matter. BC is a product of incompletely combusted gas phase condensates of biomass or fossil fuels, and has both natural and anthropogenic sources. BC has been investigated extensively in the climate science community because it strongly absorbs light (mass absorption cross section $>7.5 \pm 1.2 \text{ m}^2/\text{g}$ at 550 nm; (Bond, 2013)) and is a major contributor to positive climate forcing by warming the atmospheric layer it is in and reducing snow and ice albedo (Hansen et al., 2005; Bond et al., 2013; IPCC, 2013). Dominant mineral dust sources are desert regions; however local outcrops or land use (construction and agriculture) can also be important sources of dust emissions. Light absorption due to mineral dust is highly variable depending on the dust composition, but in general is considerably lower than BC (Clarke et al., 2004). Due to the high MAC of BC, most research on LAI in snow has focused on BC. However, recent research suggests that because dust is present in much larger concentrations than BC in some regions, dust can dominate LAI albedo reductions and melt (Kaspari et al., 2014). Organic matter can be present in snow and ice in many forms, some of which contribute to the darkening of these surfaces. It was estimated that red algae bloom can cause a decrease in snow broadband albedo of 13% over the course of

one melt season of glaciers and snow patches in various locations in the Arctic (Lutz et al., 2016). The presence of organic matter as humic substances, the matrix composing cryoconite granules (which consist of dead organic matter, algae, bacteria, mineral dust and BC particles) was reported to influence surface albedo as well (Takeuchi, 2002; Takeuchi et al., 2015a; Takeuchi et al., 2015b). Humic substances are formed by the decay of microorganisms and exhibit dark coloration due to a large amount of conjugated double bonds related mainly to phenolic and carboxylic functional groups (Kumada, 1987 #130).

Previous research investigating the role of LAI in albedo reduction has utilized chemical analysis (e.g. thermal optical methods, Single Particle Soot Photometer, mineral composition analysis) to determine the relative abundances of LAI, e.g. (Gabbi et al., 2015). For studies where snow spectral albedo measurements were not taken, various snow albedo models such as the Snow, Ice, and Aerosol Radiation (SNICAR) model (Flanner et al., 2007b; Flanner et al., 2009) have been widely used (Sandells et al., 2017). SNICAR inputs include user defined BC concentration and dust concentration and snow size distributions. A key limitation of this approach is that most users utilize generic optical properties (Dang et al., 2015) for the LAI that are based on global means, and that may not accurately reflect the unique optical properties of LAI inherent to different sampling locations. Furthermore, the optical properties of organic LAI have only minimally been investigated (Takeuchi, 2002), and are not incorporated into snow albedo models. Poorly constrained optical properties of LAI, particularly in the visible range, can result in differences in observed and modelled snow albedo (Kaspari et al., 2015). Advanced methods are needed to constrain the optical properties of LAI, which will improve our ability to identify the contribution of the different LAI constituents to albedo reductions and snow and ice melt.

The aim of this study is to establish a method to analyse the reflectance of LAI in environmental samples using a Hyperspectral Imaging Microscope Spectrometer (HIMS, called Hyperspectral Microscope by CytoViva). This instrument captures the hemispherical directional reflectance (which will be referred to as reflectance throughout this paper) of each class of LAI in a heterogeneous sample. The identification of the impurities is possible as well as the characterization of their reflectance. The use of HIMS is unique in measuring LAI in snow and on glacier surfaces, and has the potential to improve quantifying the contributions of different LAI classes to albedo reduction and therefore to attribute causes of snow and ice melt. We describe modifications made to HIMS to allow particle reflectance to be measured at the submicron scale. We present the instrument's internal calibration, a test done to identify the optimal sample substrate for measurement, and the results comparing reflectance spectra of reflectance standards, Diesel soot, mineral standards, and humic substances at the particle scale measured with the HIMS to spectra of the bulk materials obtained with a spectroradiometer that has

previously been used for measuring LAI (FieldSpec 3, ASD Inc., PANanalytical)(Kaspari et al., 2015;Naegeli et al., 2015). Lastly, for a sample collected on Plaine Morte glacier, reflectance spectra of various particles belonging to different classes of LAI were measured. These spectra provide information on how much radiation is reflected from each class of LAI and could allow quantifying the contribution of each class to the overall reflectance of the glacier surface through spectral un-mixing data obtained in the field or by remote sensing, offering the possibility to upscale to entire glacier systems.

2. Methods

2.2 Modifications of the HIMS

We used optical microscopy combined with a hyperspectral imaging spectrometer. The system included an integrated camera (Dage-MTI) and a prism-grating-prism (PGP) type spectrometer (V10D, Specim) mounted onto the camera mount of an optical microscope (BX43F, Olympus) with a motorized stage (Figure 1). When capturing a hyperspectral image the motorized stage moves the sample across the field of view, this way spectral images are created in a line scan fashion with a 10 nm step resolution. The motorized stage also allows the user to manually move the area of the sample that is viewed to select the region to be scanned.

The spectrometer's internal calibration was carried out using a mercury-argon pencil style calibration lamp (Hg (Ar) Lamp, Orel). Each wavelength corresponding to a peak in the calibration lamp was assigned to a camera line of the spectrometer and a relationship is established for the whole spectral range (400-1000 nm). Multiple calibration lamps can be used to cover the full HIMS spectral range. For example, at Central Washington University the HIMS system was calibrated with a helium lamp between 400-713 nm, and a xenon lamp between 756 and 1000 nm.

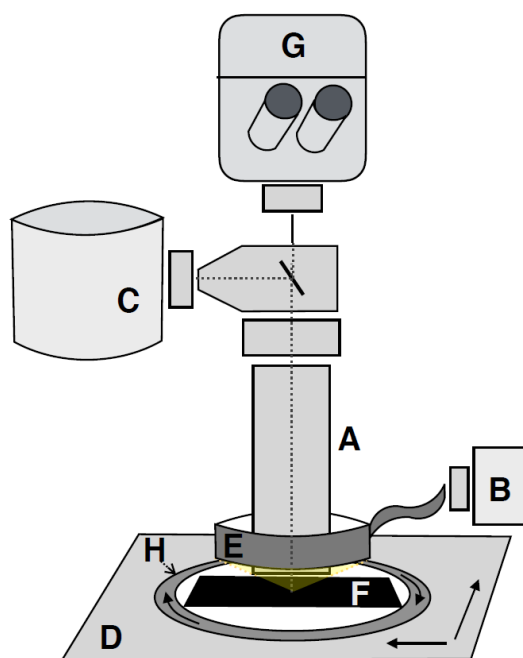


Figure 1 Scheme of the measurement setup: A) 100 x objective. B) Light source. C) Spectrometer. D) Motorized stage. E) Ring light. F) Black microscope slide. G) Camera. H) Rotatable slide holder.

The light source is a quartz halogen aluminium reflector (DC-950, Fiber-Lite) (400-2500 nm; 150 watts) used at 75% of its full power. The hyperspectral image is composed using pushbroom imaging (one line, all spectral bands) by moving the sample across the field of view with a motorized stage. Spectra are collected between 400 and 1000 nm (visible and near-infrared) with a 2.5 nm spectral resolution (Beach et al., 2015) and a spectral sampling interval of 1.2 nm. The wavelength range of the HIMS is particularly apt at measuring LAI as their main influence to snow/ice albedo is in the visible region. At 100x magnification the pixel in the hyperspectral image is $\sim 129 \text{ nm} \times 129 \text{ nm}$. One scan line has a length of $89.8 \text{ }\mu\text{m}$ equivalent to 696 pixels). By selecting, through visual inspection, a region of interest (ROI) in the hyperspectral image, an average spectrum for the selected ROI can be obtained with specific software (4.8, Harris ENVI). Hence, with the ROI tool it is possible to obtain the average spectrum of every pixel that make up the ROI, ranging from as small as one pixel to the whole hyperspectral image ($8064 \text{ }\mu\text{m}^2$). The ROI is selected along the edges of a particle, avoiding the pixels closest to the edge as they may not be representative of the particle. Typical applications of the HIMS utilize darkfield microscopy to map and characterize bacteria or pathogens in tissue (Mortimer et al., 2014) or to confirm functional groups added to nanomaterials (Roth et al., 2015). For measuring reflectance spectra of individual LAI a series of modifications were made to the microscope. Reflectance measurements require illumination from a similar geometry as the observation. For this purpose the microscope objective was fitted with a ring light of 2.8 cm inner diameter (1.125" ID, Dolan-Jenner) that minimizes shadow effects. To use the ring light the objective was changed from the regular 100x magnification objective to a long working distance 100x objective, with a Field of View (FOV) of 72° , to ensure that the sample was fully illuminated. A rotatable slide holder was added to the motorized stage of the microscope to allow collecting directional, rotational-symmetric reflectance spectra when measuring the same particle from different viewing geometries. On a daily basis a white reference (SRS-99-010, Labsphere) was measured to normalize every spectrum to unity and minimize calibration drift (also for the field spectroradiometer). The integration time was set to 0.25 s for the white reference as well as for bright materials (reflectance standards and minerals); while for darker materials (e.g. BC and humic substances) the integration time was set to 0.5 s. We assumed linearity in the instruments response, when doubling integration time (Butz et al., 2015). To create a non-interfering substrate on which to place the LAI samples, a glass microscope slide was spray painted with three layers of black matte paint of ca. $100 \text{ }\mu\text{m}$ thickness each (Black Mat, Motip Dupli).

2.3 Validation of the HIMS

Since particle reflectance at this scale has not previously been measured, we first needed to investigate how reflectance at the particle scale, measured using the HIMS method, compares to spectral reflectance of bulk samples using a common field spectroradiometer. The latter measures in the spectral range between 250–2500 nm, but for comparison with the HIMS throughout this paper only the 400 to 1000 nm range will be shown. The spectral sampling interval of the spectroradiometer is 1.4 nm (250–1000 nm) and 2 nm (1000–2500 nm), and a full width half maximum of 3 nm at 700 nm and 10 nm at 1400 nm (Analytical Spectral Devices, 2017). This instrument has been used to measure reflectance of a wide range of materials (Kokaly, 2017 #55), including snow and ice containing LAI (Kaspari et al., 2015). The measurements with the field spectroradiometer were conducted in an optical laboratory (Remote Sensing Laboratories, University of Zurich) using a collimated and stabilized tungsten halogen light source (Dedolight Aspherics 2, with stabilized power source). The FOV of the field spectroradiometer is 46° (bare fibre), the diameter of the measured area is 2 cm and consequently the distance between the sample and the fibre is 4.7 cm.

Reference materials were measured with both the field spectroradiometer and the HIMS to assess the potential of the latter instrument to collect representative reflectance spectra. With the exception of the commercial reflectance reference standards, which are provided as compressed discs, the standards for the field spectroradiometer measurement were deposited on a black microscope slide (prepared with the same black coating as for the HIMS measurement) and slightly compacted to form an optically thick layer of ca. 2 mm (Mulder et al., 2013). The reflectance measured in the micro scale of particles typical for Diesel soot, minerals and humic substances can vary depending on the size, shape and orientation of each particle (see also section 3.3). Thus, at least ten measurements of different particles of each standard material were averaged. Three reflectance standards were used for calibration: a 10% reflectance reference panel (SRS-10-010, Labsphere); a 50% reflectance reference panel (SRS-50-010, Labsphere); and a Multi-Component Wavelength Standard (MCWS) (WCS-MC-020, Labsphere). The three hemispherical reflectance spectra used in this study were provided by the producer (for the 250 – 2500 nm range) and they were measured using a dual beam spectrophotometer with Labsphere PELA-1000 integrating sphere over a wavelength range of 250 -2500 nm (Perkin Elmer Lambda 900 or Lambda 950). The 10% and 50% reflectance standards were commercially produced by mixing different amounts of white and dark particles (as is visible in Figure 5). At the macroscopic level this results in 10% and 50% reflectance, respectively, but at the microscopic level the standards are heterogeneous. To take this into account, the reflectance spectra presented in Figure 4 are based on averages of each individual

wavelength point of ten HIMS hyperspectral images (ROI of $89.8 \mu\text{m} \times 89.8 \mu\text{m}$) taken from different areas of the standard. Ten measurements were found to be sufficient in obtaining a representative average. The Diesel soot (2975) and urban dust (1649b) are from the National Institute of Standard and Technology (NIST). The mineral samples are of high purity and include hematite (44956, Fluka), quartz, chlorite, and kaolinite, which were kindly provided by Dr. M. Plözte (ETHZ) and were previously characterized by (Mulder et al., 2013). The humic substances represent a mix between Elliot Soil HA standard (Elliot soil is typical of the fertile prairie soils of the U.S. states of Indiana, Illinois, and Iowa; humic and fulvic acids were isolated from the source material) and Leonardite HA standard (Leonardite is produced by the natural oxidation of exposed lignite, a low-grade coal; and was obtained from the Gascoyne Mine in Bowman County, North Dakota, U.S.A) (mixture level 50:50%, International Humic Substance Society). The Diesel soot, minerals and humic substances were obtained dry and ground with an agate mortar and pestle to the appropriate size for measurement ($1 < x < 50 \mu\text{m}$ of diameter ca.). To investigate the influence of the particle orientation on reflectance, hematite was selected because it does not display any optical interference as was the case for the other mineral standards examined in this study (described in 3.4), and because it has more distinct spectral features than Diesel soot or humic substances. Five spectra were obtained with the HIMS from the same hematite particle rotated 360° in equal increments of 72° .

2.4 The environmental sample

The environmental sample consists of surface ice containing LAI collected in 500 ml PET containers on Plaine Morte glacier, Switzerland, on August 20th, 2015. The ice was melted at room temperature and the LAI were separated from the melted ice through vacuum filtration on a glass fibre filter (Whatman GF/B, 4 cm diameter). The sample was collected from the filter with a spatula without scraping the surface of the filter itself to avoid contamination by the glass fibres. The filtrate was then dried at 80°C overnight, weighed ($\sim 3 \text{ g}$), and a fraction of it was slightly ground in an agate mortar with the purpose of breaking apart the larger aggregates which formed during the filtration step. For the HIMS measurement a small amount of the sample was deposited with a spatula on the microscope slide to obtain as many isolated particles as possible. The observed impurities in the Plaine Morte environmental sample were assigned to different LAI classes according to their morphology and the colour perceivable to the human eye. BC particles are mostly spherical and dark (Figure 10e); minerals have angular shapes and display on average brighter colours (Figure 10c, and Figure 10a), while humic

substances compose the matrix of most of the aggregates in the sample, i.e. cryoconite granules (Figure 10i).

3. Results

3.1. Internal calibration of the HIMS

The fit of calibration lamp's wavelengths and the instrument's camera lines proved linear ($R^2 = 0.999$, Figure 2) as shown in Figure 2.

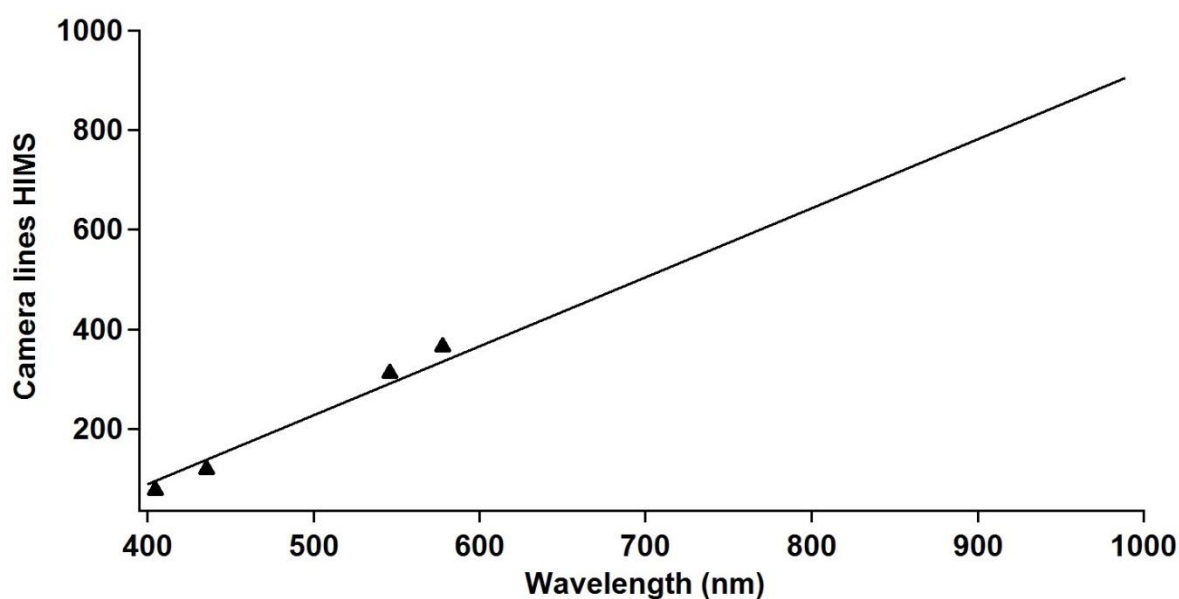


Figure 2 Linear calibration function for attributing the camera lines to a certain wavelength, based on the four known peaks of the calibration lamp at 404.66, 435.84, 546.07 and 578.01 nm.

3.2. Measurement substrate

The spectra in Figure 3 show the reflectance of a microscope slide with three layers of black spray paint, compared with just one and two layers as well as a standard low reflecting material (MetalVelvet™, Acktar) measured with the HIMS. The low reflectance of the triple paint coat ($1.17 \pm 0.12\%$ reflectance) guarantees that the measurement of the samples is not influenced by its background, and was subsequently used in all experiments. With increasing numbers of layers the noise in the range 800 to 1000 nm appears smaller, suggesting that only one or two layers might not be sufficiently opaque in that wavelength region.

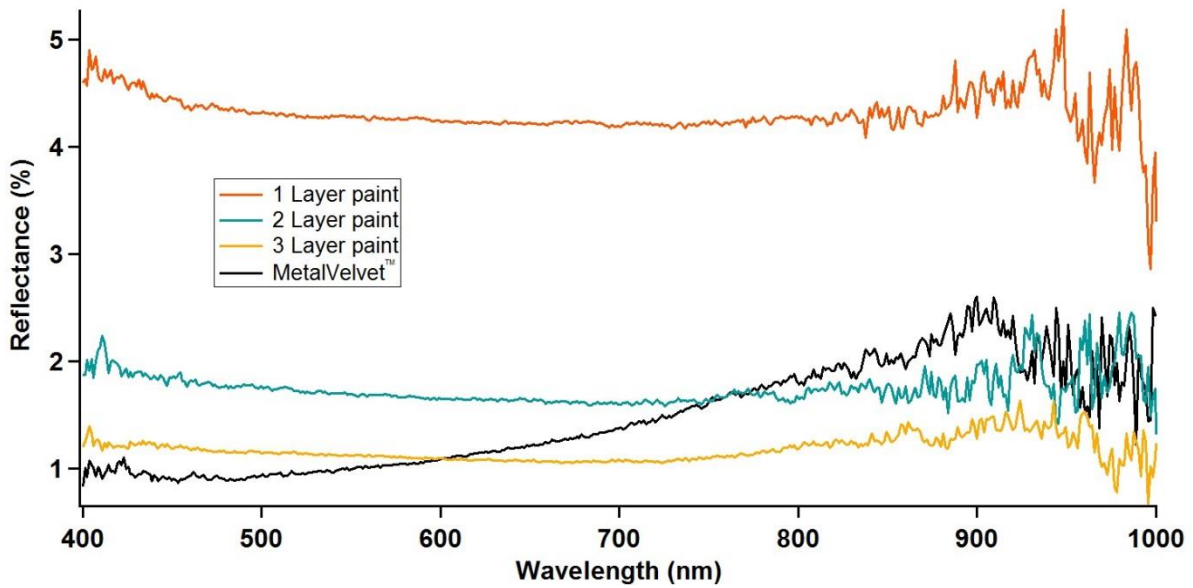


Figure 3 Reflectance spectra of a microscope slide with different numbers of black paint layers and of a low reflecting material (MetalVelvet™).

3.3. Reflectance standards

The spectra obtained for the 10% and 50% reflectance standards by the HIMS and the field spectroradiometer were compared with the respective spectra provided by the producer (Figure 4).

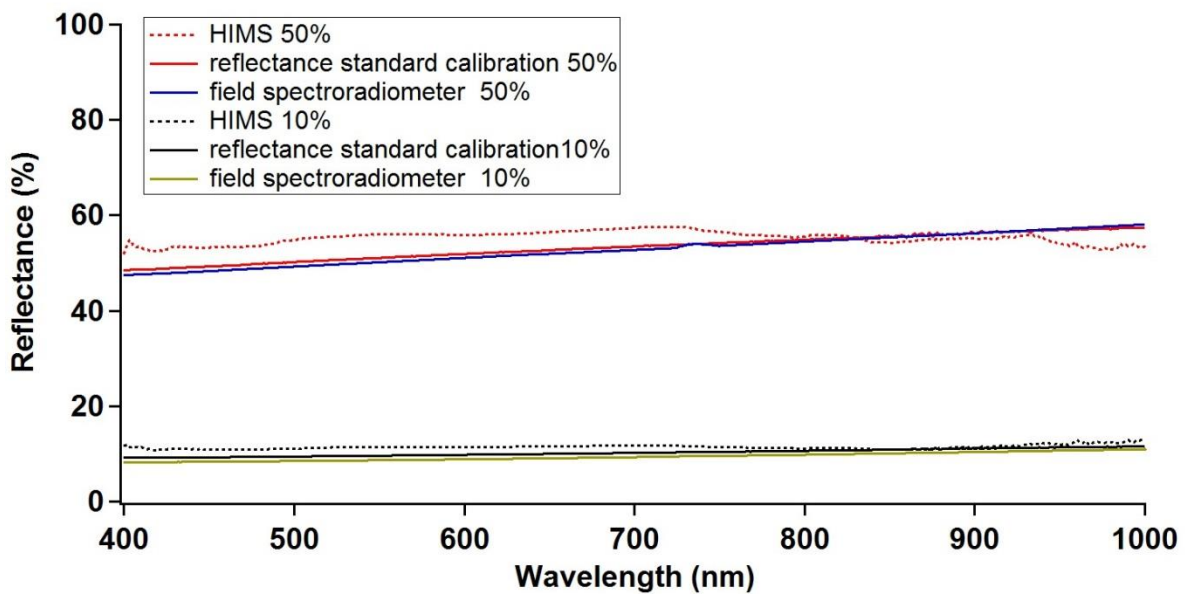


Figure 4 Reflectance spectra of the 10% and 50% reflectance standards measured with the HIMS and the field spectroradiometer and provided by the producer (Labsphere).

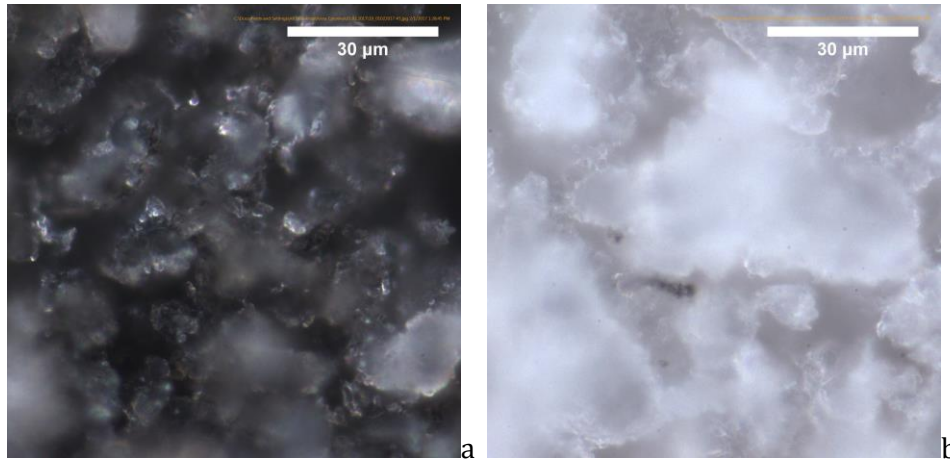


Figure 5 Microscopic images at 100x magnification of the 10% (a) and 50% (b) reflectance standards.

The average deviation of the reflectance spectra between the HIMS spectra and the calibrated spectra provided by Labsphere, over the whole spectral range, was small for both reflectance standards (1.2%, for the 10% standard and 3.2% for the 50% standard). This deviation represents the heterogeneity of the standard, visible in Figure 5, on the microscopic scale and not the uncertainty of the HIMS. In contrast to the 10% reflectance standard, the 50% reflectance spectrum obtained with the HIMS shows a wavelength dependent deviation. For the 400-830 nm range reflectance is overestimated by the HIMS, while it is underestimated for the 900-1000 nm range. The field spectroradiometer is not sensitive to the microscopic inhomogeneity of the reflectance standards; accordingly the deviation values between the spectrum provided by the producer and the one measured with the field spectroradiometer is even smaller (0.8% for the 10% standard and 0.6% for the 50% standard).

The MCWS reflectance standard has fourteen characteristic peaks in the spectral region between 400 and 1000 nm (Figure 6). The average deviation between the characteristic wavelengths given by the producer of the MCWS standard and the measured HIMS spectra is 1.1 nm, which is below the 2.5 nm spectral resolution given by the HIMS producer. This measurement shows that the spectral resolution given by the instrument's producer is valid also in the case of reflectance measurements.

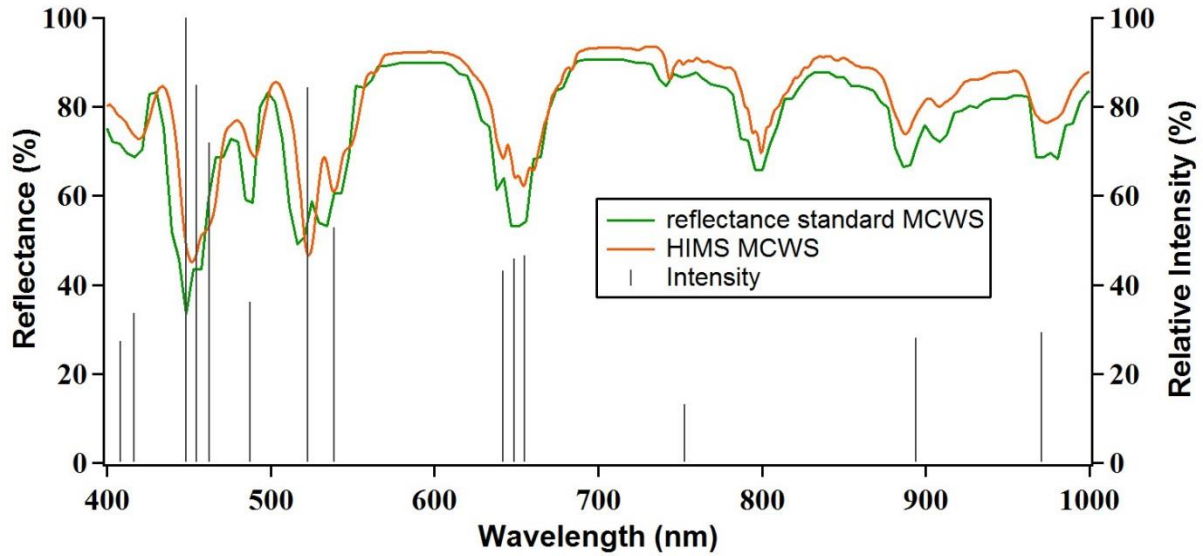


Figure 6 Reflectance spectra of the MCWS reflectance standard provided by the producer (green) and measured with the HIMS (orange) with characteristic peaks, and the relative intensity ($A_{\text{peak}}/A_{\text{max}}$, normalized to the 448.6 nm peak) reported by the company (grey lines).

3.3 Influence of particle orientation on the reflectance

The five spectra obtained by rotating a single hematite particle (visible in Figure 10a) are shown in Figure 7. The influence of orientation is negligible for wavelengths between 400 and 700 nm (average deviation of 0.2%), but is measurable in the 700 to 1000 nm range (average deviation 4.3%). This suggests that in order to acquire representative spectra several measurements with varying orientations should be averaged. The larger deviation at longer wavelengths might be due to the fact that when particle size and wavelength become more comparable in size, the orientation of the particle plays a bigger role.

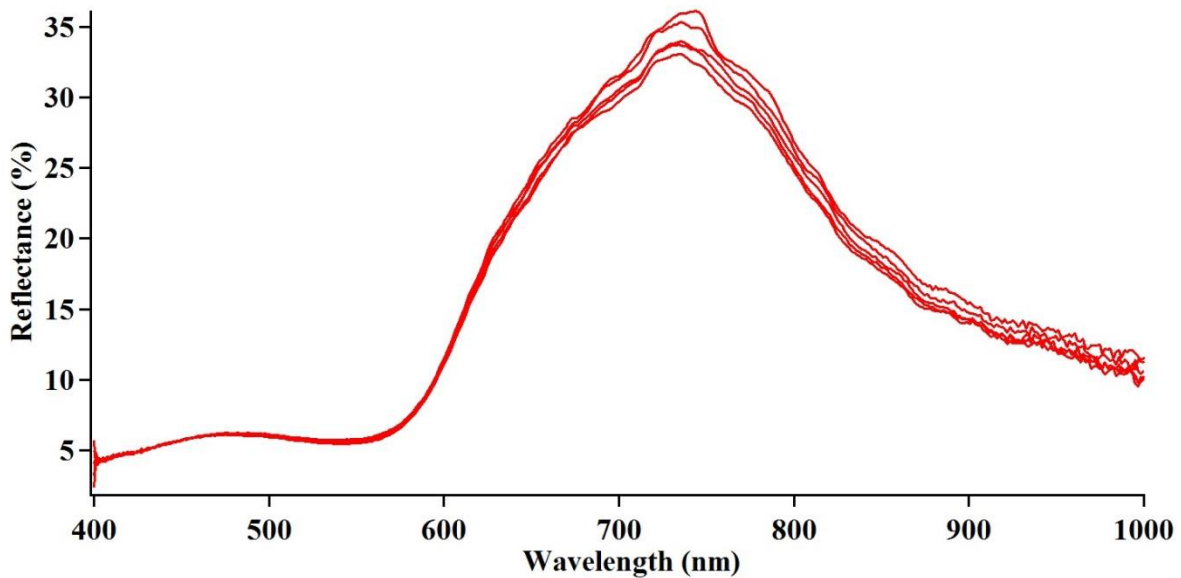


Figure 7 Five reflectance spectra of one hematite particle rotated 72° on the horizontal plane between each measurement.

3.4. Diesel soot, mineral, and organic standards:

Reflectance spectra of the standard materials Diesel soot, minerals and humic substances measured with the HIMS and the field spectroradiometer are shown in Figure 8. The comparison demonstrates that microscopic and macroscopic measurements yield comparable results, especially in the case of low reflecting materials. The absolute deviation between the corresponding spectra (R%), obtained by averaging over the entire wavelength range (400–1000 nm), are 6.79, 3.10, 6.06, 3.74, 0.86, 0.96, and 1.16 for chlorite, quartz, kaolinite, hematite, Diesel soot, urban dust and humic substances, respectively. The standard deviations obtained from the average of the 10 to 15 HIMS measurements shown in Figure 8 are the following for chlorite, quartz, kaolinite, hematite, Diesel soot, urban dust and humic substances, respectively: 79.95 ± 1.79 , 80.2 ± 3.28 , 83.74 ± 1.77 , 15.51 ± 0.59 , 1.26 ± 0.13 , 5.87 ± 0.42 and 5.81 ± 1.86 . It was found that averaging 10 to 15 measurements was enough to obtain a precise average. The small differences encountered with the particle scale measurements are intrinsic to the measurement and are due to the nature of microscopic spectrometry. Recordings from particles measured at the microscopic scale can include substrate reflections, which are not included in bulk measurements, which allow all natural re-emission of penetrating light to be picked up. The more reflective minerals (particularly quartz and chlorite) display in the HIMS spectra an interference pattern that is due to the interaction between the incoming radiation and the various semi-transparent layers of the minerals. This interference effect results in a larger deviation between the HIMS and field spectroradiometer spectra. The small feature that

appears at 743 nm in chlorite, quartz and kaolinite in all the field spectroradiometer spectra could be a hematite impurity, since it is not present in the other spectra of darker materials.

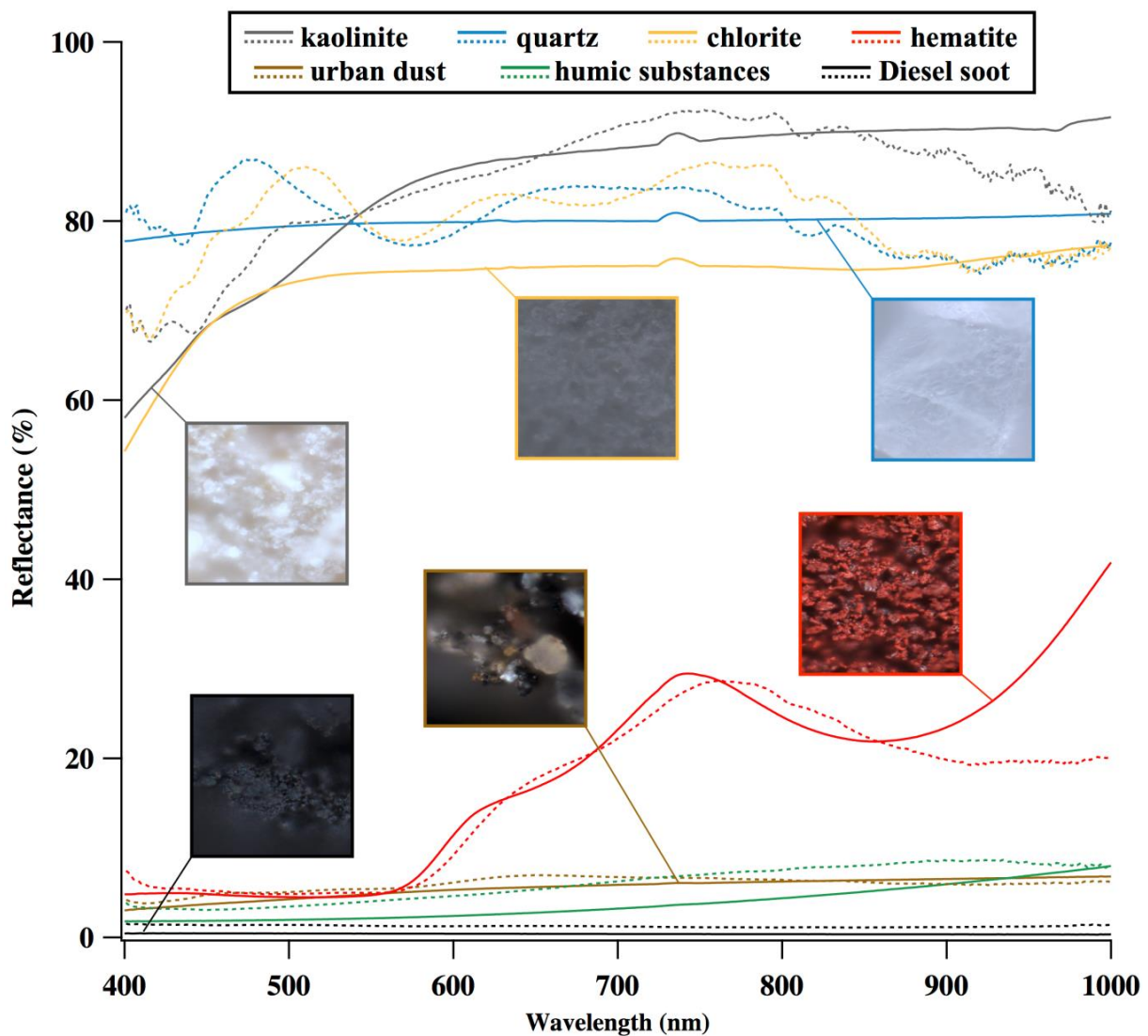


Figure 8 Reflectance spectra of the different standard materials (Diesel soot, minerals and humic substances). Dotted lines: HIMS measurements at the particle scale, solid lines: field spectroradiometer measurement of bulk samples. The images represent examples of the measured standards; the colours of the frames correspond to the spectra (humic substances are not present).

3.5 Environmental sample

The reflectance spectra of the different LAI classes contained in the environmental sample collected with the HIMS are shown in Figure 9. The spectra were obtained from a single particle for each LAI class to be able to relate the respective spectrum to the corresponding ROI in the hyperspectral image shown in Figure 10. To retrieve a representative spectrum of each LAI class measurements of 10 to 15 different particles should be averaged. The spectra collected

belong to different individual particles within the mixture of LAI in the environmental sample, and differ from the spectra shown in Figure 8 for the respective Diesel soot, mineral and humic substances standards; which were used to demonstrate the suitability of the method. This difference is expected, since emission sources and atmospheric history affect the optical properties. This finding underlines the value of the HIMS technique, which is able to collect a characteristic signal of the LAI in a heterogeneous environmental sample, rather than relying on the optical properties of standard materials.

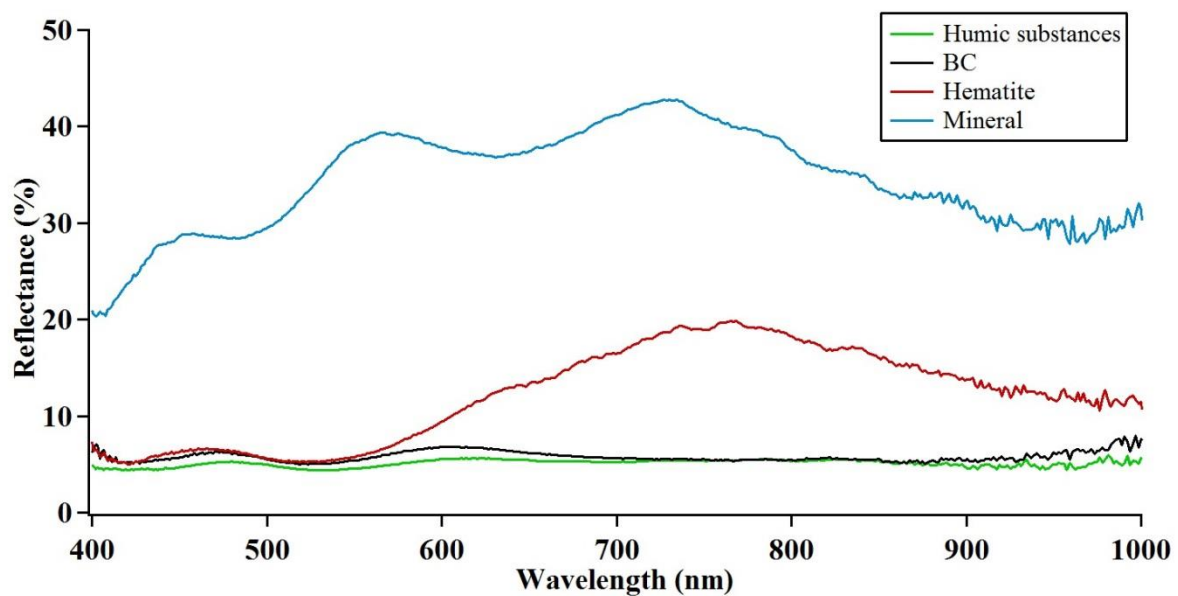
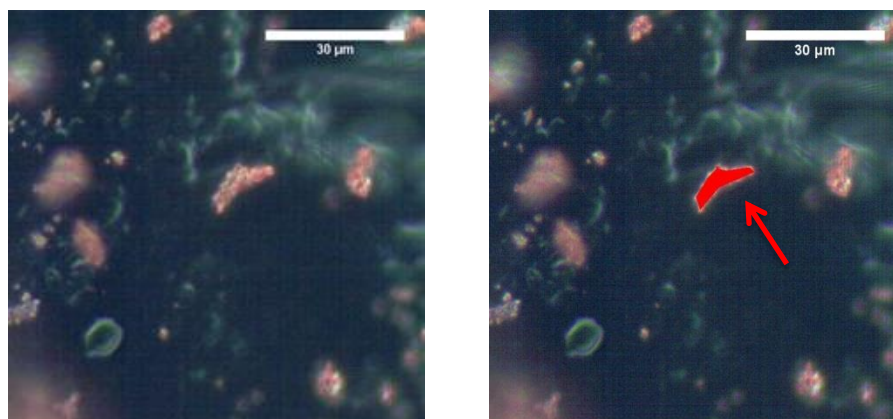


Figure 9 Individual measurements of spectral reflectance of a BC particle, a bright mineral particle, a hematite particle, and the humic substances matrix of a cryoconite granule, all originating from the Plaine Morte glacier environmental sample. The measured ROI for each reflectance measurement is shown in the images in Figure 10.



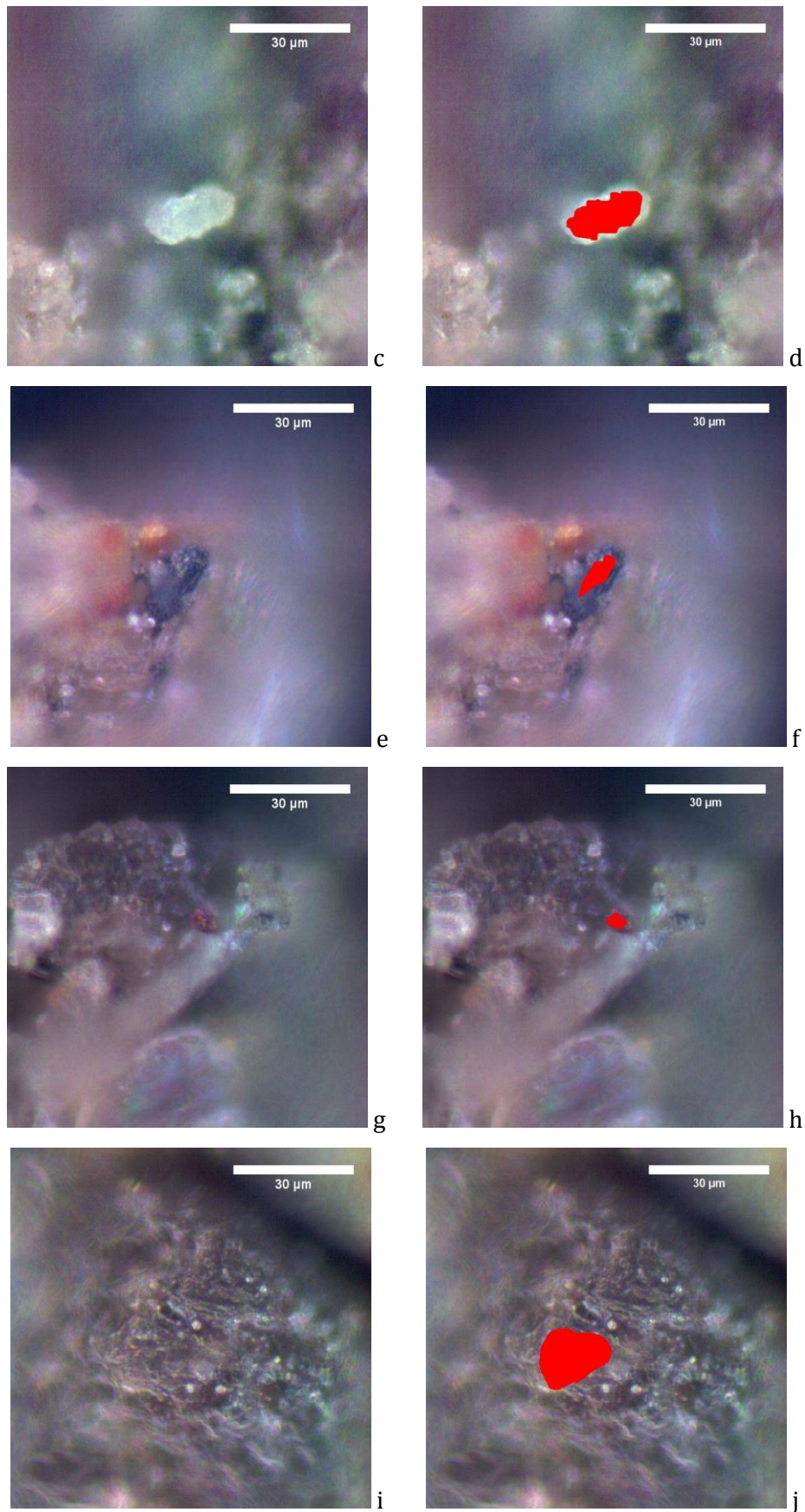


Figure 10 Images of LAI from an environmental sample from Plaine Morte glacier. a, c, e, g and i show the hyperspectral image, while in b, d, f, h and j the measured ROI is indicated in red. a, b) rotated hematite particle (ROI

indicated with a red arrow). c, d) mineral particle. e, f) BC particle. g, h) hematite particle. i, j) humic substances matrix of a cryoconite particle.

4. Conclusion

A new method using a hyperspectral imaging microscopy spectrometer (HIMS) was developed to measure the reflectivity of different types of LAI (mineral, BC and humic substances) at the submicron scale, and the method was validated by measuring the same materials at the bulk scale with a commonly used spectroradiometer. The new method yields reliable spectra for all substances, but for semi-transparent minerals interferences result in a slightly larger uncertainty. Studies on the morphology and composition of cryoconite granules could be carried out with this technique, shedding light on their formation. This new method also advances our ability to constrain the relative importance of the different LAI by allowing the reflectance of the specific LAI in a sample to be characterized as opposed to past approaches that used generic optical properties from literature. The specific optical behaviour, along with the relative abundances of LAI types can deliver a more complete picture of the effect of these impurities. As a future prospective the characteristic spectra collected could serve as endmembers for interpreting field spectra collected from the ice or snow surfaces either with in situ techniques or with remote sensing. The contribution of each endmember would be determined through non-linear spectral un-mixing as cryoconite in snow and ice constitutes an intimate mixture. The various possible applications in this research field make this a very promising method, which can pave the way to improve the understanding of the role of LAI in the surface albedo of ice and snow.

Competing interest

The authors declare that they have no conflict of interest.

Acknowledgements

We acknowledge Dr. Michael Plözte at the Department of Civil, Environmental and Geomatic Engineering of ETHZ for providing the mineral standards; Sven Avak, Dimitri Osmont, Loic Schmidely and Dr. Johannes Schindler for the help in sampling on Plaine Morte glacier. Kaspari's time was supported by a Swiss National Science Foundation short visit (IZK0Z2_160953), the Oeschger Center for Climate Change Research, and a Hans Sigrist Supplementary Grant.

4 Location and effect of light-absorbing impurities on Glacier de la Plaine Morte

Anna Dal Farra^{1,2,3}, Andrea Marinoni⁴, Kathrin Naegeli⁵, Margit Schwikowski^{1,2,3}

¹Laboratory of Environmental Chemistry, Paul Scherrer Institute, 5232 Villigen PSI, Switzerland

²Department of Chemistry and Biochemistry, University of Bern, 3012 Bern, Switzerland

³Oeschger Centre for Climate Change Research, University of Bern, 3012 Bern, Switzerland

⁴Telecommunications and Remote Sensing Laboratory, Department of Electrical, Computer and Biomedical Engineering, University of Pavia,

⁵Centre for Glaciology, Department of Geography and Earth Sciences, Aberystwyth University, UK

Correspondence to: Margit Schwikowski (margit.schwikowski@psi.ch)

Manuscript in preparation, to be submitted to Journal of Glaciology

Abstract

Light-absorbing impurities (LAI) are known to considerably influence glacier melt, accelerating the current trend of negative mass balance in the case of many glaciers, including Glacier de la Plaine Morte. The magnitude of the LAI's effect depends on their abundance on the glacier surface as well as on their optical properties. LAI are divided into three classes (black carbon (BC), organic matter, and mineral dust). An average relative abundance of 91.1, 8 and 0.9% was measured for mineral dust, organic matter and black carbon, respectively with a thermo-optical OC-EC analyser on 110 surface samples collected on Glacier de la Plaine Morte. The spatial distribution of the LAI classes revealed that mineral dust and organic matter are mostly of local origin, which was confirmed for the mineral by the composition found with X-ray diffractometry. With a novel method, using a hyperspectral imaging microscope spectrometer (HIMS) the reflectance spectrum of each LAI class was determined. These characteristic reflectance spectra along with that of bare ice were used as endmembers in the spectral unmixing of reflectance spectra measured on the glacier with a field spectroradiometer. The relative abundance determined with this method matched well with the measured values for the area where the spectra were collected (with a 0.4% average standard deviation). The same spectral unmixing was applied on a highly spatially resolved airborne hyperspectral dataset, covering the entire glacier surface. The resulting distribution of the LAI on the glacier and the

average relative abundance values agreed well with the measured data. Relatively high abundance of organic matter in the areas with particularly low albedo suggests that the latter plays an important role in glacier darkening.

4.1 Introduction

Glaciers in Switzerland hold a critical role both as a water supplier in Alpine valleys and as source of hydropower production (Finger et al., 2013; Huss et al., 2013). According to various studies, glaciers in Switzerland have strongly retreated in length and volume with estimates of the total glacier length variations for 2016 being -2482.6 m (based on 93 glaciers, GLAMOS, 2016) (Huss et al., 2008; Huss et al., 2013). Amongst the retreating glacier is Glacier de la Plaine Morte, which is situated in the western Swiss Alps, between the cantons of Valais and Bern. It forms an extensive plateau (7.88 km² in 2013) with a mean altitude of 2750 m a.s.l. Glacier de la Plaine Morte has been the subject of hydrological studies (e.g. Finger et al., 2013), which determined the flow path of the glacier runoff, and remote sensing studies (Paul, 2005; Naegeli et al., 2015), which looked at the albedo of Glacier de la Plane Morte in relation to its mass balance. In most years since 2003 at least 66% of the glacier's surface has been snow-free at the end of summer (Huss, 2013), i.e. the glacier is located below the equilibrium line altitude. The glacier's condition in the last years has resulted in a strong albedo decrease during the summer months. Albedo is defined as the ratio of the radiant flux reflected from a unit surface area into the whole hemisphere to the incident radiant flux of hemispherical angular extent (e.g. Schaepman-Strub et al., 2006). It plays an important role in the energy balance of a glacier system (Arnold et al., 1996). A glacier's surface albedo may decrease because of multiple reasons: when the bare ice surface is exposed and when liquid water or light-absorbing impurities (LAI) are present (Fujita and Ageta, 2000; Boggild et al., 2010; Box et al., 2012) (Anslow et al., 2008)(Greuell, 2000). In the case of Glacier de la Plaine Morte all these conditions are present, contributing to the acceleration of melting rates (Oerlemans and Hoogendoorn, 1989; Van De Wal et al., 1992; Hock, 2005; Naegeli et al., 2015). In this study the focus is on the characterization of the LAI classes and their distribution on the glacier. Commonly found LAI include black carbon (BC) or soot (Petzold et al., 2013), mineral dust and organic matter. BC is the product of an incomplete combustion of bio and fossil fuels, and its sources can be both natural and anthropogenic. BC is a strong contributor to positive climate forcing by directly warming the atmosphere and indirectly by reducing snow and ice albedo (Cooke and Wilson, 1996; Ramanathan and Carmichael, 2008). These positive forcings are due to the high mass absorption cross section (MAC) of $>7.5 \pm 1.2 \text{ m}^2/\text{g}$ at 550 nm of BC (Bond et al., 2013; IPCC, 2013). The radiative forcing estimated for the "soot in snow" effect is $0.65 \text{ Wm}^{-2} \pm 0.4$ (relative to the

year 1750), which is one third of the radiative forcing of CO₂, but with a much larger uncertainty. Mineral dust sources vary greatly in space and time and include desert regions, local outcrops and land use (construction, mining and agriculture). Mineral dust's light absorption is highly variable as it strongly depends on the mineral composition of the dust; although in general it is lower than for BC (Clarke et al., 2004). However, recent research suggests that in some regions the dust's higher concentration with respect to BC causes mineral dust to drive albedo reduction and consequently the melt (Skiles et al., 2012; Kaspari et al., 2014; Gabbi et al., 2015). Organic matter contributes with its many possible forms to the darkening of glacier surfaces. It was estimated that red algae blooms can cause a decrease in snow albedo of 13% over the course of one melt season (Lutz et al., 2016). The presence of organic matter in the form of cryoconite has been reported to influence surface albedo as well with an estimated decrease of approximately 30%, which is equivalent to 53.4 W m⁻² of heat gain and 13.8 mm d⁻¹ of ablation rate for the Yala glacier in the Langtang region (Kohshima, 1993; Takeuchi et al., 2001). In particular humic substances, formed by the decomposition of algae and bacteria, which make up the matrix of cryoconite granules, can display very dark colouring (Kumada, 1987). Determining the abundances of all LAI classes on a glacier is not sufficient to quantify their effect on albedo because of their different optical properties. Furthermore, only the MAC or reflective index of BC and of some minerals are known, while they have not been described for organic matter. In addition optical properties were derived from standard materials, which might not properly represent the BC and minerals present on the glacier. In this study we identified classes of LAI present on Glacier de la Plaine Morte, determined their relative abundances and distribution on the glacier as well as their sources. To obtain a characteristic reflectance spectrum for each of the different classes of LAI we applied a novel method using a Hyperspectral Imaging Microscope Spectrometer (HIMS, Hyperspectral Microscope, Cytoviva)(Dal Farra et al., submitted). The characteristic reflectance spectra obtained with the HIMS were used as endmembers for the spectral unmixing of the reflectance spectra of the glacier surface, collected both with a field spectroradiometer and with an airborne remote sensing technique, to quantify the relative contribution of each LAI class to the measured reflectance and determine the spatial distribution of the impurities.

4.2 Method

On 20th August 2015 a total of 90 surface samples were collected on Glacier de la Plaine Morte following five tracks along West-East direction and resulting in the grid shown in Figure 1. About 20 x 20 cm area of the surface of the glacier was scraped with a small plastic spatula and collected in 500 ml pre-cleaned PET containers with a plastic shovel. Sampling positions were determined by GPS for the starting point and ending point of the tracks; each sampling point was estimated by keeping equal distances during sampling. The estimated uncertainty in the sampling point is ± 25 m, and is given by the standard deviation of the distances between GPS points (green points of Figure 1). To ensure an equally spaced grid the members kept equal distance on a linear trajectory (with Glacier de la Plaine Morte being a very flat glacier the members were able to observe the positions of their adjacent members). All the samples were kept frozen until analysis. On 21st August 2015 reflectance spectra of the surface were measured under cloud free conditions between 11:00 and 13:00 Central European Summer Time (CEST) using a field spectroradiometer (FieldSpec 3, ASD Inc., PANalytical). The field spectroradiometer measures the 350–2500 nm spectral range, has a spectral sampling interval of 1.4 nm (350–1000 nm) and 2 nm (1000–2500 nm), and a full width half maximum of 3 nm at 700 nm and 10 nm at 1400 nm (Analytical Spectral Devices, I., 2014). This instrument has a Field of View (FoV) of 46°, the optic fibre was placed approximately 23 cm above the surface during measurement, resulting in a measured area of 20 cm². Unfortunately, 15 out of the 20 measurements had to be discarded due to malfunctioning of the instrument. Reflectance spectra were obtained in the area indicated in Figure 1. All spectra display reflectance in % as each measurement was light corrected with a white reference (WR, Spectralon, Labsphere) accounting for the variations of the sky condition. For each surface area 30 spectra were averaged. In addition, surface samples with a depth of 1–2 cm were collected from each 20 cm² area for which a reflectance spectrum was collected. The Airborne Prism EXperiment (APEX) spectral data presented in this study were collected during a campaign that took place 31st August 2013. Between 10:15 and 10:24 CEST under cloud-free conditions two overflights with the imaging spectrometer collected spectral data of the Glacier de la Plaine Morte. A surface projected pixel resolution of ~ 2 m was achieved by maintaining a 4000 m above ground level flying altitude combined with an instantaneous FoV of 0.0025°. APEX is a dispersive pushbroom imaging spectrometer which covers the 400–2500 nm spectral wavelength range in 313 narrow continuous spectral bands (Schaepman et al., 2015).

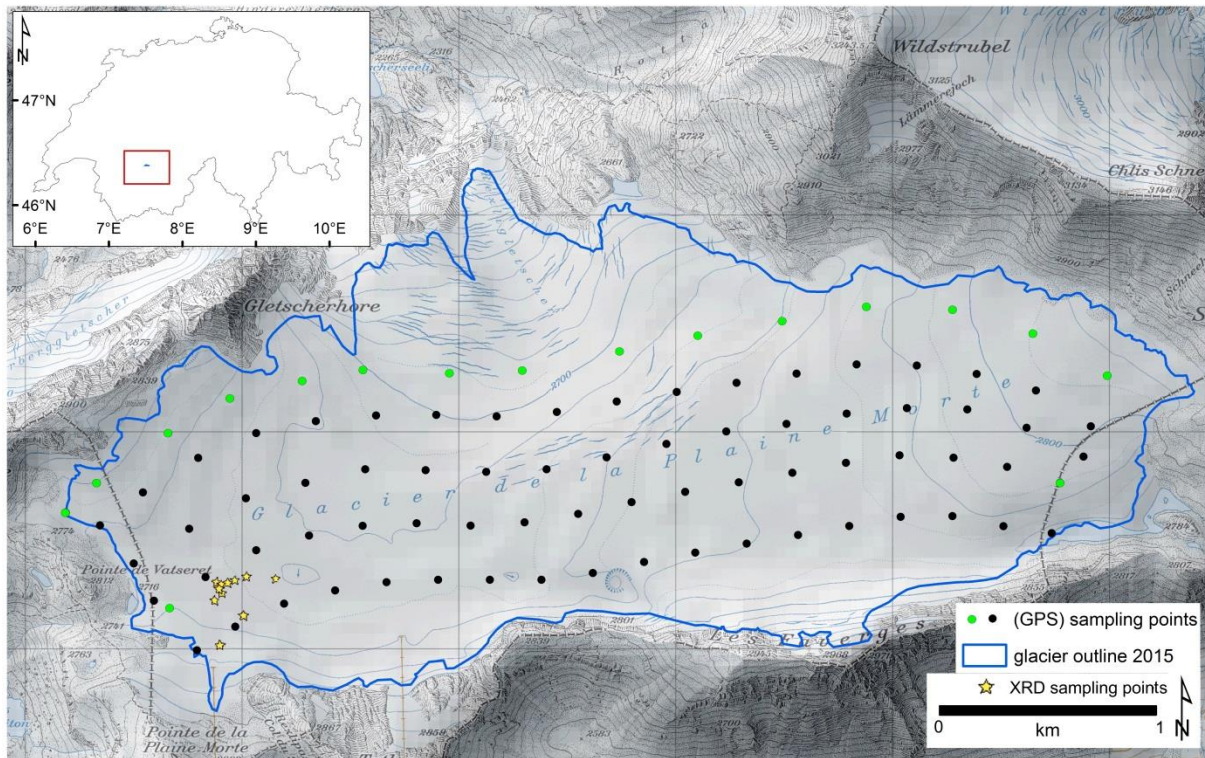


Figure 1 Topographic map of Glacier de la Plaine Morte and its location within Switzerland (inset). The grid-like dotted pattern represents the sampling locations; the green points indicate GPS position taken while the black points have an uncertainty of $25 \pm \text{m}$. The location of the sampling points for the XRD measurements are highlighted by the yellow stars (adapted from Swiss office of Topography).

Organic carbon (OC) and elemental carbon (EC) were determined with a thermal optical analyser, for this the 110 samples were melted at room temperature and filtered with a vacuum pump onto glass fibre filters (Whatman GF/B, 4 cm diameter). The filtrate was dried overnight in an oven at 80°C and the weight of each was determined after cooling. The filtrate was grinded and mixed in an agate mortar. Between 2.7 and 4 mg of the samples were weighted and placed in polypropylene vial, which were then filled with 30 ml of ultra-pure water and sonicated for 30 minutes to break apart large aggregates. The suspensions were then filtered onto preheated quartz fibre filters (Pallflex Tissuquartz, 2500QA0UP) and combusted with a thermo-optical OC-EC analyser (Model4L, Sunset Laboratory Inc., USA), using the Swiss_4S protocol for OC-EC separation (Zhang et al., 2012). Here EC (elemental carbon) is used as a proxy for BC (Lavanchy et al., 1999), while, to obtain organic matter, the OC was multiplied by 2, as suggested by (Pribyl, 2010). By subtracting the amount of organic matter and BC from the sample's initial weight the mass purely composed of minerals was determined, assuming that the non-combusted fraction is purely composed of minerals.

The relative abundances were interpolated to obtain the spatial distribution of the LAI on the glacier with an Inverse Distance Weighting (ESRI ArcGIS, version 10.4). A novel method (Dal Farra et al., submitted) was used to determine the characteristic reflectance spectrum of each class of LAI directly in the LAI samples collected. This has the advantage that little to no sample treatment is required and that characteristic reflectance spectra were obtained without the need to separate the mixture. The analysis proceeded as follows: amongst the 110 samples the ones with the highest abundance of BC, minerals and organic matter respectively, were identified. These specific samples were taken as dried filtrate and slightly grinded in an agate mortar with the purpose of breaking apart the larger aggregates. 2 to 3 mg of the sample was positioned on a glass microscope slide; which had been painted with three coatings of black matte paint (Motip Dupli, Black Mat) to ensure minimal interference from the background. A characteristic reflectance spectrum for each of the classes of LAI was obtained by averaging 10 to 15 measurements of particles belonging to the respective LAI class. The particles observed through the 100x magnification microscope were divided into the three LAI classes based on their morphology and perceived colour. BC particles are mostly spherical and dark; minerals have angular shapes and display on average brighter colours, while humic substances compose the matrix of most of the aggregates in the sample, i.e. cryoconite granules. All the spectra were normalized with a white reference (WR, Spectralon, Labsphere). Measurement times varied depending on the brightness of each particle but were all normalized according to (1).

$$R (\%) = \frac{I_s * Mt_s}{I_{WR} * Mt_{WR}} \quad (1)$$

Where R is the reflectance, I_s and I_{WR} are the intensity of the signal of sample and WR, respectively, while Mt_s and Mt_{WR} are the measuring time for sample and WR.

The mineralogical composition of 11 samples (location shown in Figure 1) was determined with X-Ray Diffractometry (XRD, XPertPro, MPD Panalytical) using a Cu ka radiation at 40 kV/40 mA with a detection limit of about 0.5 wt%. About 1.5 g of the filtered and dried samples was grinded with an automatic grinding ball mill for 2 min, to guarantee that the size of the individual particles was small (5-10 μm diameter) and homogenous enough for the XRD measurement.

To determine the contribution of each LAI class to the glacier surface reflectance, hyperspectral unmixing based on a p-linear mixture model (p-LMM) was applied (Marinoni and Gamba, 2015). p-LMM is a physics-related nonlinear mixture model, which relies on describing physical interactions among the materials in the given hyperspectral dataset. This model has been developed to improve the description of macroscopic scale interactions among the constituent

elements, typically without prior knowledge of the ground-truth. These schemes aim at retrieving an accurate reconstruction of the dataset as well as a precise quantification of the fractional distribution of the materials in the scene by approximating their interactions at the same order of magnitude of the sensor resolution as powers of products of reflectance. Among nonlinear mixture models, p-LMM is able to characterize higher order combinations of materials within the given hyperspectral records. Specifically, p-LMM describes the spectral signature of the l -th sample $\underline{y}_l = [y_{l_n}]_{n=1, \dots, N}$ (where N is the number of bands) as follows:

$$\underline{y}_l = \sum_{r=1}^R \alpha_{rl} \underline{m}_r + \sum_{k=2}^p \sum_{r'=1}^R \beta_{r'kl} \underline{m}_{r'}^k \quad (2)$$

Where $\underline{m}_r = [m_{r_n}]_{n=1, \dots, N}$ is the spectral signature of the r -th elements in the scene, whereas $\underline{m}_i^k = [m_{i_n}^k]_{n=1, \dots, N}$. Moreover, the α and β coefficients are used to outline the linear and nonlinear contributions provided by each LAI class and a bare ice spectrum, which is reported as “bright ice” in (Naegeli et al., 2015), to the target spectral signature, respectively. As p-LMM is able to achieve a precise outline of the higher order nonlinear interactions among elements, this mixture model is typically suitable to characterize spectrally and geometrically complex scenarios, such as those acquired on a glacial surface. To determine the α and β parameters a polytope decomposition (POD) scheme (Marinoni and Gamba, 2015; Marinoni et al., 2015) is used to perform p-LMM-based unmixing. Then, a volumetric distance is employed in order to ultimately achieve an accurate understanding of the distribution of the materials in each sample. Specifically, it allows to write each spectral component of \underline{y}_l as $y_{l_n} = \sum_{r=1}^R \varphi_{rl_n} m_{r_n}$, where φ_{rl_n} represents the overall contribution of the r -th element to the reconstruction of the l -th sample on the n -th band. Thus, φ_{rl_n} is a function of the α and β coefficients. Then, it is possible to obtain a reliable quantification of the elements in the samples by computing the actual proportion of each material to the overall polytope induced by the given samples in the N -dimensional space (Marinoni and Gamba, 2015), as follows:

$$\hat{\alpha}_{rl} = \frac{\prod_{n=1}^N \varphi_{rl_n}}{\sum_{t=1}^R \prod_{m=1}^N \varphi_{tl_m}} \quad (3)$$

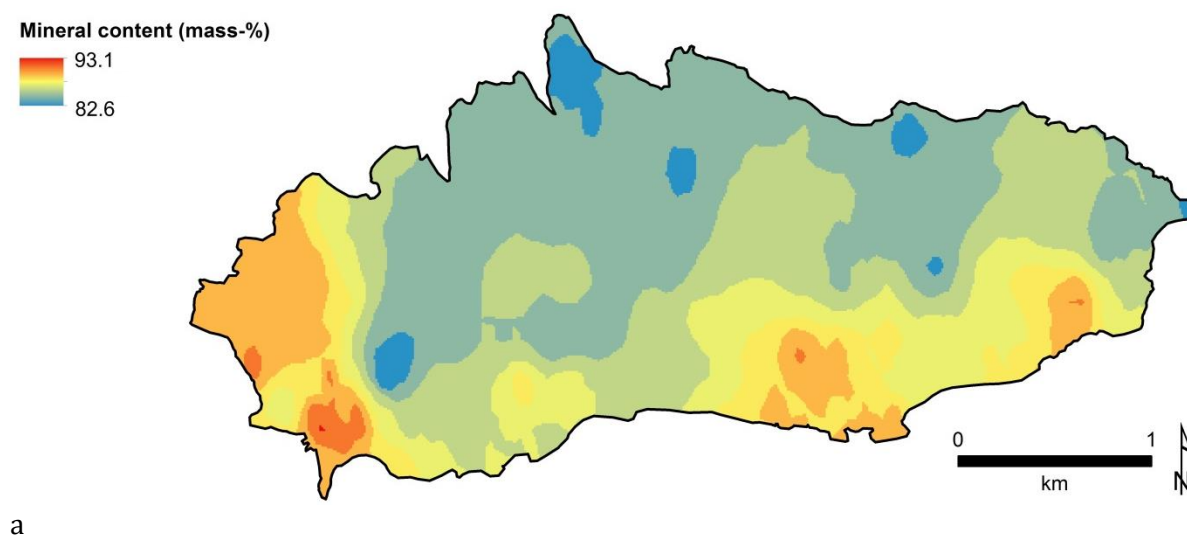
Hence, the $\hat{\alpha}$ abundance index is suitable to deliver an overall description of the contributions provided by the endmembers to the target spectrum by collecting the whole spectral nonlinear

effects in closed form. Moreover, it can be ultimately used to characterize the physical-chemical composition of the surface spectra obtained on site or remotely.

4.3 Results and discussion

4.3.1 Relative abundances of mineral, organic matter and BC

Considering the 110 samples, the obtained average relative abundances of mineral dust, organic matter and BC were $91.1 \pm 3.7\%$ (range 76.2 – 98), $8 \pm 3.5\%$ (range 0.6 – 22.4) and $0.9 \pm 0.4\%$ (range 0.2 – 2.2), respectively. Thus, mineral dust represents the overwhelming majority of LAI on Glacier de la Plaine Morte. The average organic matter abundance is also relatively high compared to other glaciers (Takeuchi et al., 2001). Overall the variability of the relative abundances is small, indicating a mostly homogeneous composition, which is also visible in the relative abundance maps of LAI on Plaine Morte in Figure 2. The higher abundance of minerals at the southern and the western side of Glacier de la Plaine Morte is most likely due to the presence of steep slopes (see map, Figure 1 and Figure 2a). Mineral dust is transported from the slopes in many water paths conveying to the glacier or by wind erosion, becoming more and more enriched each year at the surface, since Glacier de la Plaine Morte does not have any accumulation area. The organic matter distribution is heterogeneous with four hot spots (Figure 2b). This is consistent with what we know about of biota proliferation on glaciers. The ideal conditions for proliferation are when nutrients (both minerals and organics) and liquid water are present (Liu et al., 2017), which might be found in different patches on the glacier. The BC abundance is overall low and its distribution rather homogeneous. This is expected, since BC is transported to Glacier de la Plaine Morte from the surrounding emission sources, which are located within or even outside Switzerland.



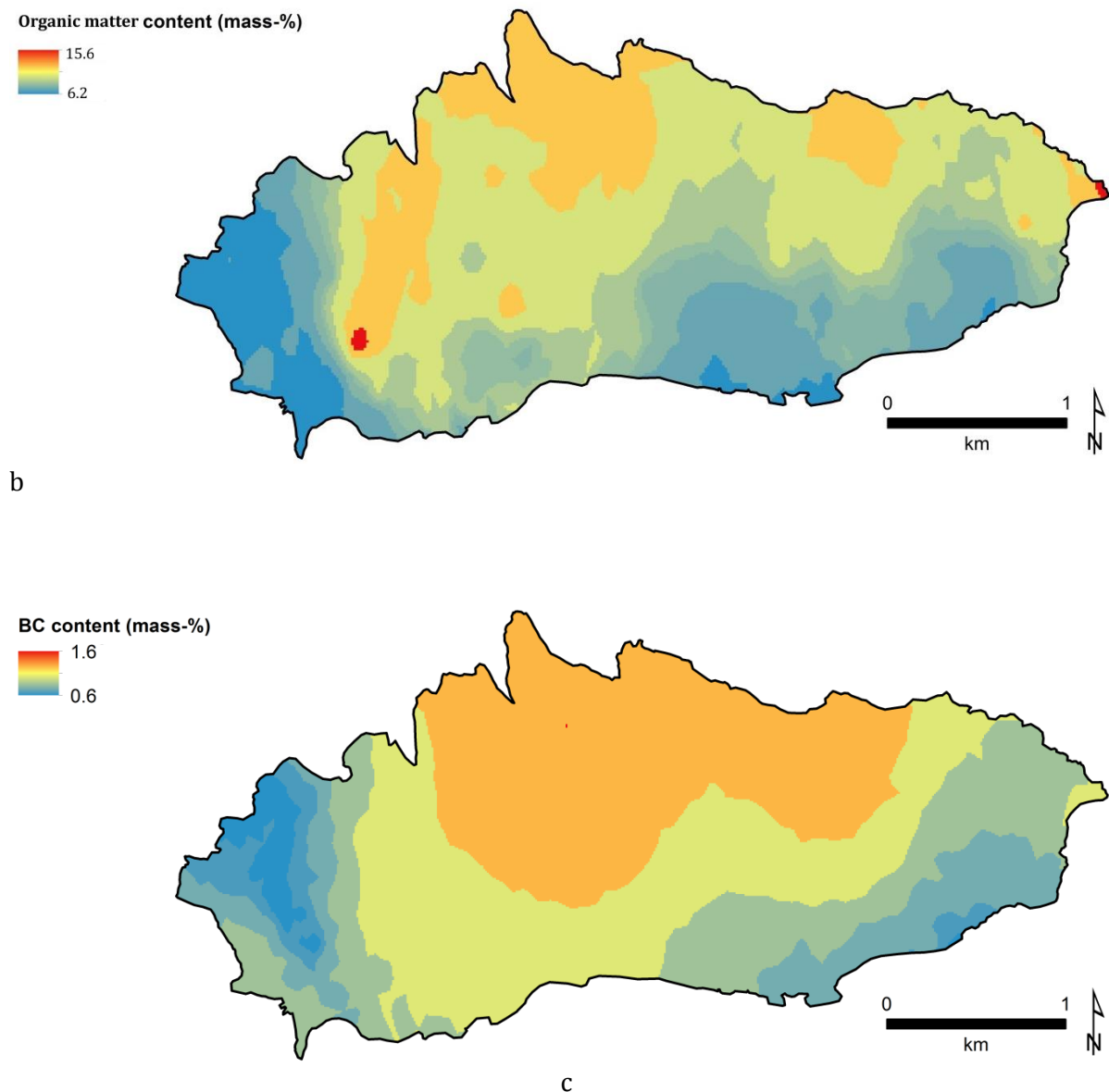


Figure 2 Relative abundances of minerals (a), organic matter (b) and BC (c) on Glacier de la Plaine Morte.

4.3.3 Mineral composition

The mineral composition (Table 1) is dominated by quartz, followed by clay minerals (plagioclase and K-feldspar). This reflects greatly the local geology, which is composed generally of limestone with marl beds, calcareous phyllite and marly shale. Phyllite is a type of metamorphic rock created from slate and primarily consists of quartz, sericite mica, and chlorite (Atlas of Switzerland). While calcite is definitely predominant in the local rock

(limestone) its higher solubility in water (0.013 g/L at 25°C), compared to the silicate based minerals, can explain the small portion that is present on the glacier surface after runoff. In addition, the filtration procedure applied to the samples might further deplete the calcite. Hematite was not detected, although present in Saharan dust, which is regularly transported to the Alps (Schwikowski et al., 1995; Gabbi et al., 2015). Thus, the hematite abundance is below 0.5%, which is due to the dominant and continuous input of local mineral dust versus the less frequent events of Saharan dust deposition.

Table 1 Mineral composition of LAI from Glacier de la Plaine Morte, shown in relative abundances along with the overall average and standard deviation.

Sample	97	99	100	101	102	103	104	105	107	108	109	Average(%)
Calcite	0.8	0.8	11.9	14.7	0.7	0.8	2.9	0.7	0.8	15.4	4.3	4.9 ± 5.5
Dolomite	0.8	0.8	0.7	0.7	0.7	0.0	0.7	0.0	1.6	0.0	0.0	0.5 ± 0.5
K-feldspar	4.7	6.2	5.9	8.8	4.4	6.0	4.3	7.0	12.4	6.2	4.3	6.4 ± 2.2
Plagioclase	17.2	18.5	11.9	10.3	17.8	15.0	15.7	16.8	14.0	12.3	17.1	15.1 ± 2.5
Quartz	76.6	73.8	69.6	66.2	74.1	78.2	72.9	72.7	69.8	66.2	68.6	71.7 ± 3.6
Amphibole	0.8	0.8	0.7	0.0	3.0	0.0	4.3	2.8	1.6	0.0	5.7	1.8 ± 1.8

4.3.4 Characteristic reflectance spectra of different LAI classes

The characteristic reflectance spectra for the different LAI classes BC, organic matter and mineral dust obtained with the HIMS together with a bare ice spectrum are presented in Figure 3. The BC has a low reflectance as expected. The reflectance of organic matter can vary greatly depending on what type of organic matter is dominant on the glacier. In the case of Glacier de la Plaine Morte the organic matter is primarily composed of humic substances, which are as dark as BC (Figure 3). Mineral dust has a lower reflectance than the bare ice, but it is considerably higher than that of BC and organic matter. The spectra in Figure 4 were used as endmembers for calculating the contribution of each LAI class to the reflectance of the glacier surface. Averaging 10–15 measurements was sufficient to obtain a representative spectrum since further measurements did not change the average substantially.

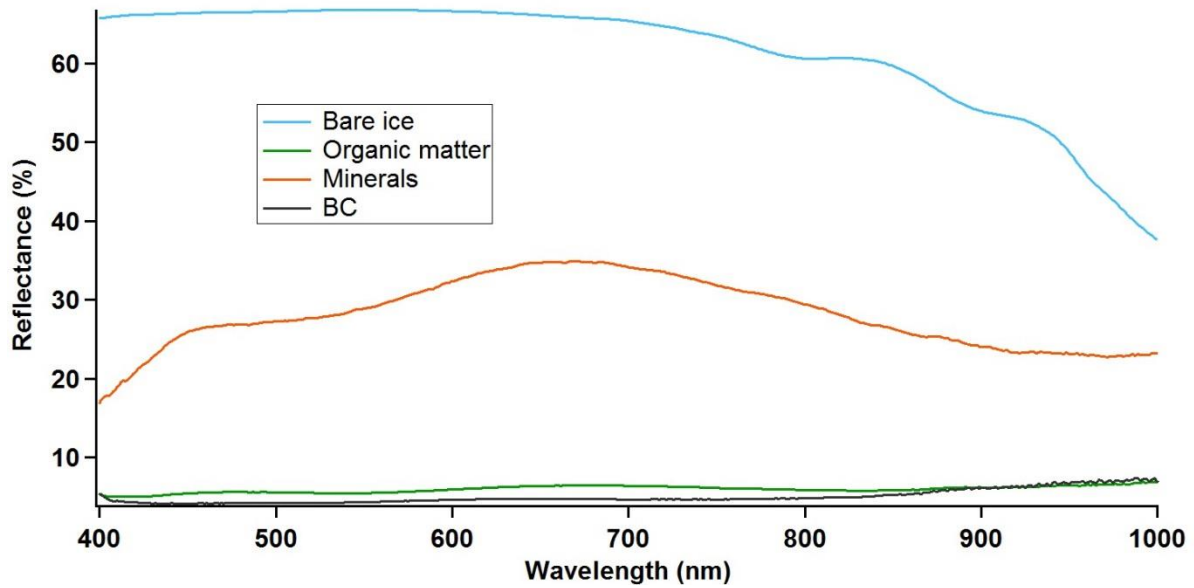


Figure 3 Reflectance spectra used as endmember for the p-LMM, which include the characteristic spectra of the three major LAI classes determined with the HIMS and the bare ice spectrum from Plaine Morte collected with the field spectroradiometer.

4.3.5 Contribution of each LAI class to the glacier surface reflectance

For testing the suitability of the p-LMM, the relative abundance of each LAI class (mineral dust, organic matter, and BC) was retrieved by unmixing the surface reflectance spectra measured on-site with the field spectroradiometer (Figure 4) using the endmembers shown in Figure 3. The obtained relative abundances agree reasonably well with the measured relative abundances (Table 2) with an average deviation of 0.4%. Compared to the overall relative abundances, the variability of the surface LAI composition of this sample subset is understandably small, most probably because of the limited area covered.

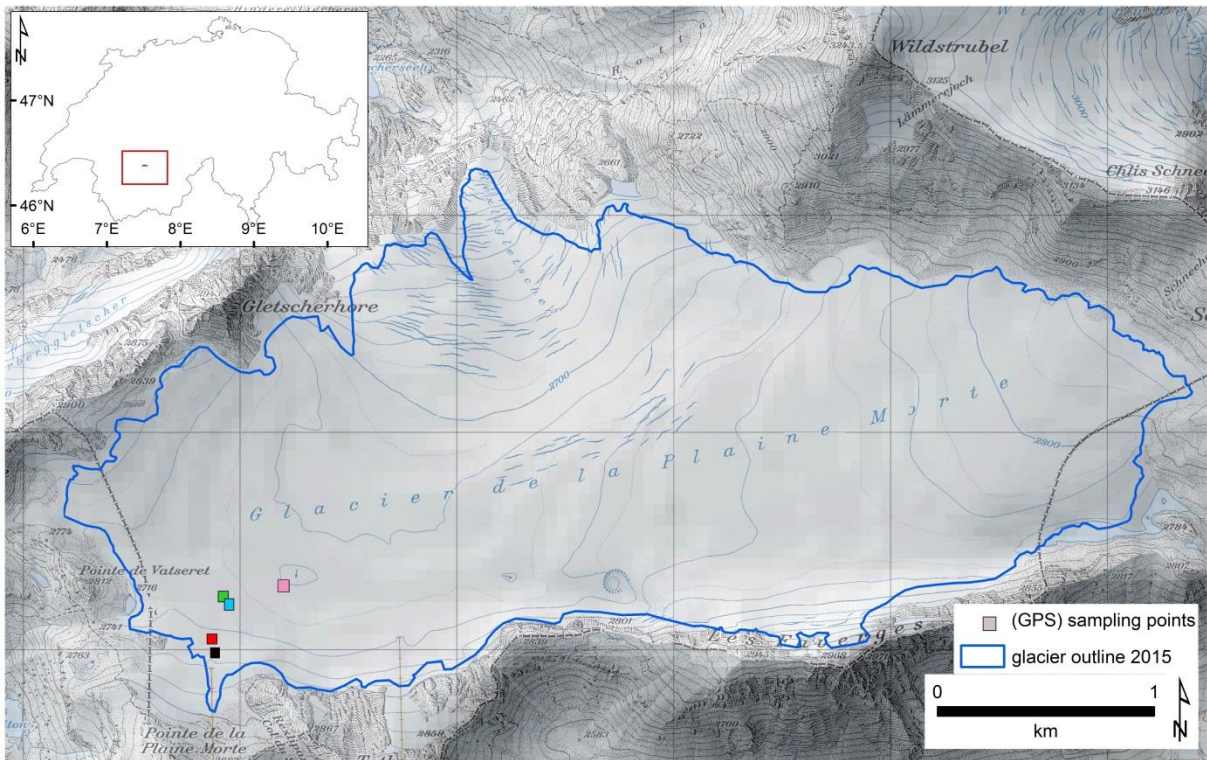


Figure 4 Location of the sampling points of the field spectroradiometer measurements. The colour of the squares corresponds to the colour of the spectra in the Figure 6.

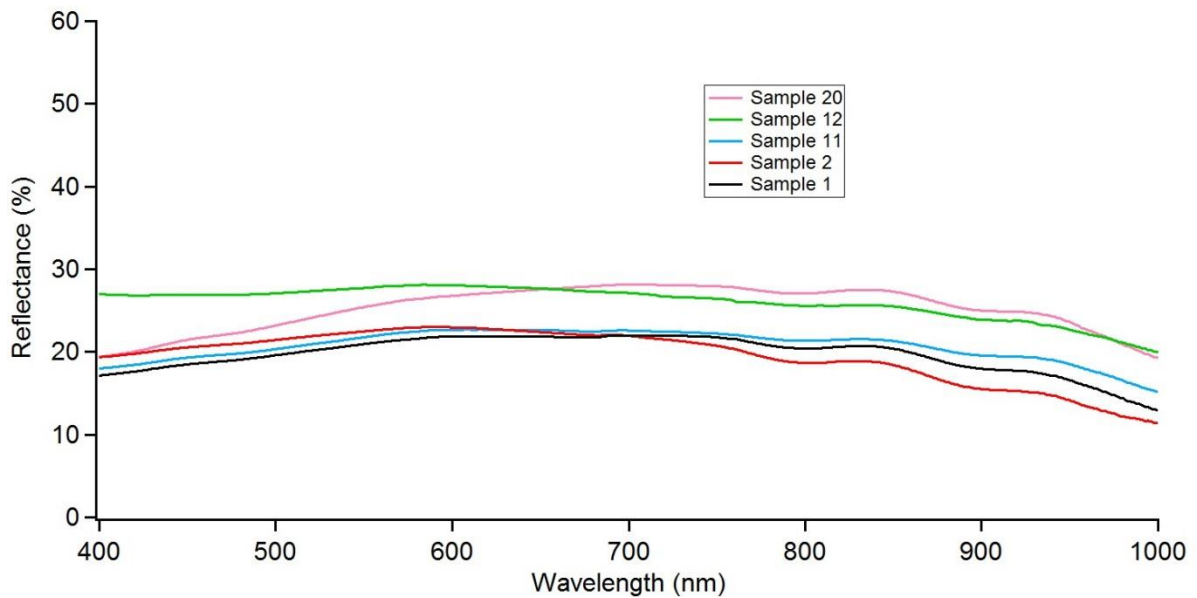


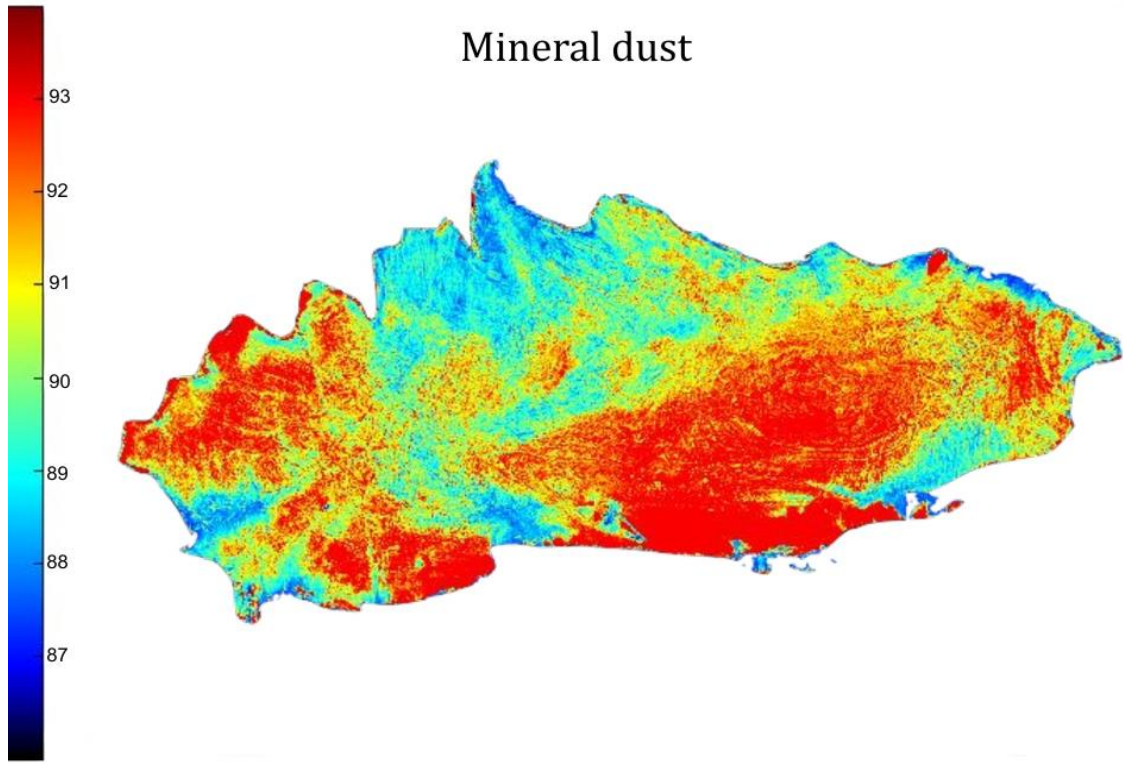
Figure 5 Reflectance spectra collected with the field spectroradiometer on the surface of Glacier de la Plaine Morte.

Table 2 Relative abundances of the different LAI classes measured with the thermal optical method and calculated with p-LMM in percent (%) and the absolute deviation between the values (Abs. dev).

Sam #	Mineral Rel. ab. %			BC Rel. ab. %			Organic matter Rel. ab. %		
	Calculated	Measured	Abs. dev	Calculated	Measured	Abs. dev	Calculated	Measured	Abs. dev
1	96.65	97.03	0.38	1.34	0.55	0.79	2	2.42	0.42
2	96.08	95.28	0.8	0.92	0.32	0.6	2.99	4.4	1.41
12	95.58	94.6	0.98	1.12	0.32	0.8	3.29	5.08	1.79
13	96.52	95.86	0.66	0.82	0.26	0.56	2.65	3.88	1.23
20	96.95	97	0.05	0.99	0.22	0.77	2.06	2.78	0.72
Average	96.4	96	0.4	1	0.3	0.7	2.6	3.7	1.1

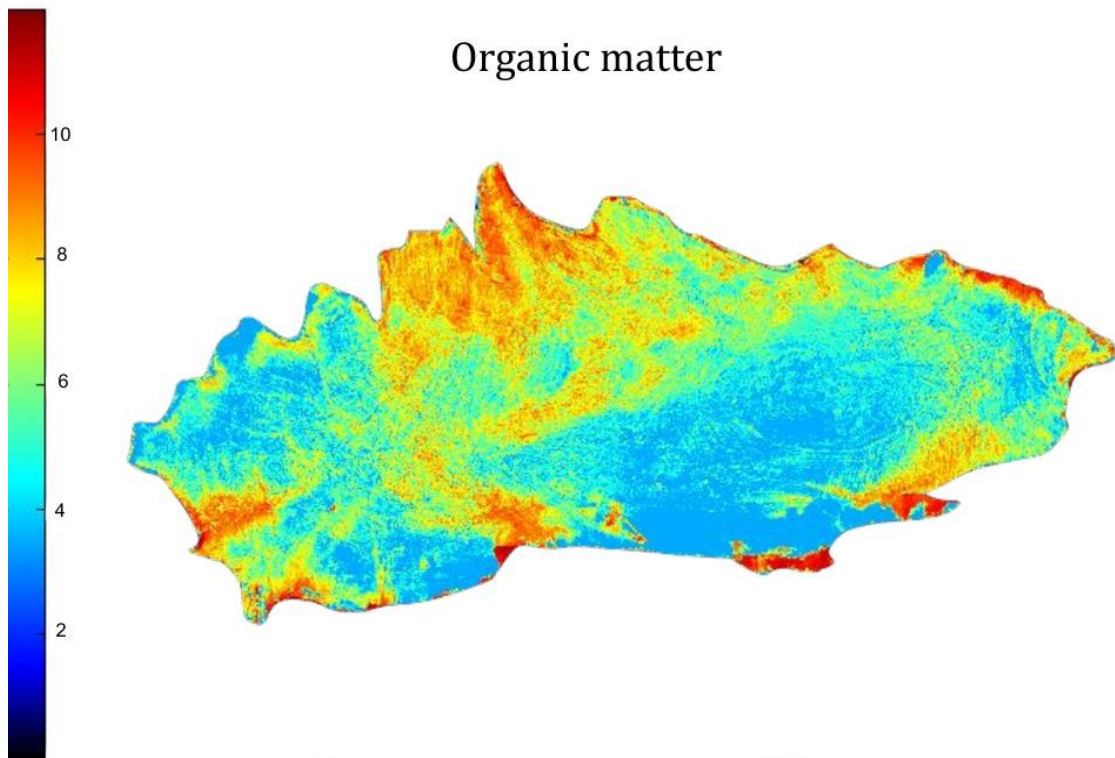
To obtain a high spatially resolved relative abundance map of the entire glacier, unmixing of the APEX reflectance spectra was performed using the same procedure as for the field spectrometer reflectance spectra. Overall the average abundance obtained by spectral unmixing of 91.6, 4.9 and 3.3% for minerals, organic matter and BC, respectively is in good agreement with the measured ones (chapter 4.3.1), indicating that the unmixing procedure using the characteristic endmembers spectra gives reliable results. Also the spatial distribution of mineral and organic matter agree well with the abundance maps obtained by interpolation (Figure 6a and 6b and Figure 2a and 2b). This is reasonable since both LAI classes are characterized by large variability and an uneven distribution on the glacier. There is no agreement in the spatial abundance of BC, BC has a low abundance and variability, since it is the only class of LAI whose sources are predominantly remote from the glacier and is therefore expected to be evenly distributed on the surface. Thus, spectral unmixing of the reflectance spectra is a suitable method to retrieve the overall abundance of major LAI classes on the glacier, but cannot resolve the variability of BC, which has an extremely low abundance.

Mineral dust



a

Organic matter



b

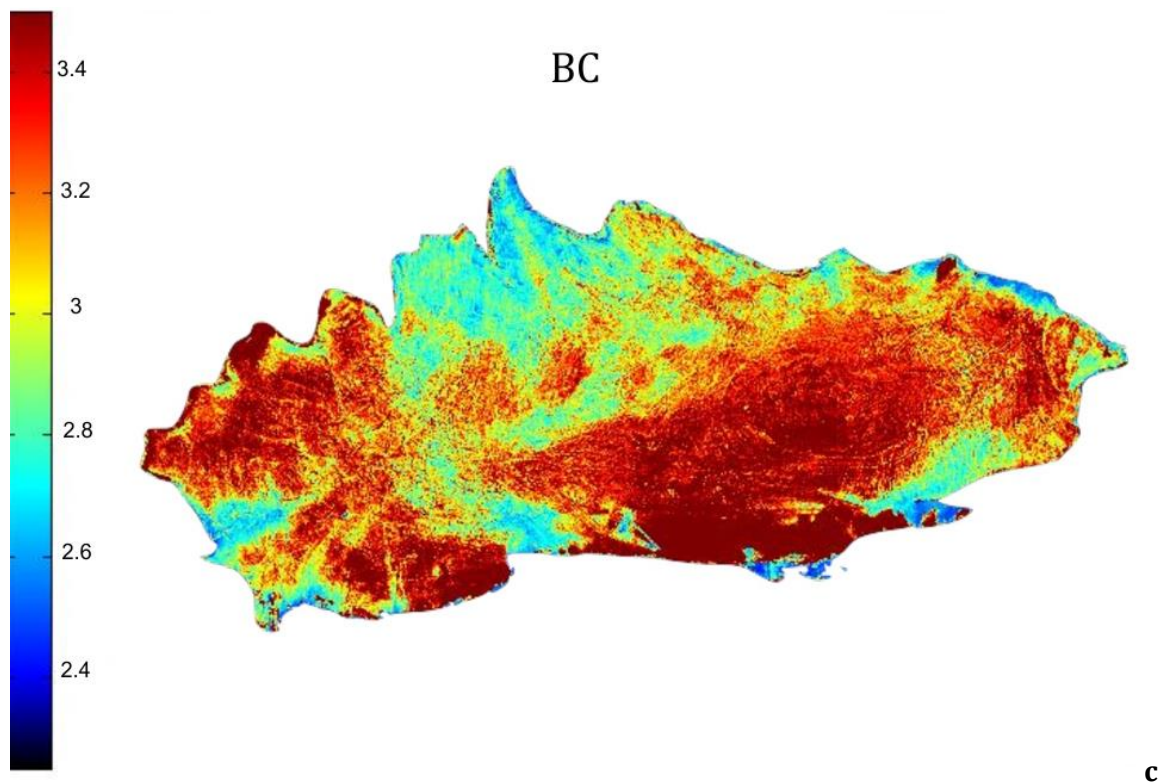


Figure 6 Relative abundance maps of a) mineral dust, b) organic matter and c) BC on Glacier de la Plaine Morte, obtained by unmixing APEX reflectance spectra, abundances are given in %.

To determine the effect of each LAI class on the glacier albedo, the abundance maps obtained by spectral unmixing were compared to the spectral albedo map ($\lambda = 400\text{--}2500\text{ nm}$) of Glacier de la Plaine Morte, computed from APEX data, (Naegeli et al., 2015)(Figure 7). The mean albedo determined from this spectral albedo map is 0.29 ± 0.12 . The lowest albedo is found at the small tongue of the glacier (north side) as well as in the edges of the glacier, especially in the south side. The high albedo at 136312 and from 606000 to 607375 is due to a cloud and is not representative of the actual surface. By comparing the albedo map in Figure 7 with the distribution of LAI in Figure 6b it becomes clear that organic matter plays a role in lowering the albedo of the glacier. In contrast, the areas where mineral is present in higher percentage appear to have higher albedo (Figure 6a). This is reasonable since the broadband albedo of organic matter (5.9%, 400-1000 nm) is much lower than that of mineral (28.2%, Figure 3). Although the nature of the surface (snow/brittle ice/compact ice/liquid water) might have an influence, our results indicate that in the case of Glacier de la Plaine Morte the amount of organic matter has a detectable effect in lowering albedo.

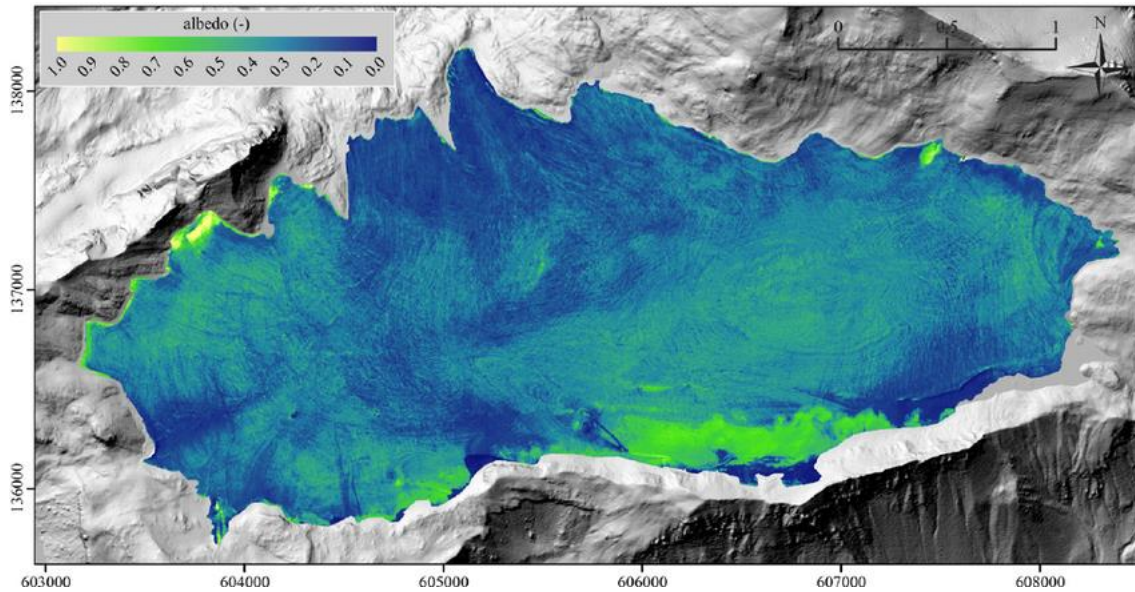


Figure 7 Glacier surface albedo derived from APEX data (Naegeli et al., 2015). The coordinates use the Swiss national grid (CH19203).

4.4 Conclusions

On glacier de la Plaine Morte the dominant LAI class is mineral, with an abundance of $91.1 \pm 3.7\%$, followed by organic matter ($8 \pm 3.5\%$) and BC ($0.9 \pm 0.4\%$). Quartz is the most abundant mineral, followed by other types of silicate minerals as well as a smaller fraction of calcite; all consistent with the local mineralogy. Mineral dust is more abundant towards the south side of the glacier confirming a major contribution from the surrounding rock, especially where steep slopes feed the glacier with mineral particles. Organic matter is present in patches throughout the glacier with a particular enrichment in the glacier tongue. Low abundance and variability in the distribution of BC are explained by the fact that the sources of BC are external to the glacier and are expected to have a homogeneous distribution. To relate the relative abundances of the LAI classes to the albedo of the glacier, p-LMM spectral unmixing was performed on the APEX hyperspectral reflectance data, using a characteristic reflectance spectrum of each LAI class obtained with the HIMS as endmembers, along with a spectrum of base bare ice. The resulting abundance maps agree with the maps determined by the interpolation of the measured abundances, especially for mineral and organic matter, indicating that it is possible to obtain the composition of LAI by spectral unmixing of remote sensing data. The contribution of each LAI class to the measured albedo was determined by comparing the abundance maps with the albedo map, both derived from APEX data. A very good correlation between low albedo areas of the glacier and organic matter rich areas was found. Although mineral dust is most abundant, and contributes to some extent to the decreased albedo, organic matter plays a more important

role. This is due to the fact that organic matter has much lower reflectance (5.9%) than mineral dust (28.2%). Overall the APEX data, along with the HIMS endmembers and the p-LMM spectral unmixing proved very effective in determining the relative abundance of the LAI classes, their spatial distribution, and their influence on albedo reduction.

Acknowledgements

We acknowledge Dr. Chiara Uglietti from the Paul Scherrer Institute for the help with the Thermal Optical Analyser and Dr. Urs Eggenberger from the University of Bern, Institute for Geology (Minerology group) for the XRD measurements. Sven Avak, Dimitri Osmont, Loic Schmidely and Dr. Johannes Schindler for the help in sampling on Glacier de la Plaine Morte.

5 Conclusion and Outlook

5.1 Conclusions

The aim of this thesis was to define the composition of the LAI of Glacier de la Plaine Morte, determine their distribution on the surface and their effect to the albedo of the glacier. To obtain this information an exhaustive characterization of the glacier LAI was done, and the LAI themselves were divided into three classes, mineral dust, organic matter and BC. The characterization was achieved through a number of techniques: (SEM-EDX), Raman micro-spectroscopy, ICP-OES. To measure the reflectivity of the different classes of LAI measuring at the submicron scale was considered as separation of the different classes proved too challenging. To measure at the submicron scale a novel method was developed using a hyperspectral imaging microscopy spectrometer (HIMS). The HIMS was validated through the comparison of the reflectance measurements of a number of different materials with a spectroradiometer, therefore comparing particle measurements to the bulk measurements. The new method yielded reliable spectra for all materials measured with an average deviation between the spectra of 3.2% for the 400 to 1000 nm wavelength range. Only semi-transparent minerals displayed interferences which resulted in a slightly larger uncertainty between the particle measurement and the bulk measurement. The LAI on Glacier de la Plaine Morte were analysed to determine their relative abundance; mineral dominated the composition, with an abundance of $91.1 \pm 3.7\%$, followed by organic matter ($8 \pm 3.5\%$) and BC ($0.9 \pm 0.4\%$). The mineral composition was consistent with the local mineralogy; with quartz being the most abundant mineral, most of the remaining minerals were silicate base with the exception of a smaller fraction of calcite. The spatial distribution of the relative abundances of LAI was determined by interpolating the results from the measurements of the relative abundance of the LAI classes from the samples collected from a large portion of the glacier surface in a grid-like manner. Mineral dust was found to be especially abundant along the south side of the Glacier de la Plaine Morte, where steep slopes feed the glacier with mineral particles, confirming a major contribution from the surrounding rock. Organic matter was found in patches throughout the glacier with the glacier tongue being particularly enriched. To relate the albedo of the glacier to the relative abundances of the LAI classes, p-LMM spectral unmixing was performed on the

APEX hyperspectral reflectance data. The spectral unmixing was done using the characteristic reflectance spectra of all the LAI classes obtained with the HIMS as endmembers, along with a spectrum of base ice. The distribution maps obtained with the APEX spectra agree well with the ones determined with the interpolated measurement data, especially for mineral dust and organic matter. Furthermore, a comparison between the albedo map and the APEX distribution map reveals that, even though mineral dust is very abundant throughout the surface, a very good correlation is found between low albedo areas of the glacier and organic matter rich areas. This is understandable, organic matter has much lower reflectance (5.9%) than mineral dust (28.2%), it is therefore clear that organic matter plays an important role in the decrease of albedo in Glacier de la Plaine Morte. Overall the APEX data, along with the HIMS endmembers and the p-LMM proved very effective in determining the relative abundance of the LAI classes as well as their spatial distribution.

4.4 Outlook

On the example of the study carried out in Glacier de la Plaine Morte, in which the abundance maps of the different LAI classes were retrieved using the HIMS spectra and spectral unmixing on the APEX remote sensing data, other glaciers could be subjected to the same method. For other glaciers, which may be less accessible or much larger, obtaining samples with a good coverage through the whole glacier can be demanding, slow and dangerous, especially in those cases this type of method would be beneficial. However, the retrieval of some samples would still be necessary to collect enough LAI to determine the classes present, and measure their characteristic reflectance spectrum. Glacier located in different geographical areas can have a lot of variance in the composition and optical properties of the LAI, based on location, elevation, pollution, sources, geology etc. Unfortunately retrieving airborne data is costly and limited in the geographical coverage. APEX is a small Swiss Belgian consortium from which most of the scientific community can't take advantage of. Satellites would allow better coverage, they have been employed in the study of glaciers for a long time providing information on glaciers spatial extent (Kulkarni et al., 2007), bottom and surface topography (Joughin et al., 1998), surface flow field, ablation and accumulation rates (mass balance)(Huggel et al., 2002;Berthier et al., 2007), changes in these quantities over time and albedo (Konig et al., 2001;Racoviteanu et al., 2008)(Paul, 2005) etc.

Satellites cover large geographical areas but lack in sensitivity, spectral range and present a limited spatial resolution. The spatial resolution for the satellites Sentinel-2 and Landsat 8 used in (Naegeli, 2017 #330) to determine surface albedo is about 20 to 30 m²; compared to the 2 to 5 m² resolved by the APEX. Furthermore sensors on board of satellites do not measure in continuous spectra but only at specific wavelength as summarized in Figure 21. The wider spatial resolution might cause losses in the details of the distribution, but could overall still provide information, especially for the total relative abundances of LAI classes on the surface. Tests should be carried out to assess if p-LMM, using the HIMS endmembers, can be applied to the reflectance spectra measured from satellites to determine LAI relative abundances on a glacier.

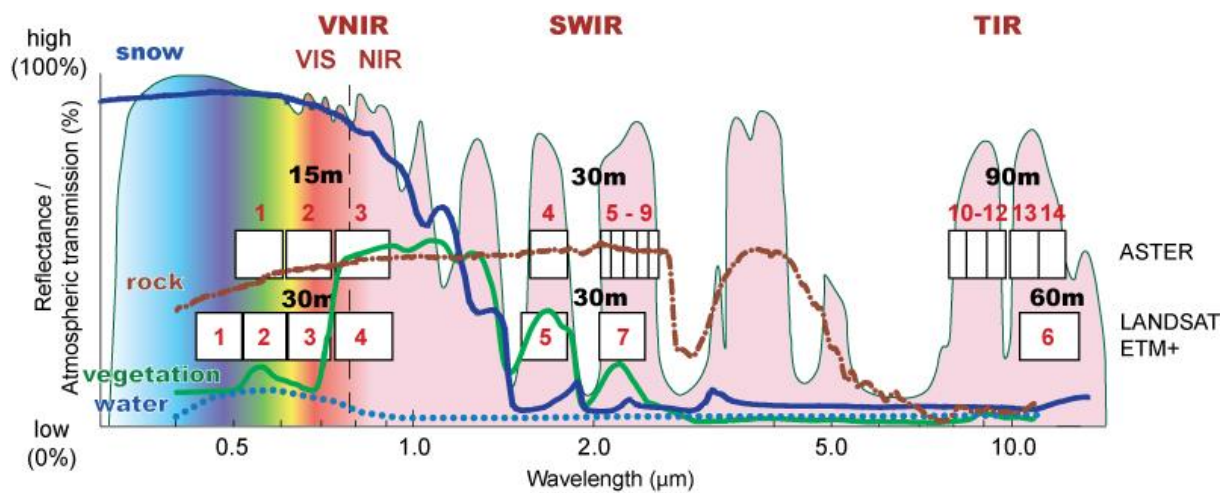


Figure 21 Reflectance curves of snow, water, vegetation and rock (coloured lines). Wavelength range of the channels of the ASTER and the Landsat ETM+ (and TM) sensors with their spatial resolution (numbered boxes). Coloured area: atmospheric transmission; high values indicate that a high degree of solar radiation passes through the atmosphere and low values indicate that large parts of solar radiation are blocked by atmospheric gasses (Casey, 2011 #348).

It is known that glacier LAI vary in composition, optical properties and amount. A study using HIMS to assess difference in the reflectance spectra from LAI of different glaciers could provide information on how much the characteristic reflectance of the LAI changes; this would be linked to what the different sources of LAI are and how much they contribute to lowering albedo.

A more complete approach could be taken with the use of the “Integrated Raman & Hyperspectral Microscopy” instrument produces by the same company which produced the HIMS. With this instrument a micro RAMAN spectrum can be measured at any location of the hyperspectral image confirming visual identification of all LAI, especially in the case of mineral

dust. The newest version of the HIMS can measure a wider wavelength range from 400 1700 nm. That would provide more information on the reflectance in general and also improve the performance towards the 800 to 1000 nm range, in which the HIMS which had sometimes a higher noise compared to the rest of the spectra. Higher magnification on the HIMS than 100X (used throughout this thesis) might allow the investigation of smaller particles, such as the ones present in snow. In general the method described in this thesis work offers many possibilities for improvement as well as application to different conditions.

In the framework of this project remote sensing was considered as a fast and efficient tool with which to collect information on the location of certain classes of LAI on the surface of a glacier and how those classes effect albedo. Remote sensing has given a great contribution to the study of glaciers, making it possible to collect data from hard to reach glaciers which would otherwise involve lengthy and possibly dangerous expeditions. Some of these contributions include obtaining information on a glacier's spatial extent (Kulkarni et al., 2007), bottom and surface topography (Joughin et al., 1998), surface flow field, ablation and accumulation rates (mass balance)(Huggel et al., 2002;Berthier et al., 2007), changes in these quantities over time and albedo (Konig et al., 2001;Racoviteanu et al., 2008). The remote sensing studies which have been executed on Glacier de la Plaine Morte have all focused on its changing albedo. Different aspects of a glacier's albedo have been considered e.g. as a consequence of the extreme glacier melt condition faced in 2003 using the Landsat Thematic Mapper in a comparison between various years as shown in Figure 21 in a study comparing the albedo from Airborne and Satellite (Sentinel-2 and Landsat 8) optical data (Naegeli et al., 2017) and in a study of the glacier's various surface types and their albedo using the an airborne imaging spectrometer)(Naegeli et al., 2015).

References

- Agrawala, S. (2007). "The European alps: Location, economy and climate," in *Climate Change in the European Alps: Adapting Winter Tourism and Natural Hazards Management.*, 17-23.
- Alfaro, S.C., Lafon, S., Rajot, J.L., Formenti, P., Gaudichet, A., and Maillé, M. (2004). Iron oxides and light absorption by pure desert dust: An experimental study. *Journal of Geophysical Research: Atmospheres* 109, n/a-n/a.
- Analytical Spectral Devices (2017). "fieldspec spectroradiometers fieldspec".).
- Anisimov, O.A. (2007). Potential feedback of thawing permafrost to the global climate system through methane emission. *Environmental Research Letters* 2, 045016.
- Anslow, F.S., Hostetler, S., Bidlake, W.R., and Clark, P.U. (2008). Distributed energy balance modeling of South Cascade Glacier, Washington and assessment of model uncertainty. *Journal of Geophysical Research-Earth Surface* 113, 18.
- Aoki, T., Kuchiki, K., Niwano, M., Kodama, Y., Hosaka, M., and Tanaka, T. (2011). Physically based snow albedo model for calculating broadband albedos and the solar heating profile in snowpack for general circulation models. *Journal of Geophysical Research-Atmospheres* 116, 22.
- Arnold, N.S., Willis, I.C., Sharp, M.J., Richards, K.S., and Lawson, W.J. (1996). A distributed surface energy-balance model for a small valley glacier .1. Development and testing for Haut Glacier d'Arolla, Valais Switzerland. *Journal of Glaciology* 42, 77-89.
- Attenborough, D. (1995). The private life of plants. *The private life of plants.*
- Barnett, T.P., Adam, J.C., and Lettenmaier, D.P. (2005). Potential impacts of a warming climate on water availability in snow-dominated regions. *Nature* 438, 303-309.
- Beach, J.M., Uertz, J.L., and Eckhardt, L.G. (2015). Hyperspectral interferometry: Sizing microscale surface features in the pine bark beetle. *Microscopy Research and Technique* 78, 873-885.
- Berthier, E., Arnaud, Y., Kumar, R., Ahmad, S., Wagnon, P., and Chevallier, P. (2007). Remote sensing estimates of glacier mass balances in the Himachal Pradesh (Western Himalaya, India). *Remote Sensing of Environment* 108, 327-338.
- Boggild, C.E., Brandt, R.E., Brown, K.J., and Warren, S.G. (2010). The ablation zone in northeast Greenland: ice types, albedos and impurities. *Journal of Glaciology* 56, 101-113.
- Bond, T.C., Doherty, S.J., Fahey, D.W., Forster, P.M., Berntsen, T., Deangelo, B.J., Flanner, M.G., Ghan, S., Kärcher, B., Koch, D., Kinne, S., Kondo, Y., Quinn, P.K., Sarofim, M.C., Schultz, M.G., Schulz, M., Venkataraman, C., Zhang, H., Zhang, S., Bellouin, N., Guttikunda, S.K., Hopke, P.K., Jacobson, M.Z., Kaiser, J.W., Klimont, Z., Lohmann, U., Schwarz, J.P., Shindell, D., Storelvmo, T., Warren, S.G., and Zender, C.S. (2013). Bounding the role of black carbon in the climate system: A scientific assessment. *Journal of Geophysical Research: Atmospheres* 118, 5380-5552.
- Bony, S., Colman, R., Kattsov, V.M., Allan, R.P., Bretherton, C.S., Dufresne, J.L., Hall, A., Hallegatte, S., Holland, M.M., Ingram, W., Randall, D.A., Soden, B.J., Tselioudis, G., and Webb, M.J. (2006). How well do we understand and evaluate climate change feedback processes? *Journal of Climate* 19, 3445-3482.
- Box, J.E., Fettweis, X., Stroeve, J.C., Tedesco, M., Hall, D.K., and Steffen, K. (2012). Greenland ice sheet albedo feedback: thermodynamics and atmospheric drivers. *Cryosphere* 6, 821-839.
- Brun, E. (2017). Investigation on Wet-Snow Metamorphism in Respect of Liquid-Water Content. *Annals of Glaciology* 13, 22-26.
- Bühlmann (2011). Influence of particulate matter on observed albedo reductions on Plaine Morte glacier, Swiss Alps
- Butz, C., Grosjean, M., Fischer, D., Wunderle, S., Tylmann, W., and Rein, B. (Year). "Hyperspectral imaging spectroscopy: a promising method for the biogeochemical analysis of lake sediments": SPIE), 20.

- Charlson, R.J., Schwartz, S.E., Hales, J.M., Cess, R.D., Coakley, J.A., Hansen, J.E., and Hofmann, D.J. (1992). Climate Forcing by Anthropogenic Aerosols. *Science* 255, 423-430.
- Clarke, A.D., Shinozuka, Y., Kapustin, V.N., Howell, S., Huebert, B., Doherty, S., Anderson, T., Covert, D., Anderson, J., Hua, X., Moore, K.G., Mcnaughton, C., Carmichael, G., and Weber, R. (2004). Size distributions and mixtures of dust and black carbon aerosol in Asian outflow: Physiochemistry and optical properties. *Journal of Geophysical Research-Atmospheres* 109.
- Coakley, J. (2003). "Reflectance and albedo, surface". Academic).
- Colbeck, S.C. (1979). Grain clusters in wet snow. *Journal of Colloid and Interface Science* 72, 371-384.
- Cooke, W.F., and Wilson, J.J.N. (1996). A global black carbon aerosol model. *Journal of Geophysical Research-Atmospheres* 101, 19395-19409.
- Corripio, J.G. (2004). Snow surface albedo estimation using terrestrial photography. *International Journal of Remote Sensing* 25, 5705-5729.
- Cutler, P.M., and Scott Munro, D. (2017). Visible and near-infrared reflectivity during the ablation period on Peyto Glacier, Alberta, Canada. *Journal of Glaciology* 42, 333-340.
- Dang, C., Brandt, R.E., and Warren, S.G. (2015). Parameterizations for narrowband and broadband albedo of pure snow and snow containing mineral dust and black carbon. *Journal of Geophysical Research: Atmospheres* 120, 5446-5468.
- Dong, Z.W., Kang, S.C., Qin, D.H., Li, Y., Wang, X.J., Ren, J.W., Li, X.F., Yang, J., and Qin, X. (2016). Provenance of cryoconite deposited on the glaciers of the Tibetan Plateau: New insights from Nd-Sr isotopic composition and size distribution. *Journal of Geophysical Research-Atmospheres* 121, 7371-7382.
- Dozier, J., and Painter, T.H. (2004). Multispectral and hyperspectral remote sensing of alpine snow properties. *Annu. Rev. Earth Planet. Sci.* 32, 465-494.
- Fatehi, P., Damm, A., Schaepman, M., and Kneubühler, M. (2015). Estimation of Alpine Forest Structural Variables from Imaging Spectrometer Data. *Remote Sensing* 7, 15830.
- Finger, D., Hugentobler, A., Huss, M., Voinesco, A., Wernli, H., Fischer, D., Weber, E., Jeannin, P.Y., Kauzlaric, M., Wirz, A., Vennemann, T., Husler, F., Schadler, B., and Weingartner, R. (2013). Identification of glacial meltwater runoff in a karstic environment and its implication for present and future water availability. *Hydrology and Earth System Sciences* 17, 3261-3277.
- Flanner, M.G., Zender, C.S., Hess, P.G., Mahowald, N.M., Painter, T.H., Ramanathan, V., and Rasch, P.J. (2009). Springtime warming and reduced snow cover from carbonaceous particles. *Atmos. Chem. Phys.* 9, 2481-2497.
- Flanner, M.G., Zender, C.S., Randerson, J.T., and Rasch, P.J. (2007a). Present-day climate forcing and response from black carbon in snow. *Journal of Geophysical Research: Atmospheres* 112, n/a-n/a.
- Flanner, M.G., Zender, C.S., Randerson, J.T., and Rasch, P.J. (2007b). Present-day climate forcing and response from black carbon in snow. *Journal of Geophysical Research: Atmospheres (1984–2012)* 112.
- Fujita, K., and Ageta, Y. (2000). Effect of summer accumulation on glacier mass balance on the Tibetan Plateau revealed by mass-balance model. *Journal of Glaciology* 46, 244-252.
- Gabbi, J., Huss, M., Bauder, A., Cao, F., and Schwikowski, M. (2015). The impact of Saharan dust and black carbon on albedo and long-term mass balance of an Alpine glacier. *The Cryosphere* 9, 1385-1400.
- Gardner, A.S., and Sharp, M.J. (2010). A review of snow and ice albedo and the development of a new physically based broadband albedo parameterization. *Journal of Geophysical Research-Earth Surface* 115, 15.
- Grenfell, T.C., Light, B., and Sturm, M. (2002). Spatial distribution and radiative effects of soot in the snow and sea ice during the SHEBA experiment. *Journal of Geophysical Research: Oceans* 107, SHE 7-1-SHE 7-7.
- Greuell, W. (2000). Melt-water accumulation on the surface of the Greenland ice sheet: Effect on albedo and mass balance. *Geografiska Annaler Series a-Physical Geography* 82A, 489-498.

- Hall, D.K., Bindschadler, R.A., Foster, J.L., Chang, A.T.C., and Siddalingaiah, H. (1990). Comparison of in situ and satellite-derived reflectances of Forbindels Glacier, Greenland. *International Journal of Remote Sensing* 11, 493-504.
- Hansen, J., and Nazarenko, L. (2004). Soot climate forcing via snow and ice albedos. *Proceedings of the National Academy of Sciences of the United States of America* 101, 423-428.
- Hansen, J., Sato, M., Ruedy, R., Nazarenko, L., Lacis, A., Schmidt, G.A., Russell, G., Aleinov, I., Bauer, M., Bauer, S., Bell, N., Cairns, B., Canuto, V., Chandler, M., Cheng, Y., Del Genio, A., Faluvegi, G., Fleming, E., Friend, A., Hall, T., Jackman, C., Kelley, M., Kiang, N., Koch, D., Lean, J., Lerner, J., Lo, K., Menon, S., Miller, R., Minnis, P., Novakov, T., Oinas, V., Perlwitz, J., Perlwitz, J., Rind, D., Romanou, A., Shindell, D., Stone, P., Sun, S., Tausnev, N., Thresher, D., Wielicki, B., Wong, T., Yao, M., and Zhang, S. (2005). Efficacy of climate forcings. *Journal of Geophysical Research D: Atmospheres* 110, 1-45.
- Hock, R. (2005). Glacier melt: a review of processes and their modelling. *Progress in Physical Geography* 29, 362-391.
- Hoover, R.B., and Gilichinsky, D. (2001). "Significance to Astrobiology of Micro-Organisms in Permafrost and Ice," in *Permafrost Response on Economic Development, Environmental Security and Natural Resources*, eds. R. Paepe, V.P. Melnikov, E. Van Overloop & V.D. Gorokhov. (Dordrecht: Springer Netherlands), 553-579.
- Huggel, C., Kaab, A., Haeblerli, W., Teyssie, P., and Paul, F. (2002). Remote sensing based assessment of hazards from glacier lake outbursts: a case study in the Swiss Alps. *Canadian Geotechnical Journal* 39, 316-330.
- Huss, M., Bauder, A., Funk, M., and Hock, R. (2008). Determination of the seasonal mass balance of four Alpine glaciers since 1865. *Journal of Geophysical Research-Earth Surface* 113, 11.
- Huss, M., Dhulst, L., and Bauder, A. (2017). New long-term mass-balance series for the Swiss Alps. *Journal of Glaciology* 61, 551-562.
- Huss, M., Voinesco, A., and Hoelzle, M. (2013). Implications of climate change on Glacier de la Plaine Morte, Switzerland. *Geogr. Helv.* 68, 227-237.
- Ippcc (2013). *Climate Change 2013: The Physical Science Basis. Contribution of Working Group I to the Fifth Assessment Report of the Intergovernmental Panel on Climate Change*. Cambridge, United Kingdom and New York, NY, USA: Cambridge University Press.
- Jacobi, H.W., Lim, S., Menegoz, M., Ginot, P., Laj, P., Bonasoni, P., Stocchi, P., Marinoni, A., and Arnaud, Y. (2015). Black carbon in snow in the upper Himalayan Khumbu Valley, Nepal: observations and modeling of the impact on snow albedo, melting, and radiative forcing. *Cryosphere* 9, 1685-1699.
- Jacobson, M.Z. (2004). Climate response of fossil fuel and biofuel soot, accounting for soot's feedback to snow and sea ice albedo and emissivity. *Journal of Geophysical Research-Atmospheres* 109, 15.
- Jansson, P., Hock, R., and Schneider, T. (2003). The concept of glacier storage: a review. *Journal of Hydrology* 282, 116-129.
- Joughin, I.R., Kwok, R., and Fahnestock, M.A. (1998). Interferometric estimation of three-dimensional ice-flow using ascending and descending passes. *IEEE Transactions on Geoscience and Remote Sensing* 36, 25-37.
- Kaspari, S., McKenzie Skiles, S., Delaney, I., Dixon, D., and Painter, T.H. (2015). Accelerated glacier melt on Snow Dome, Mount Olympus, Washington, USA, due to deposition of black carbon and mineral dust from wildfire. *Journal of Geophysical Research: Atmospheres* 120, 2793-2807.
- Kaspari, S., Painter, T.H., Gysel, M., Skiles, S.M., and Schwikowski, M. (2014). Seasonal and elevational variations of black carbon and dust in snow and ice in the Solu-Khumbu, Nepal and estimated radiative forcings. *Atmospheric Chemistry and Physics* 14, 8089-8103.

- Kaspari, S.D., Schwikowski, M., Gysel, M., Flanner, M.G., Kang, S., Hou, S., and Mayewski, P.A. (2011). Recent increase in black carbon concentrations from a Mt. Everest ice core spanning 1860-2000 AD. *Geophysical Research Letters* 38.
- Kohshima, S. (1993). Biotic acceleration of glacier melting in Yala glacier, Langtang region, Nepal Himalaya. *IAHS-AISH publication* 214.
- Konig, M., Winther, J.G., and Isaksson, E. (2001). Measuring snow and glacier ice properties from satellite. *Reviews of Geophysics* 39, 1-27.
- Kulkarni, A.V., Bahuguna, I.M., Rathore, B.P., Singh, S.K., Randhawa, S.S., Sood, R.K., and Dhar, S. (2007). Glacial retreat in Himalaya using Indian Remote Sensing satellite data. *Current Science* 92, 69-74.
- Kumada, K., and Kumada, K. (1987). *Chemistry of soil organic matter*.
- Laborde, M., Mertes, P., Zieger, P., Dommen, J., Baltensperger, U., and Gysel, M. (2012). Sensitivity of the Single Particle Soot Photometer to different black carbon types. *Atmospheric Measurement Techniques* 5, 1031-1043.
- Lafon, S., Sokolik, I.N., Rajot, J.L., Caquineau, S., and Gaudichet, A. (2006). Characterization of iron oxides in mineral dust aerosols: Implications for light absorption. *Journal of Geophysical Research: Atmospheres* 111, n/a-n/a.
- Lavanchy, V.M.H., Gäggeler, H.W., Nyeki, S., and Baltensperger, U. (1999). Elemental carbon (EC) and black carbon (BC) measurements with a thermal method and an aethalometer at the high-alpine research station Jungfrauoch. *Atmospheric Environment* 33, 2759-2769.
- Lenton, T.M. (1998). Gaia and natural selection. *Nature* 394, 439-447.
- Liechti, M. (2015). Investigation of black carbon analysis in snow and ice core samples. *Bachelor Thesis, Department of Chemistry and Biochemistry at the University of Bern*.
- Lim, S., Fain, X., Zanatta, M., Cozic, J., Jaffrezo, J.L., Ginot, P., and Laj, P. (2014). Refractory black carbon mass concentrations in snow and ice: method evaluation and inter-comparison with elemental carbon measurement. *Atmospheric Measurement Techniques* 7, 3307-3324.
- Linke, C., Möhler, O., Veres, A., Mohácsi, Á., Bozóki, Z., Szabó, G., and Schnaiter, M. (2006). Optical properties and mineralogical composition of different Saharan mineral dust samples: a laboratory study. *Atmos. Chem. Phys.* 6, 3315-3323.
- Liu, Y., Vick-Majors, T.J., Prisco, J.C., Yao, T., Kang, S., Liu, K., Cong, Z., Xiong, J., and Li, Y. (2017). Biogeography of cryoconite bacterial communities on glaciers of the Tibetan Plateau. *FEMS Microbiology Ecology* 93.
- Lutz, S., Anesio, A.M., Raiswell, R., Edwards, A., Newton, R.J., Gill, F., and Benning, L.G. (2016). The biogeography of red snow microbiomes and their role in melting arctic glaciers. *Nature Communications* 7.
- Marcinkowska, A., Zagajewski, B., Ochtyra, A., Jarocińska, A., Raczko, E., Kupková, L., Stych, P., and Meuleman, K. (2014). "Mapping vegetation communities of the Karkonosze National Park using APEX hyperspectral data and Support Vector Machines", in: *Miscellanea Geographica*.
- Marinoni, A., and Gamba, P. (2015). A Novel Approach for Efficient p-Linear Hyperspectral Unmixing. *IEEE Journal of Selected Topics in Signal Processing* 9, 1156-1168.
- Marinoni, A., Plaza, J., Plaza, A., and Gamba, P. (2015). Nonlinear Hyperspectral Unmixing Using Nonlinearity Order Estimation and Polytope Decomposition. *IEEE Journal of Selected Topics in Applied Earth Observations and Remote Sensing* 8, 2644-2654.
- Megahan, W.F., and Meiman, J.R. (1968). *EFFECT OF ALBEDO-REDUCING MATERIALS ON NET ALL-WAVE RADIATION AT A SNOW SURFACE*. 49 Meeting Abstract.
- Ming, J., Xiao, C., Cachier, H., Qin, D., Qin, X., Li, Z., and Pu, J. (2009). Black Carbon (BC) in the snow of glaciers in west China and its potential effects on albedos. *Atmospheric Research* 92, 114-123.

- Mortimer, M., Gogos, A., Bartolomé, N., Kahru, A., Bucheli, T.D., and Slaveykova, V.I. (2014). Potential of Hyperspectral Imaging Microscopy for Semi-quantitative Analysis of Nanoparticle Uptake by Protozoa. *Environmental Science & Technology* 48, 8760-8767.
- Moustafa, S.E., Rennermalm, A.K., Smith, L.C., Miller, M.A., Mioduszewski, J.R., Koenig, L.S., Hom, M.G., and Shuman, C.A. (2015). Multi-modal albedo distributions in the ablation area of the southwestern Greenland Ice Sheet. *Cryosphere* 9, 905-923.
- Mulder, V.L., De Bruin, S., Weyermann, J., Kokaly, R.F., and Schaepman, M.E. (2013). Characterizing regional soil mineral composition using spectroscopy and geostatistics. *Remote Sensing of Environment* 139, 415-429.
- Musilova, M., Tranter, M., Bamber, J.L., Takeuchi, N., and Anesio, A.M.B. (2016). Experimental evidence that microbial activity lowers the albedo of glaciers. *Geochemical Perspectives Letters* 2, 105-116.
- Myhre, G., Samset, B.H., Schulz, M., Balkanski, Y., Bauer, S., Bernsten, T.K., Bian, H., Bellouin, N., Chin, M., Diehl, T., Easter, R.C., Feichter, J., Ghan, S.J., Hauglustaine, D., Iversen, T., Kinne, S., Kirkevåg, A., Lamarque, J.F., Lin, G., Liu, X., Lund, M.T., Luo, G., Ma, X., Van Noije, T., Penner, J.E., Rasch, P.J., Ruiz, A., Seland, Ø., Skeie, R.B., Stier, P., Takemura, T., Tsigaridis, K., Wang, P., Wang, Z., Xu, L., Yu, H., Yu, F., Yoon, J.H., Zhang, K., Zhang, H., and Zhou, C. (2013). Radiative forcing of the direct aerosol effect from AeroCom Phase II simulations. *Atmos. Chem. Phys.* 13, 1853-1877.
- Naegeli, K., Damm, A., Huss, M., Schaepman, M., and Hoelzle, M. (2015). Imaging spectroscopy to assess the composition of ice surface materials and their impact on glacier mass balance. *Remote Sensing of Environment* 168, 388-402.
- Naegeli, K., Damm, A., Huss, M., Wulf, H., Schaepman, M., and Hoelzle, M. (2017). Cross-Comparison of Albedo Products for Glacier Surfaces Derived from Airborne and Satellite (Sentinel-2 and Landsat 8) Optical Data. *Remote Sensing* 9.
- Nagatsuka, N., Takeuchi, N., Uetake, J., and Shimada, R. (2014). Mineralogical composition of cryoconite on glaciers in northwest Greenland. *Bulletin of Glaciological Research* 32, 107-114.
- Nagatsuka, N., Takeuchi, N., Uetake, J., Shimada, R., Onuma, Y., Tanaka, S., and Nakano, T. (2016). Variations in Sr and Nd Isotopic Ratios of Mineral Particles in Cryoconite in Western Greenland. *Frontiers in Earth Science* 4.
- Nolin, A.W., and Dozier, J. (2000). A Hyperspectral Method for Remotely Sensing the Grain Size of Snow. *Remote Sensing of Environment* 74, 207-216.
- Oerlemans, J., and Hoogendoorn, N.C. (1989). Mass-balance gradients and climatic change. *Journal of Glaciology* 35, 399-405.
- Painter, T.H., Berisford, D.F., Boardman, J.W., Bormann, K.J., Deems, J.S., Gehrke, F., Hedrick, A., Joyce, M., Laidlaw, R., Marks, D., Mattmann, C., Mcgurk, B., Ramirez, P., Richardson, M., Skiles, S.M., Seidel, F.C., and Winstral, A. (2016). The Airborne Snow Observatory: Fusion of scanning lidar, imaging spectrometer, and physically-based modeling for mapping snow water equivalent and snow albedo. *Remote Sensing of Environment* 184, 139-152.
- Paul, M., Kääh (2005). ON THE IMPACT OF GLACIER ALBEDO UNDER CONDITIONS OF EXTREME GLACIER MELT: THE SUMMER OF 2003 IN THE ALPS *EARSeL eProceedings* 4, 11.
- Pautler, B.G., Dubnick, A., Sharp, M.J., Simpson, A.J., and Simpson, M.J. (2013). Comparison of cryoconite organic matter composition from Arctic and Antarctic glaciers at the molecular-level. *Geochimica et Cosmochimica Acta* 104, 1-18.
- Petzold, A., Ogren, J.A., Fiebig, M., Laj, P., Li, S.M., Baltensperger, U., Holzer-Popp, T., Kinne, S., Pappalardo, G., Sugimoto, N., Wehrli, C., Wiedensohler, A., and Zhang, X.Y. (2013). Recommendations for reporting "black carbon" measurements. *Atmos. Chem. Phys.* 13, 8365-8379.

- Popp, C., Brunner, D., Damm, A., Van Roozendaal, M., Fayt, C., and Buchmann, B. (2012). High-resolution NO₂ remote sensing from the Airborne Prism EXperiment (APEX) imaging spectrometer. *Atmos. Meas. Tech.* 5, 2211-2225.
- Pribyl, D.W. (2010). A critical review of the conventional SOC to SOM conversion factor. *Geoderma* 156, 75-83.
- Racoviteanu, A.E., Williams, M.W., and Barry, R.G. (2008). Optical remote sensing of glacier characteristics: A review with focus on the Himalaya. *Sensors* 8, 3355-3383.
- Ramanathan, V., and Carmichael, G. (2008). Global and regional climate changes due to black carbon. *Nature Geosci* 1, 221-227.
- Ramanathan, V., Li, F., Ramana, M.V., Praveen, P.S., Kim, D., Corrigan, C.E., Nguyen, H., Stone, E.A., Schauer, J.J., Carmichael, G.R., Adhikary, B., and Yoon, S.C. (2007). Atmospheric brown clouds: Hemispherical and regional variations in long-range transport, absorption, and radiative forcing. *Journal of Geophysical Research Atmospheres* 112.
- Roth, G.A., Tahiliani, S., Neu-Baker, N.M., and Brenner, S.A. (2015). Hyperspectral microscopy as an analytical tool for nanomaterials. *Wiley Interdisciplinary Reviews: Nanomedicine and Nanobiotechnology* 7, 565-579.
- Sandells, M., Essery, R., Rutter, N., Wake, L., Leppänen, L., and Lemmetyinen, J. (2017). Microstructure representation of snow in coupled snowpack and microwave emission models. *The Cryosphere* 11, 229-246.
- Schaepman-Strub, G., Schaepman, M.E., Painter, T.H., Dangel, S., and Martonchik, J.V. (2006). Reflectance quantities in optical remote sensing—definitions and case studies. *Remote Sensing of Environment* 103, 27-42.
- Schaepman, M.E., Jehle, M., Hueni, A., D'odorico, P., Damm, A., Weyermann, J., Schneider, F.D., Laurent, V., Popp, C., Seidel, F.C., Lenhard, K., Gege, P., Kuchler, C., Brazile, J., Kohler, P., De Vos, L., Meuleman, K., Meynart, R., Schläpfer, D., Kneubühler, M., and Itten, K.I. (2015). Advanced radiometry measurements and Earth science applications with the Airborne Prism Experiment (APEX). *Remote Sensing of Environment* 158, 207-219.
- Schilt, A., Baumgartner, M., Blunier, T., Schwander, J., Spahni, R., Fischer, H., and Stocker, T.F. (2010). Glacial-interglacial and millennial-scale variations in the atmospheric nitrous oxide concentration during the last 800,000 years. *Quaternary Science Reviews* 29, 182-192.
- Schwarz, J.P., Gao, R.S., Fahey, D.W., Thomson, D.S., Watts, L.A., Wilson, J.C., Reeves, J.M., Darbeheshti, M., Baumgardner, D.G., Kok, G.L., Chung, S.H., Schulz, M., Hendricks, J., Lauer, A., Kärcher, B., Slowik, J.G., Rosenlof, K.H., Thompson, T.L., Langford, A.O., Loewenstein, M., and Aikin, K.C. (2006). Single-particle measurements of midlatitude black carbon and light-scattering aerosols from the boundary layer to the lower stratosphere. *Journal of Geophysical Research: Atmospheres* 111, n/a-n/a.
- Schwikowski, M., Seibert, P., Baltensperger, U., and Gäggeler, H.W. (1995). A study of an outstanding Saharan dust event at the high-Alpine site Jungfrauoch, Switzerland. *Atmospheric Environment* 29, 1829-1842.
- Skiles, S.M., Painter, T.H., Deems, J.S., Bryant, A.C., and Landry, C.C. (2012). Dust radiative forcing in snow of the Upper Colorado River Basin: 2. Interannual variability in radiative forcing and snowmelt rates. *Water Resources Research* 48, n/a-n/a.
- Soden, B.J., and Held, I.M. (2006). An assessment of climate feedbacks in coupled ocean-atmosphere models. *Journal of Climate* 19, 3354-3360.
- Suzuki, K. (2006). Characterisation of airborne particulates and associated trace metals deposited on tree bark by ICP-OES, ICP-MS, SEM-EDX and laser ablation ICP-MS. *Atmospheric Environment* 40, 2626-2634.
- Takeuchi, N. (2002). "Optical characteristics of cryoconite (surface dust) on glaciers: the relationship between light absorbency and the property of organic matter contained in the cryoconite," in *Annals of Glaciology, Vol 34, 2002*, eds. J.G. Winther & R. Solberg. (Cambridge: Int Glaciological Soc), 409-414.

- Takeuchi, N., Fujisawa, Y., Kadota, T., Tanaka, S., Miyairi, M., Shirakawa, T., Kusaka, R., Fedorov, A.N., Konstantinov, P., and Ohata, T. (2015a). The Effect of Impurities on the Surface Melt of a Glacier in the Suntar-Khayata Mountain Range, Russian Siberia. *Frontiers in Earth Science* 3.
- Takeuchi, N., Fujisawa, Y., Kadota, T., Tanaka, S., Miyairi, M., Shirakawa, T., Kusaka, R., Fedorov, A.N., Konstantinov, P., and Ohata, T. (2015b). "The effect of impurities on the surface melt of a glacier in the Suntar-Khayata mountain range, Russian Siberia", in: *Frontiers in Earth Sciences*).
- Takeuchi, N., Kohshima, S., and Seko, K. (2001). Structure, Formation, and Darkening Process of Albedo-Reducing Material (Cryoconite) on a Himalayan Glacier: A Granular Algal Mat Growing on the Glacier. *Arctic, Antarctic, and Alpine Research* 33, 115-122.
- Takeuchi, N., Nagatsuka, N., Uetake, J., and Shimada, R. (2014). Spatial variations in impurities (cryoconite) on glaciers in northwest Greenland. *Bulletin of Glaciological Research* 32, 85-94.
- Tedesco, M., Foreman, C.M., Anton, J., Steiner, N., and Schwartzman, T. (2013). Comparative analysis of morphological, mineralogical and spectral properties of cryoconite in Jakobshavn Isbræ, Greenland, and Canada Glacier, Antarctica. *Annals of Glaciology* 54, 147-157.
- Tegen, I., and Fung, I. (1994). Modeling of mineral dust in the atmosphere: Sources, transport, and optical thickness. *Journal of Geophysical Research: Atmospheres* 99, 22897-22914.
- Thomas, W.H., and Duval, B. (1995). SIERRA-NEVADA, CALIFORNIA, USA, SNOW ALGAE - SNOW ALBEDO CHANGES, ALGAL BACTERIAL INTERRELATIONSHIPS, AND ULTRAVIOLET-RADIATION EFFECTS. *Arctic and Alpine Research* 27, 389-399.
- Thuillier, G., Floyd, L., Woods, T.N., Cebula, R., Hilsenrath, E., Hersé, M., and Labs, D. (2004). Solar irradiance reference spectra for two solar active levels. *Advances in Space Research* 34, 256-261.
- Uetake, J., Tanaka, S., Segawa, T., Takeuchi, N., Nagatsuka, N., Motoyama, H., and Aoki, T. (2016). Microbial community variation in cryoconite granules on Qaanaaq Glacier, NW Greenland. *FEMS Microbiology Ecology* 92, fiw127-fiw127.
- Van De Wal, R.S.W., Oerlemans, J., and Van Der Hage, J.C. (1992). A study of ablation variations on the tongue of Hintereisferner, Austrian Alps. *Journal of Glaciology* 38, 319-324.
- Walther, G.R., Post, E., Convey, P., Menzel, A., Parmesan, C., Beebee, T.J.C., Fromentin, J.M., Hoegh-Guldberg, O., and Bairlein, F. (2002). Ecological responses to recent climate change. *Nature* 416, 389-395.
- Wendl, I.A., Menking, J.A., Farber, R., Gysel, M., Kaspari, S.D., Laborde, M.J.G., and Schwikowski, M. (2014). Optimized method for black carbon analysis in ice and snow using the Single Particle Soot Photometer. *Atmospheric Measurement Techniques* 7, 2667-2681.
- Wiscombe, W.J., and Warren, S.G. (1980). A Model for the Spectral Albedo of Snow. I: Pure Snow. *Journal of the Atmospheric Sciences* 37, 2712-2733.
- Wood, A.J., Ackland, G.J., Dyke, J.G., Williams, H.T.P., and Lenton, T.M. (2008). Daisyworld: A review. *Reviews of Geophysics* 46, n/a-n/a.
- Xuan, J., and Sokolik, I.N. (2002). Characterization of sources and emission rates of mineral dust in Northern China. *Atmospheric Environment* 36, 4863-4876.
- Yasunari, T.J., Bonasoni, P., Laj, P., Fujita, K., Vuillermoz, E., Marinoni, A., Cristofanelli, P., Duchi, R., Tartari, G., and Lau, K.M. (2010). Estimated impact of black carbon deposition during pre-monsoon season from Nepal Climate Observatory - Pyramid data and snow albedo changes over Himalayan glaciers. *Atmospheric Chemistry and Physics* 10, 6603-6615.
- Zhang, Y.L., Perron, N., Ciobanu, V.G., Zotter, P., Minguillón, M.C., Wacker, L., Prévôt, A.S.H., Baltensperger, U., and Szidat, S. (2012). On the isolation of OC and EC and the optimal strategy of radiocarbon-based source apportionment of carbonaceous aerosols. *Atmos. Chem. Phys.* 12, 10841-10856.

Appendix

Table 1 Weight of dry filtered samples of the 2015 campaign.

Sample	Weight (g)	Sample	Weight (g)	Sample	Weight (g)
1	11.548	38	4.187	75	3.443
2	2.271	39	16.506	76	9.771
3	8.784	40	9.936	77	43.292
4	8.358	41	2.612	78	11.944
5	4.935	42	14.576	79	4.164
6	7.925	43	21.524	80	4.456
7	3.900	44	4.187	81	15.215
8	4.5863	45	24.250	82	6.957
9	5.320	46	32.830	83	14.005
10	4.851	47	19.937	84	11.935
11	4.988	48	8.429	85	5.701
12	2.218	49	4.346	86	6.160
13	3.359	50	2.970	87	30.626
14	3.531	51	3.961	88	1.501
15	44.884	52	16.525	89	9.557
16	4.727	53	4.270	90	N.A
17	25.390	54	5.076	91	9.021
18	10.631	55	7.307	92	1.985
19	4.809	56	3.695	93	2.431
20	3.469	57	58.149	94	2.301
21	1.328	58	66.364	95	2.335
22	12.067	59	13.823	96	1.954
23	7.853	60	12.917	97	2.239
24	5.523	61	32.816	98	1.350
25	2.004	62	48.320	99	1.914
26	1.328	63	28.924	100	2.155
27	8.304	64	17.534	101	4.185
28	1.720	65	17.683	102	3.183
29	1.256	66	11.662	103	8.550
30	1.489	67	19.579	104	2.766
31	2.712	68	9.204	105	2.521
32	2.558	69	46.462	106	1.912
33	3.637	70	28.331	107	0.974
34	1.848	71	17.692	108	1.792
35	1.725	72	19.159	109	2.333
36	1.019	73	17.120	110	0.924

37	5.3957
----	--------

74	13.292
----	--------

--	--

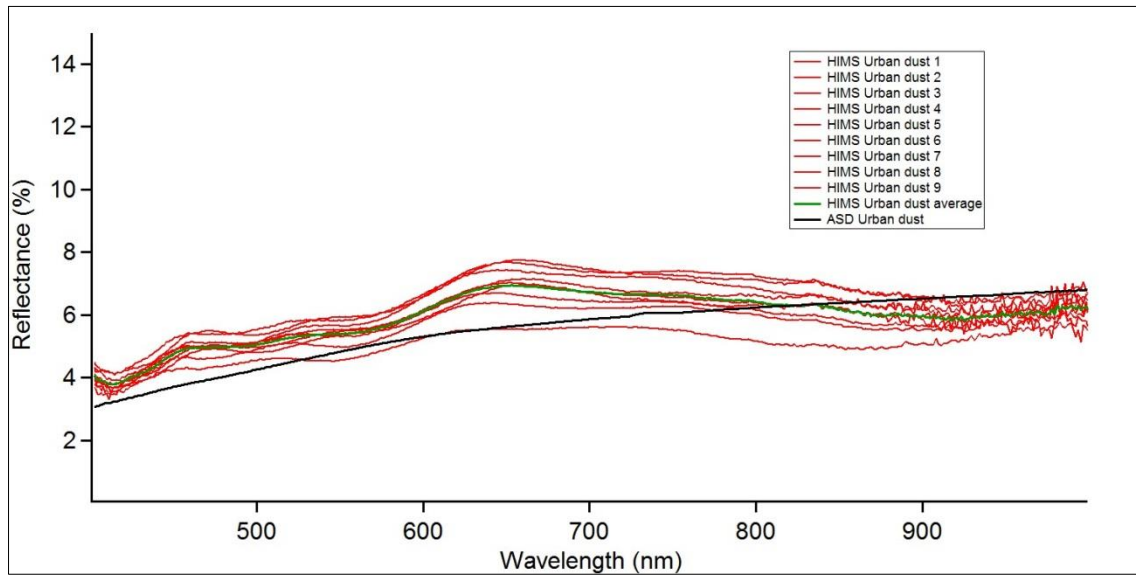
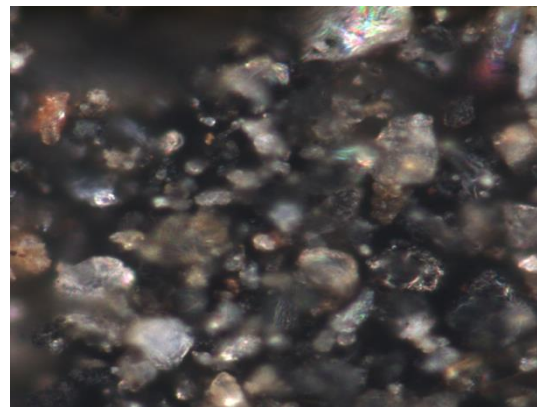
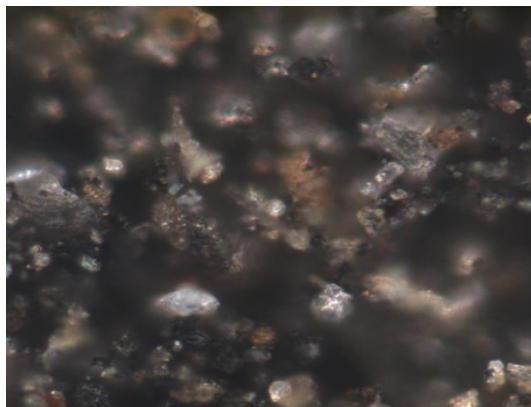
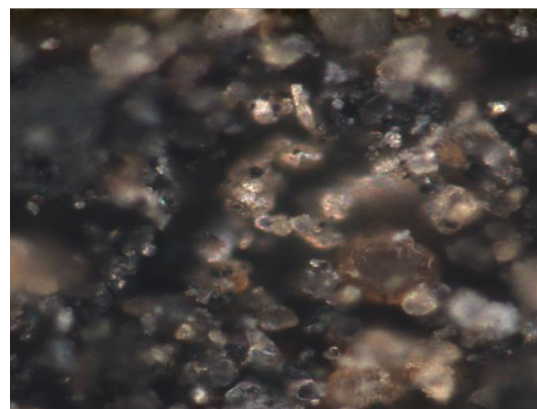
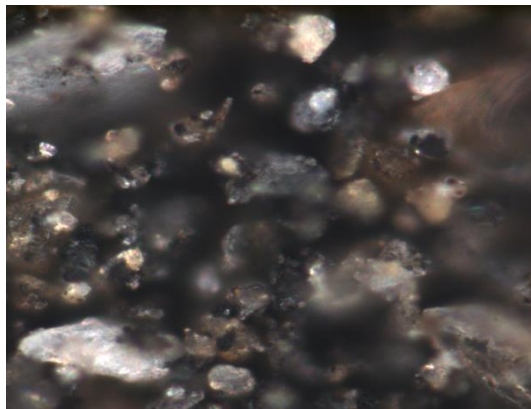


Figure 22 Reflectance spectra measured with HIMS of urban dust (red lines). The green line represents the average of 9 HIMS spectra and the black line is the spectrum obtained with the field spectroradiometer.



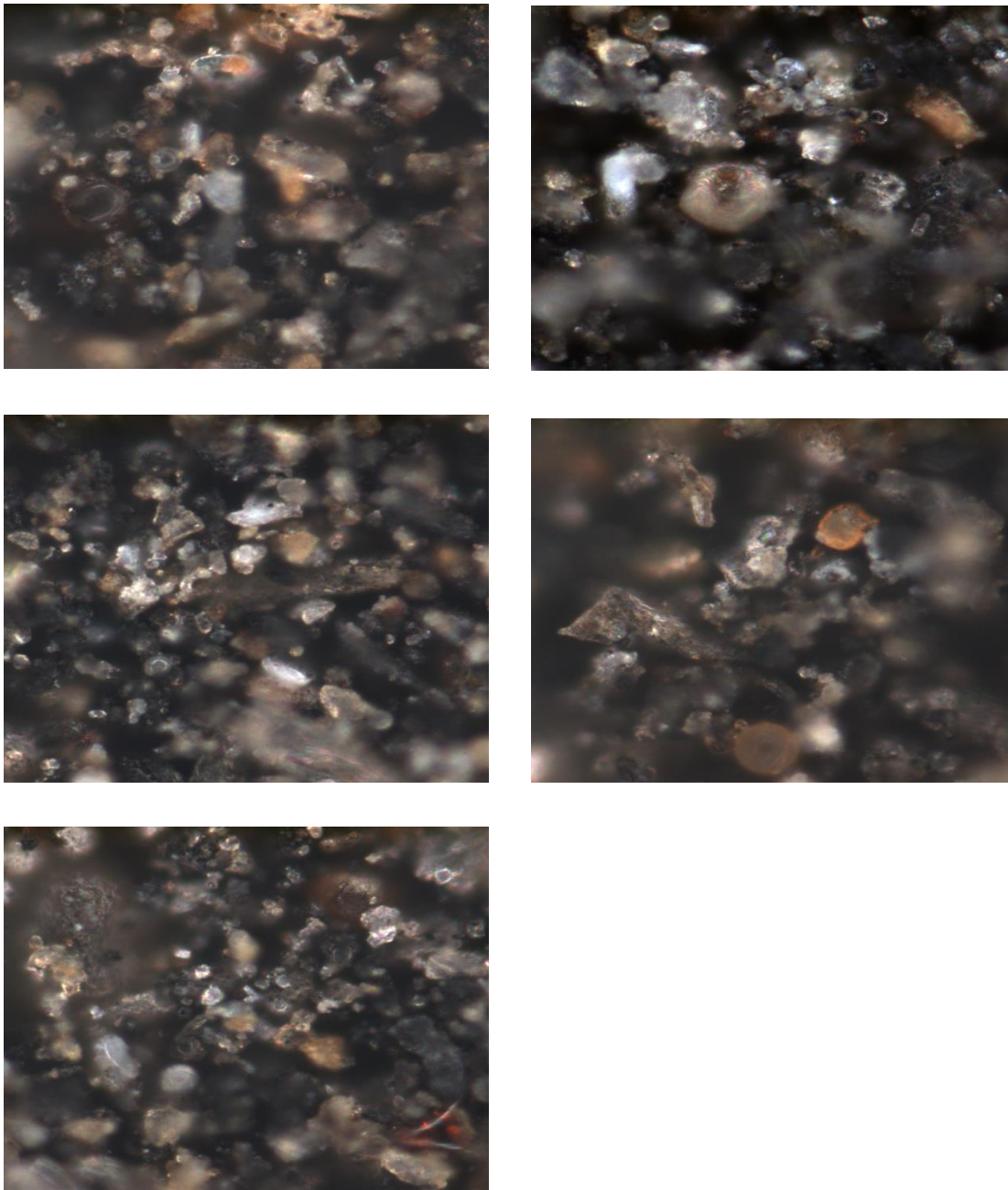


Figure 23 Microscopic images of measured areas of the spectra shown in Figure 29.

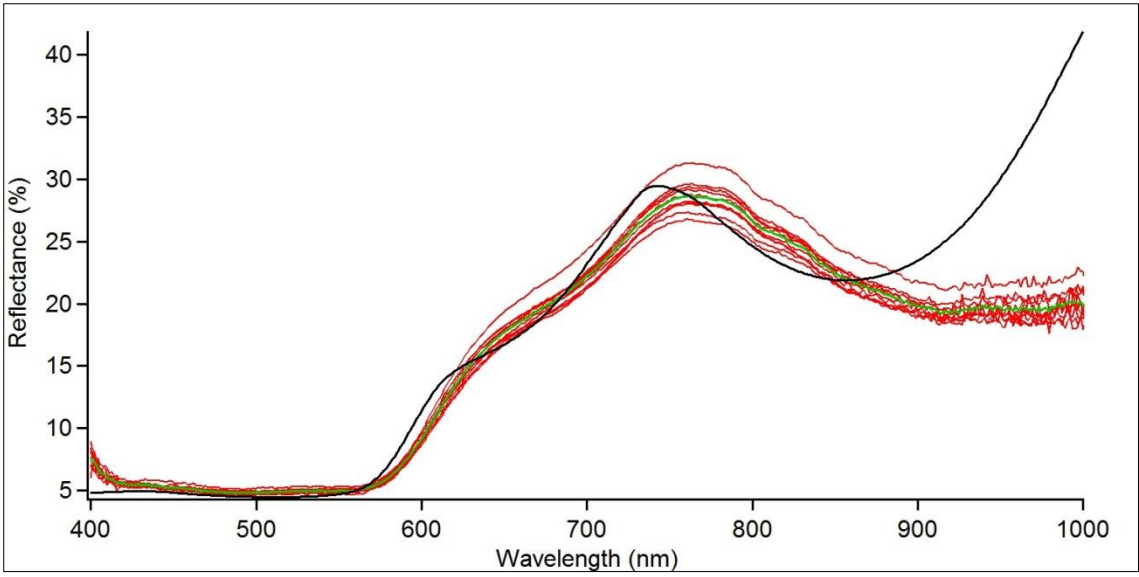
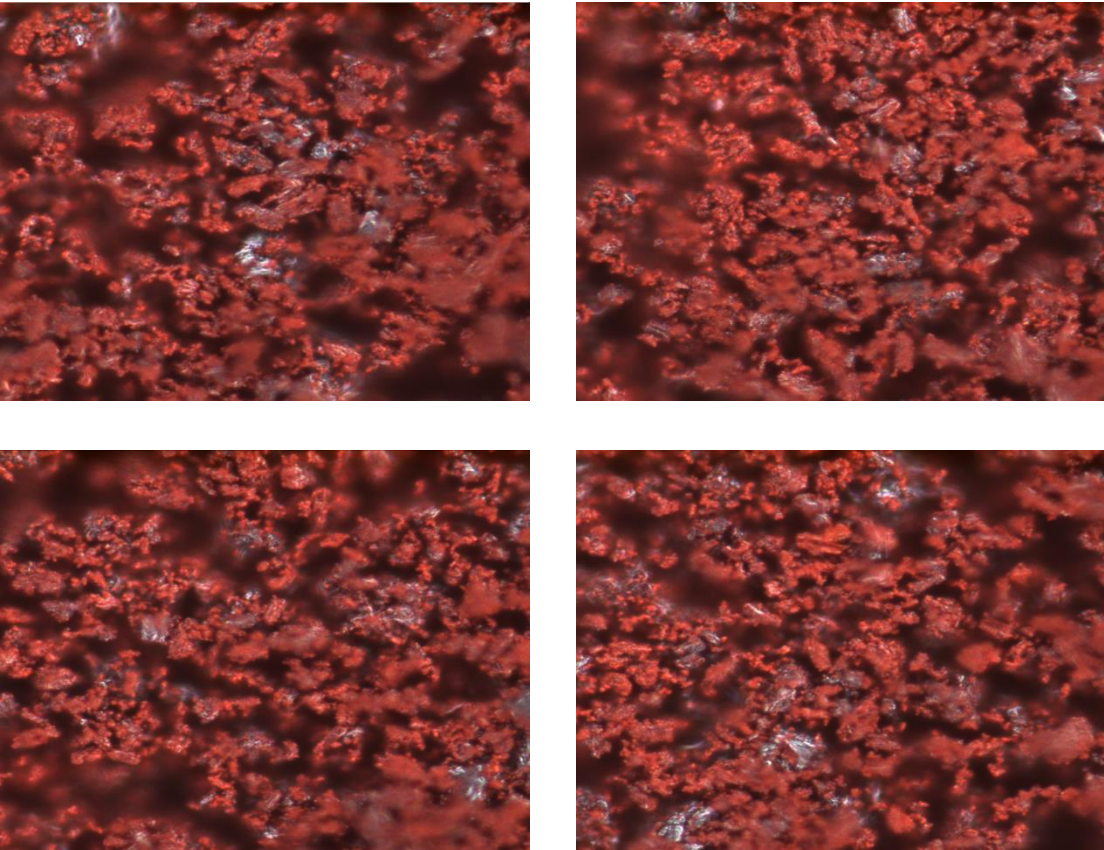


Figure 24 Reflectance spectra measured with HIMS of hematite (red lines). The green line represents the average of 10 HIMS spectra and the black line is the spectrum obtained with the field spectroradiometer.



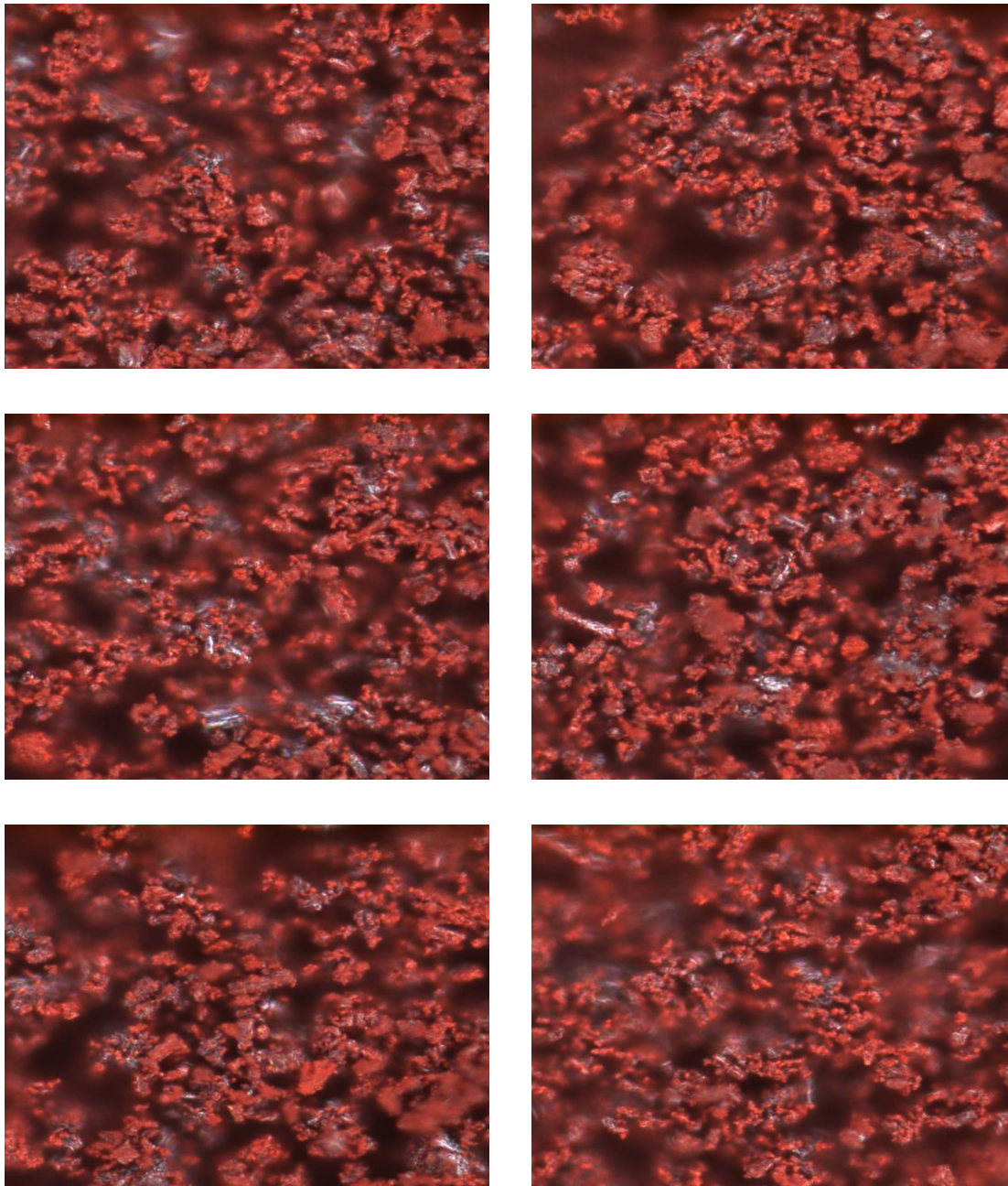


Figure 25 Microscopic images of measured areas of the spectra shown in Figure 31.

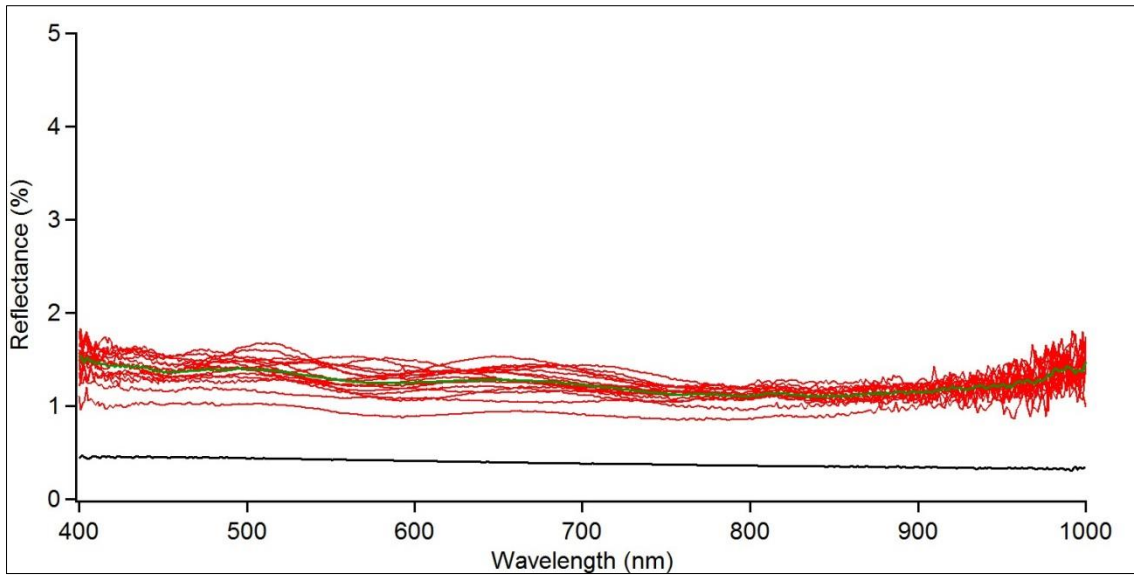
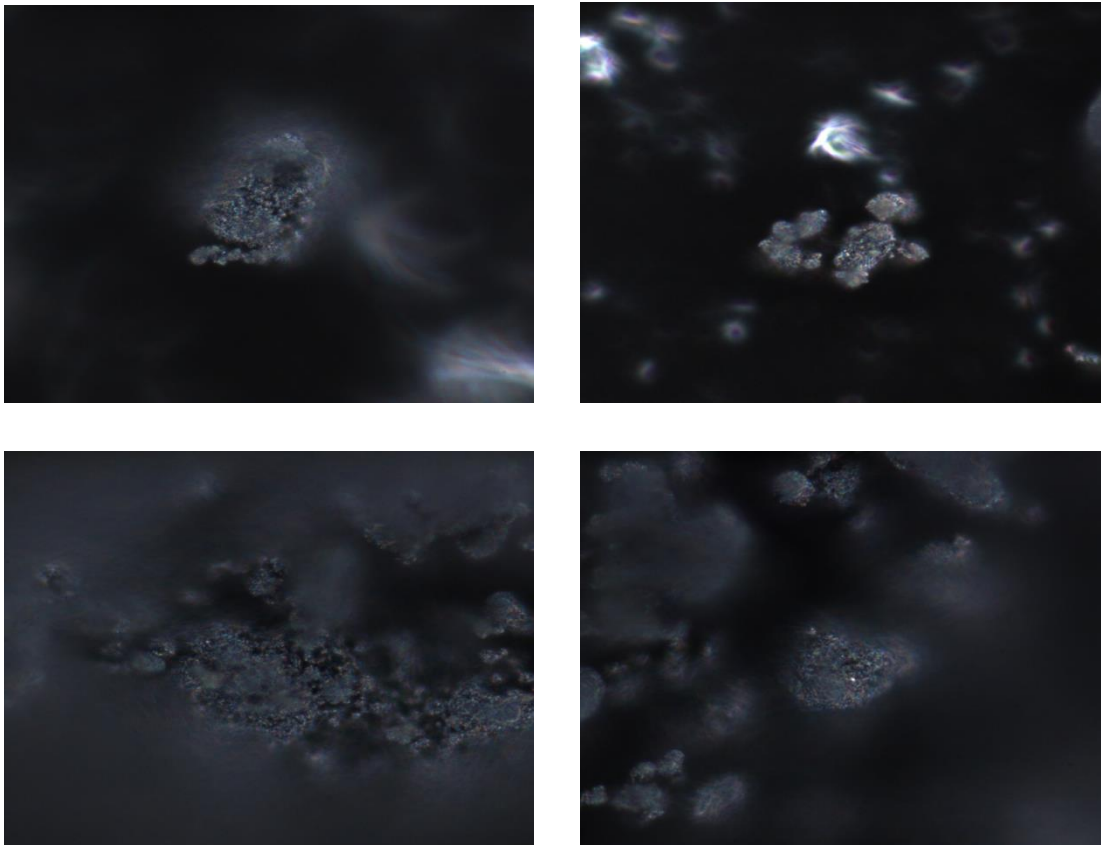


Figure 26 Reflectance spectra measured with HIMS of Diesel soot (red lines). The green line represents the average of 10 HIMS spectra and the black line is the spectrum obtained with the field spectroradiometer.



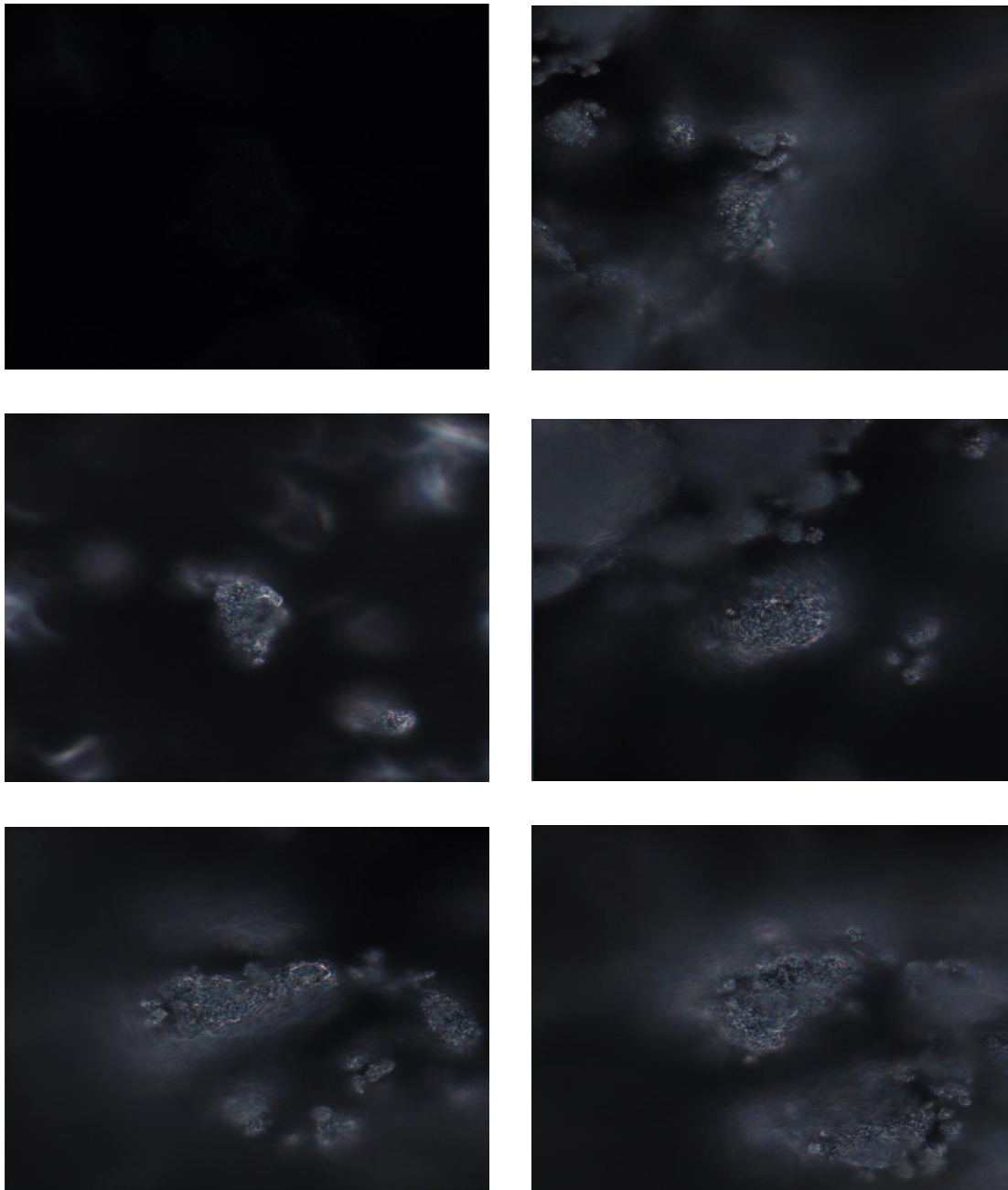


Figure 27 Microscopic images of measured areas of the spectra shown in Figure 33.

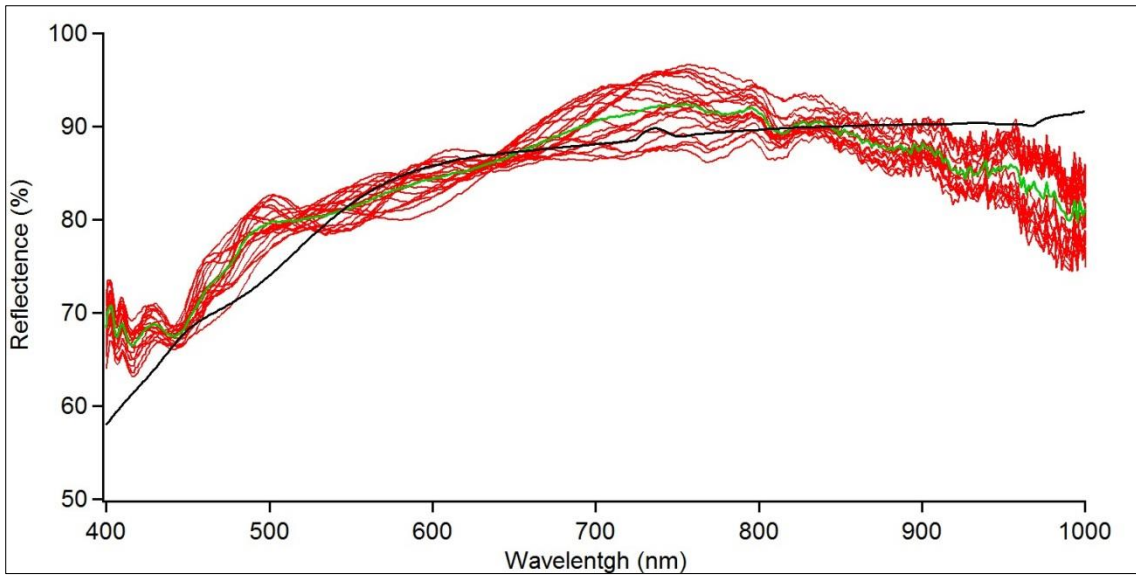
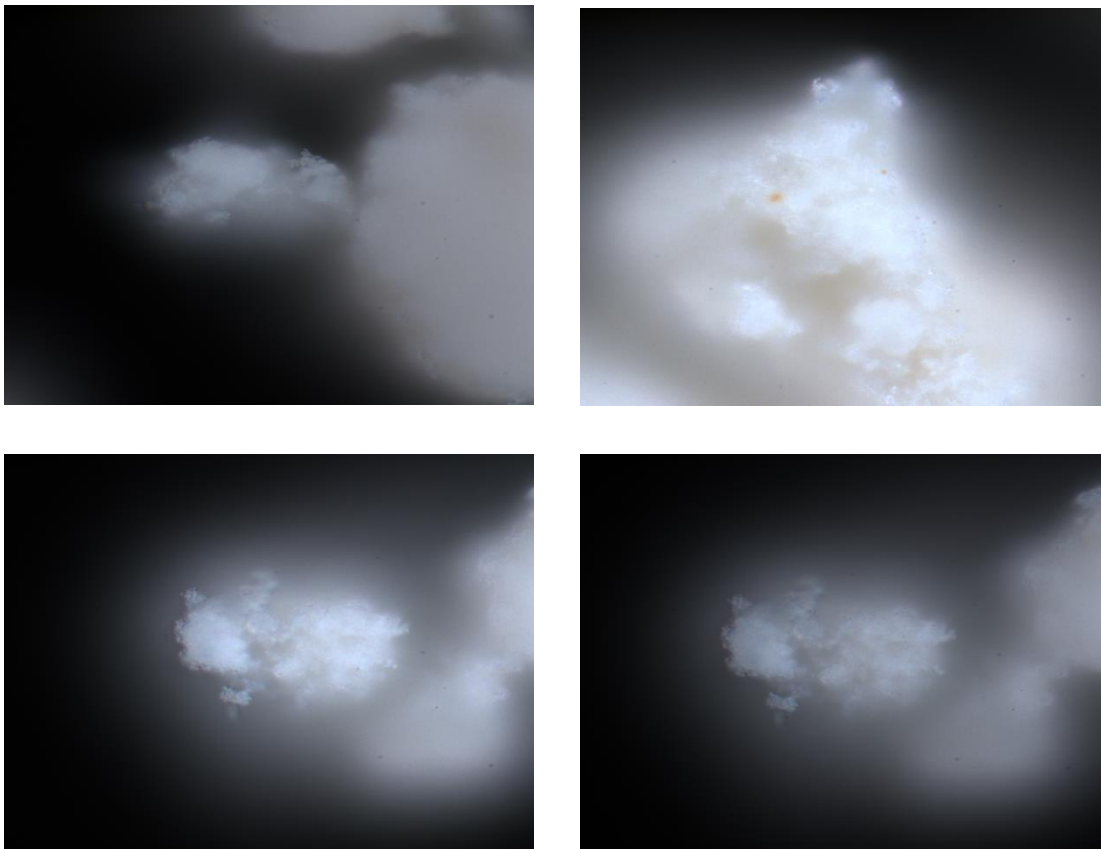
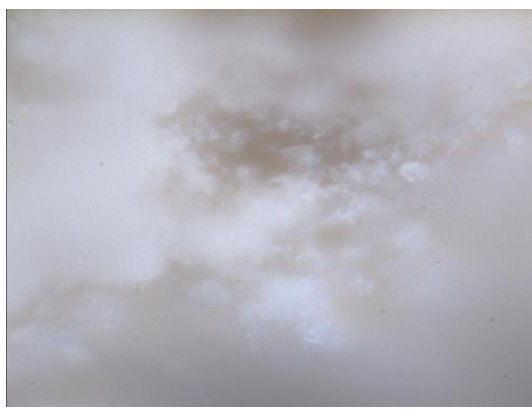
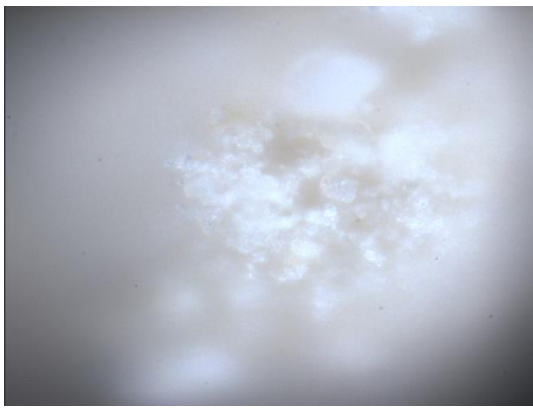
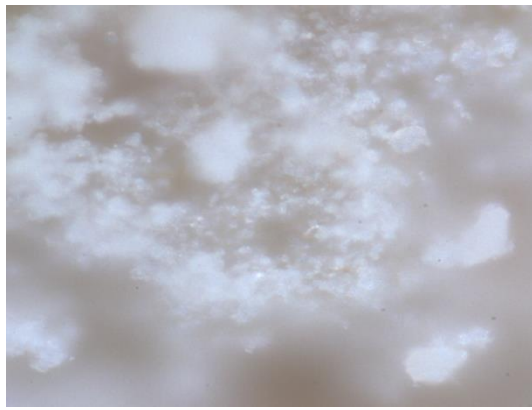


Figure 28 Reflectance spectra measured with HIMS of kaolinite (red lines). The green line represents the average of 19 HIMS spectra and the black line is the spectrum obtained with the field spectroradiometer.





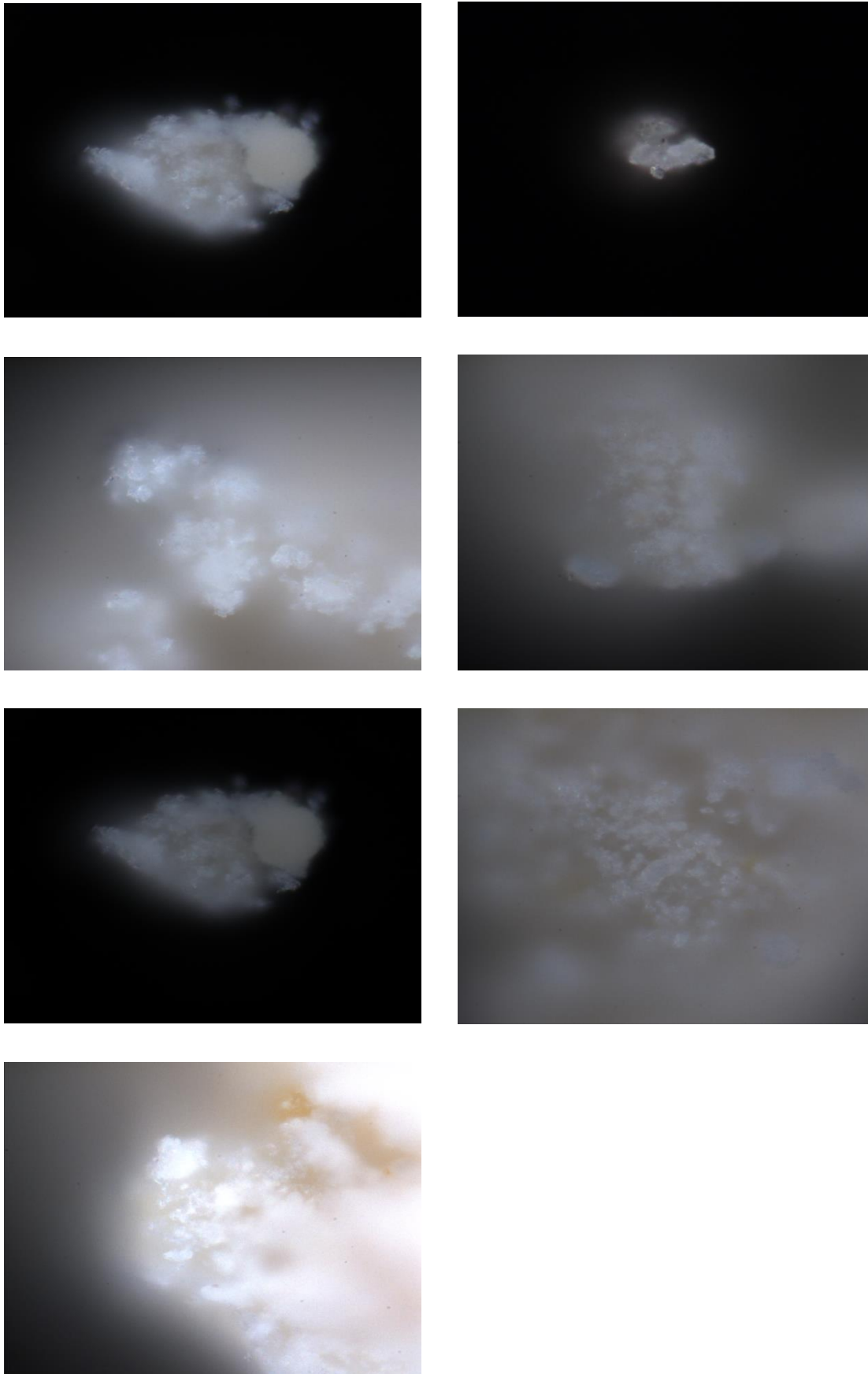


Figure 29 Microscopic images of measured areas of the spectra shown in Figure 35.

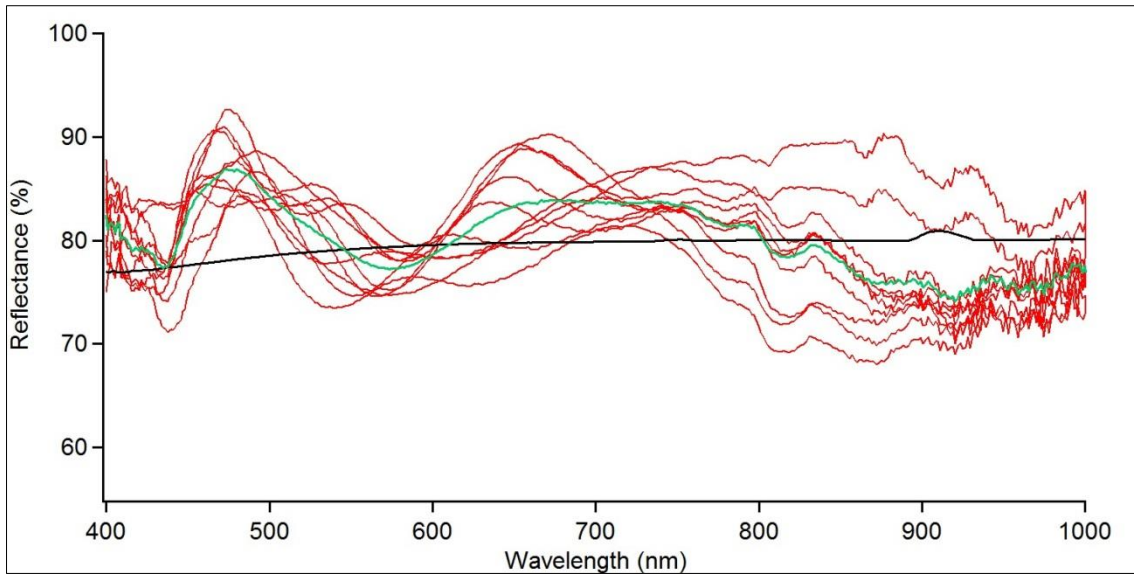
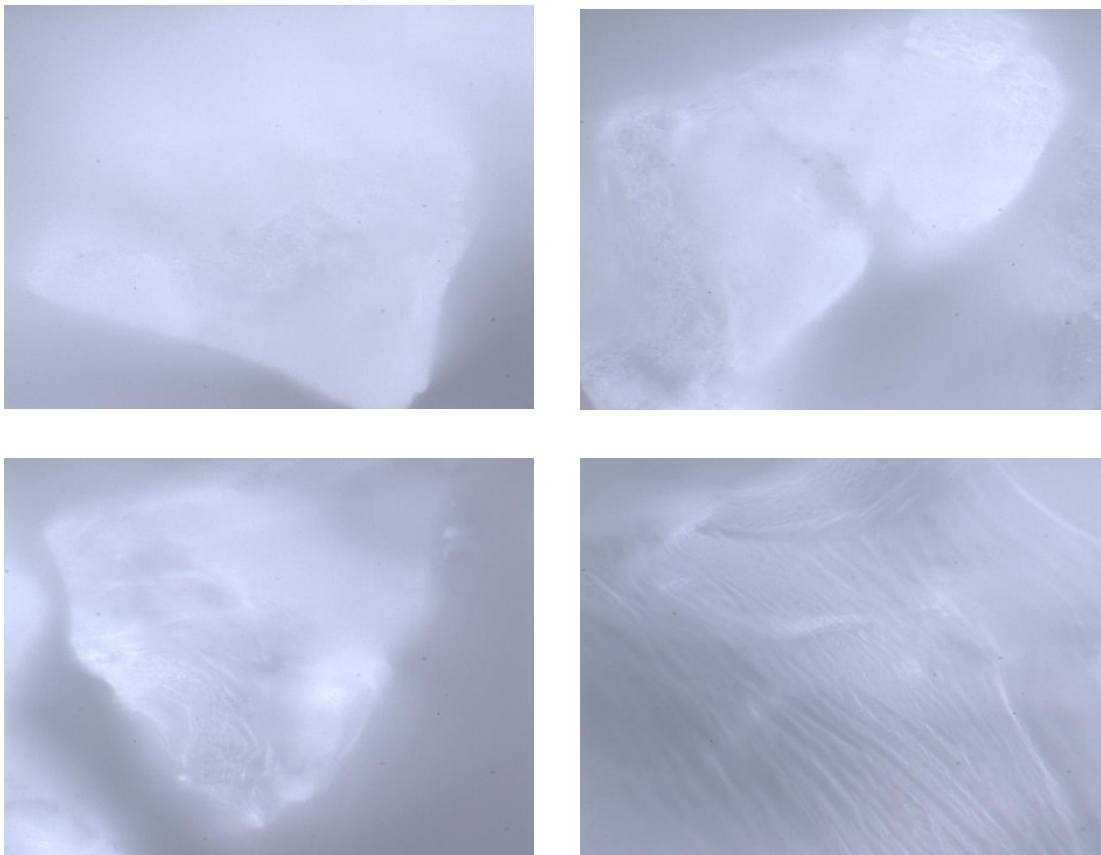


Figure 30 Reflectance spectra measured with HIMS of quartz (red lines). The green line represents the average of 10 HIMS spectra and the black line is the spectrum obtained with the field spectroradiometer.



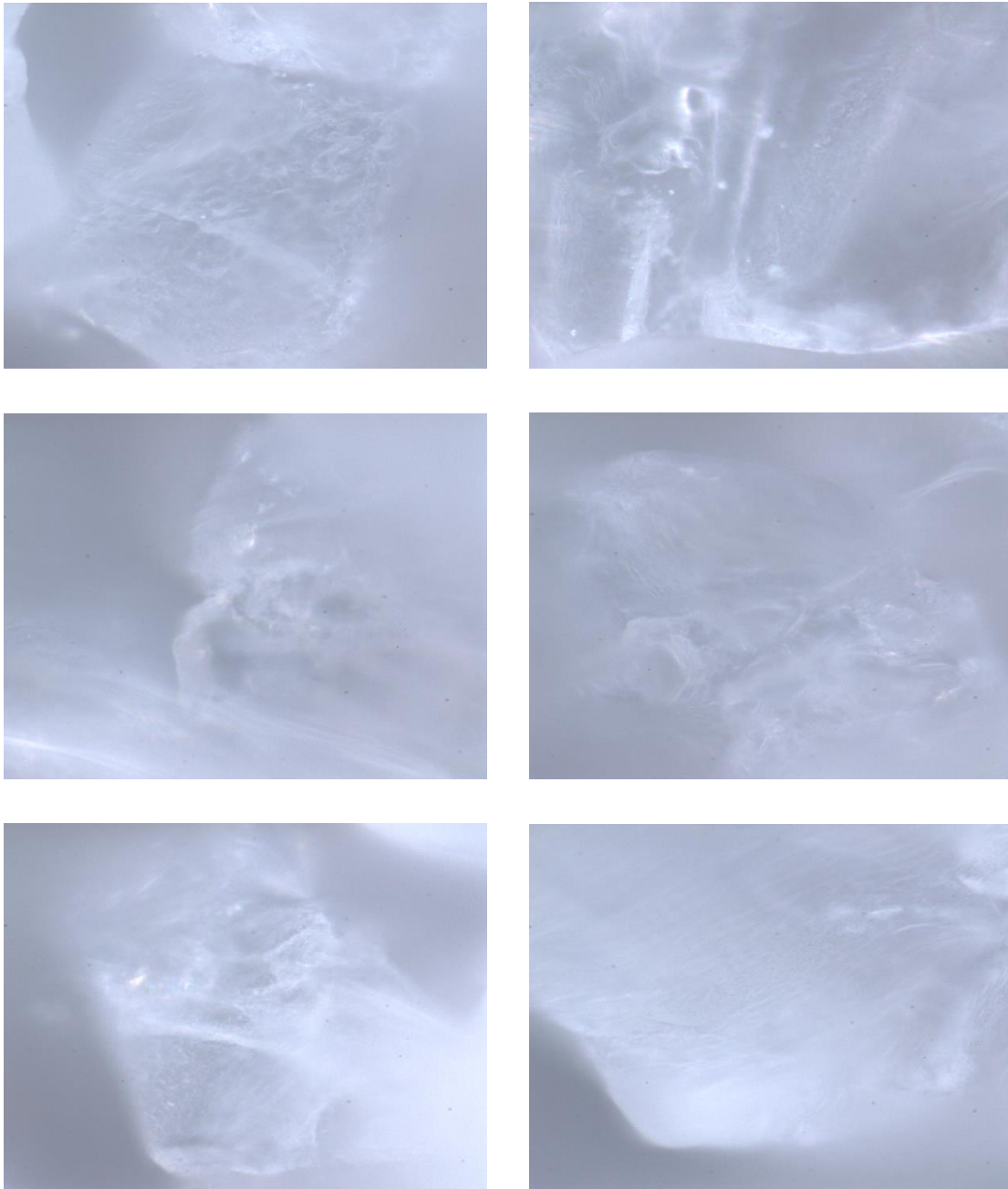


Figure 31 Microscopic images of measured areas of the spectra shown in Figure 37.

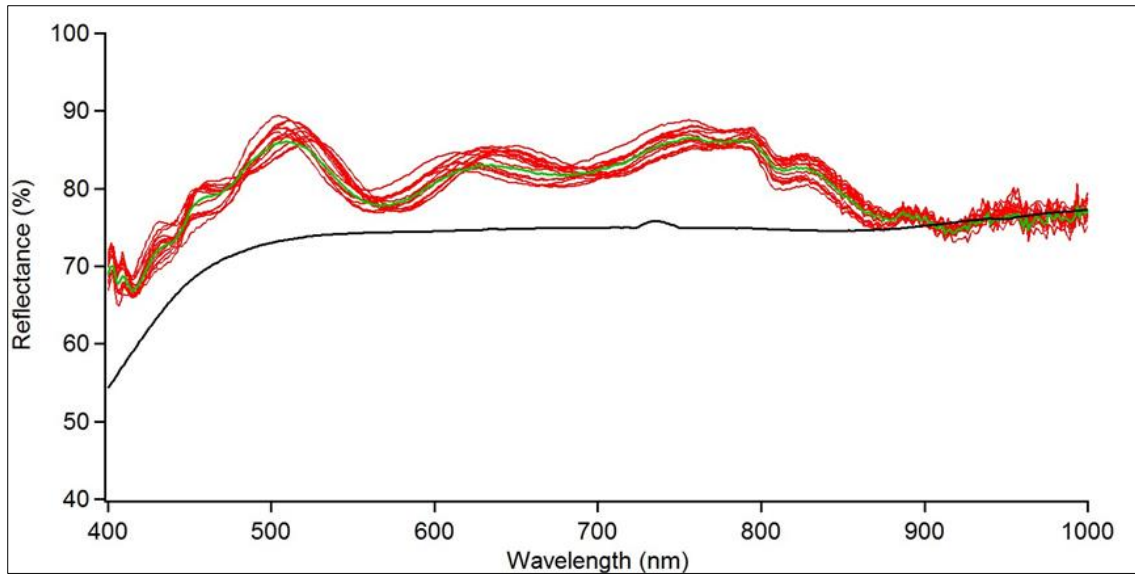
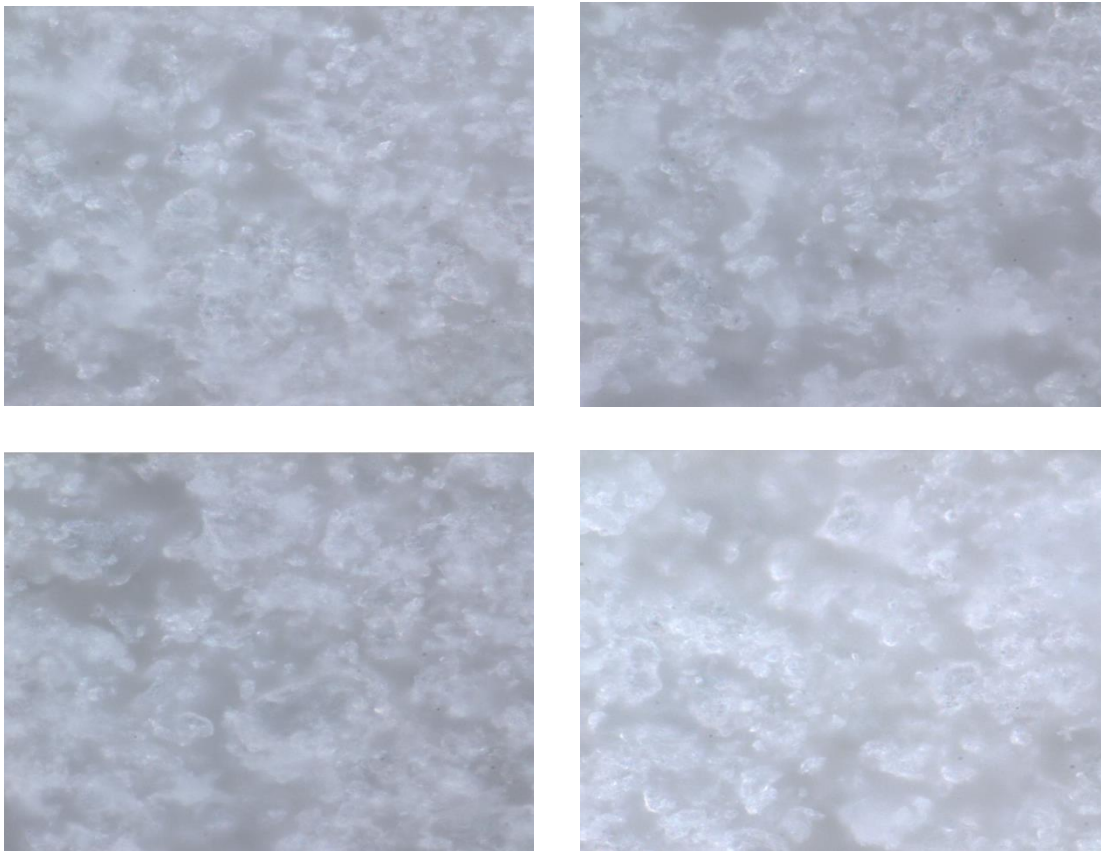
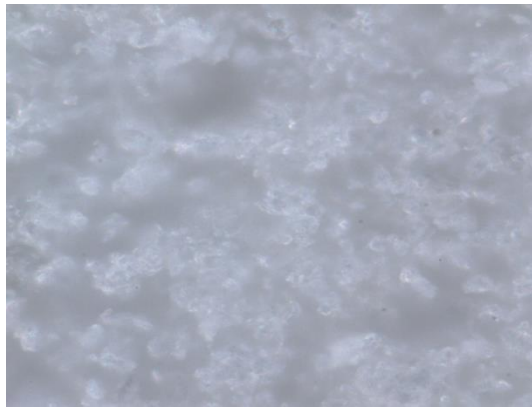


Figure 32 Reflectance spectra measured with HIMS of chlorite (red lines). The green line represents the average of 10 HIMS spectra and the black line is the spectrum obtained with the field spectroradiometer.





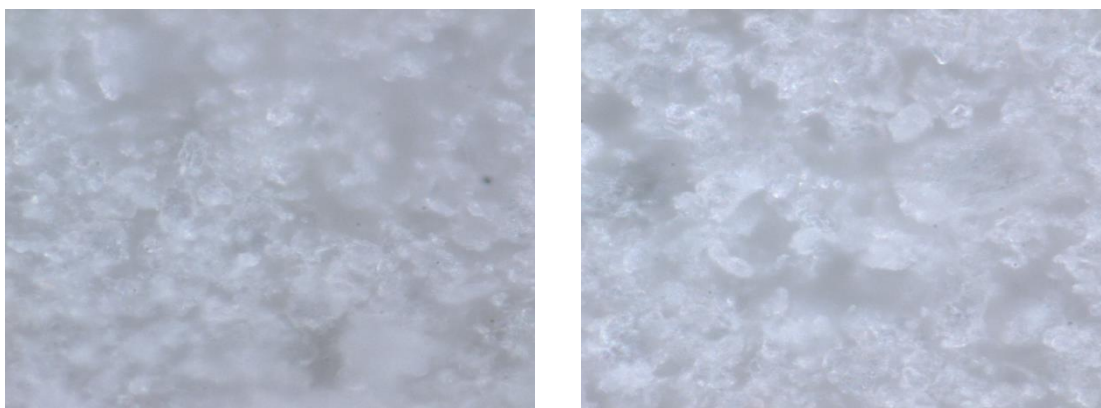


Figure 21 Microscopic images of measured areas of the spectra shown in Figure 39.

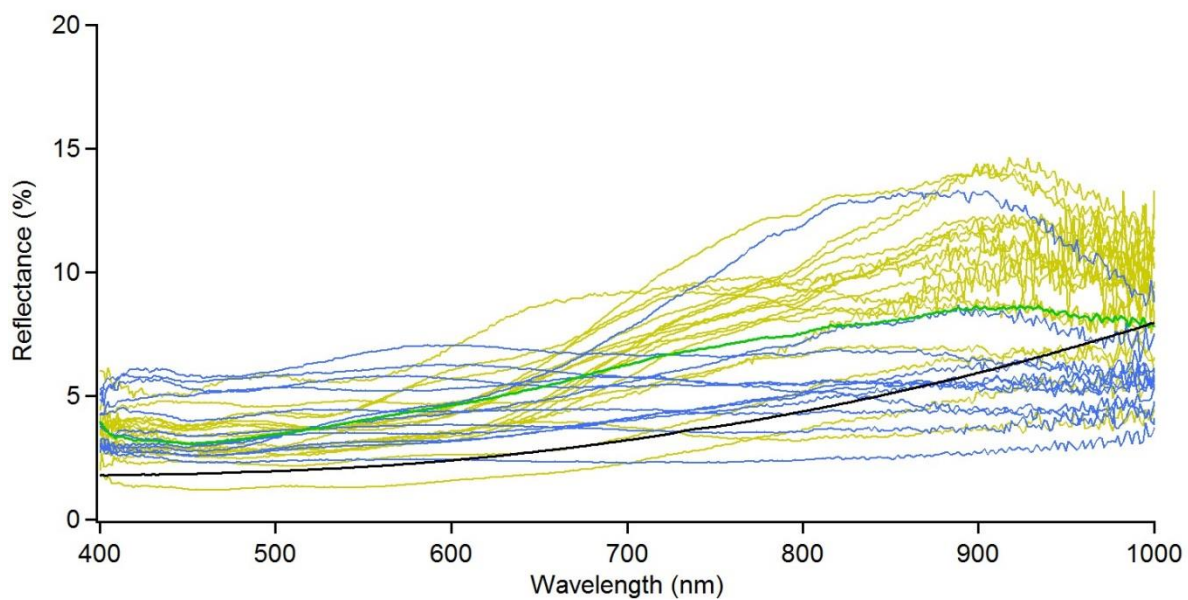
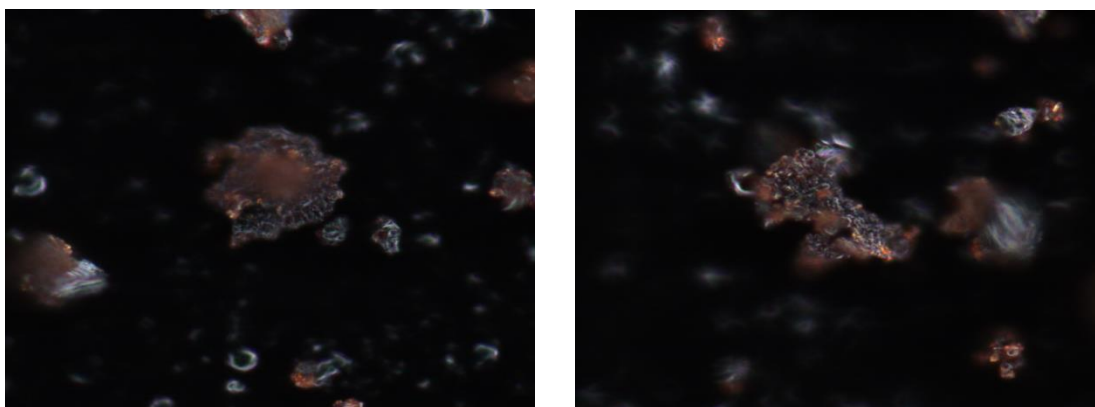
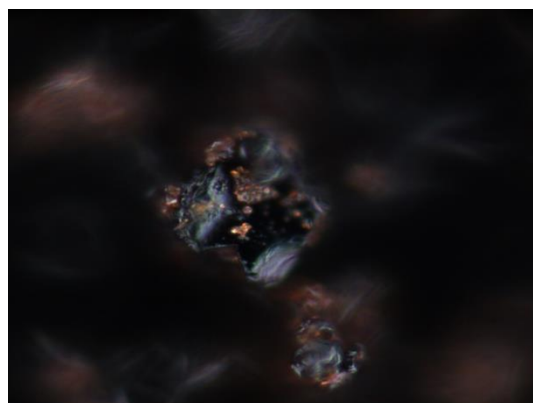
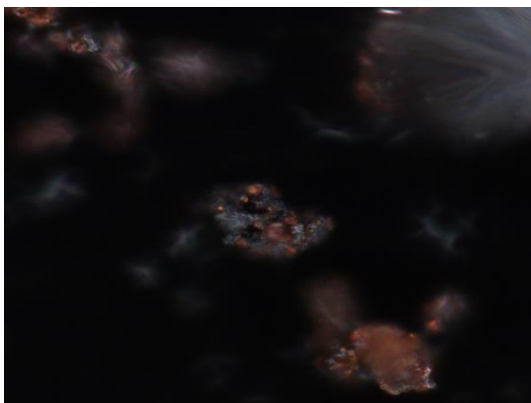
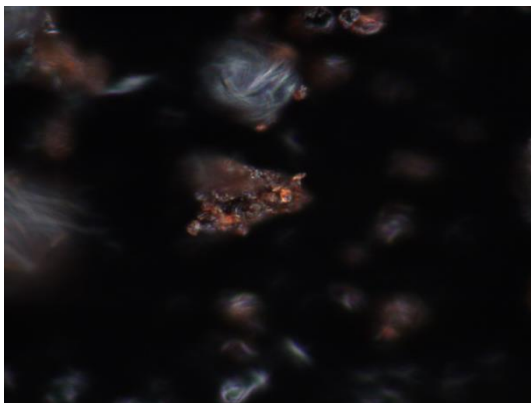
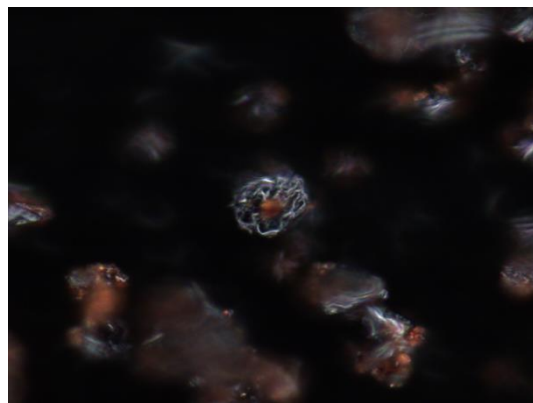
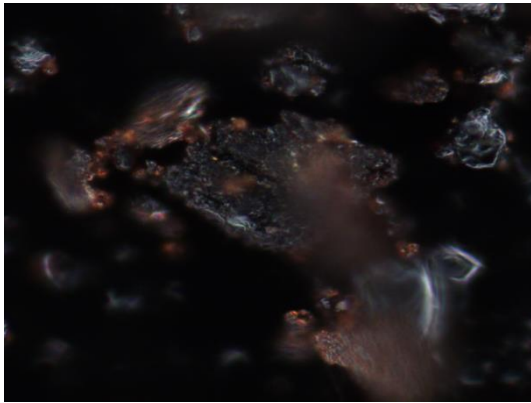
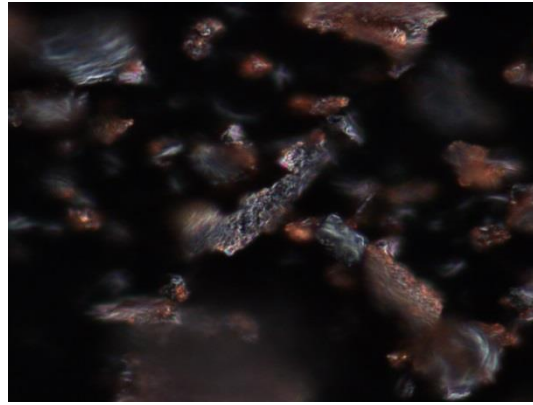
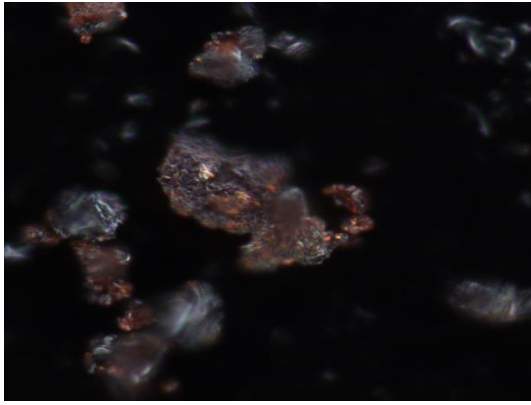


Figure 22 Reflectance spectra measured with HIMS of humic substances (blue for Elliot Soil, yellow for Leonardite). The green line represents the average of 10 HIMS spectra and the black line is the spectrum obtained with the field spectroradiometer.





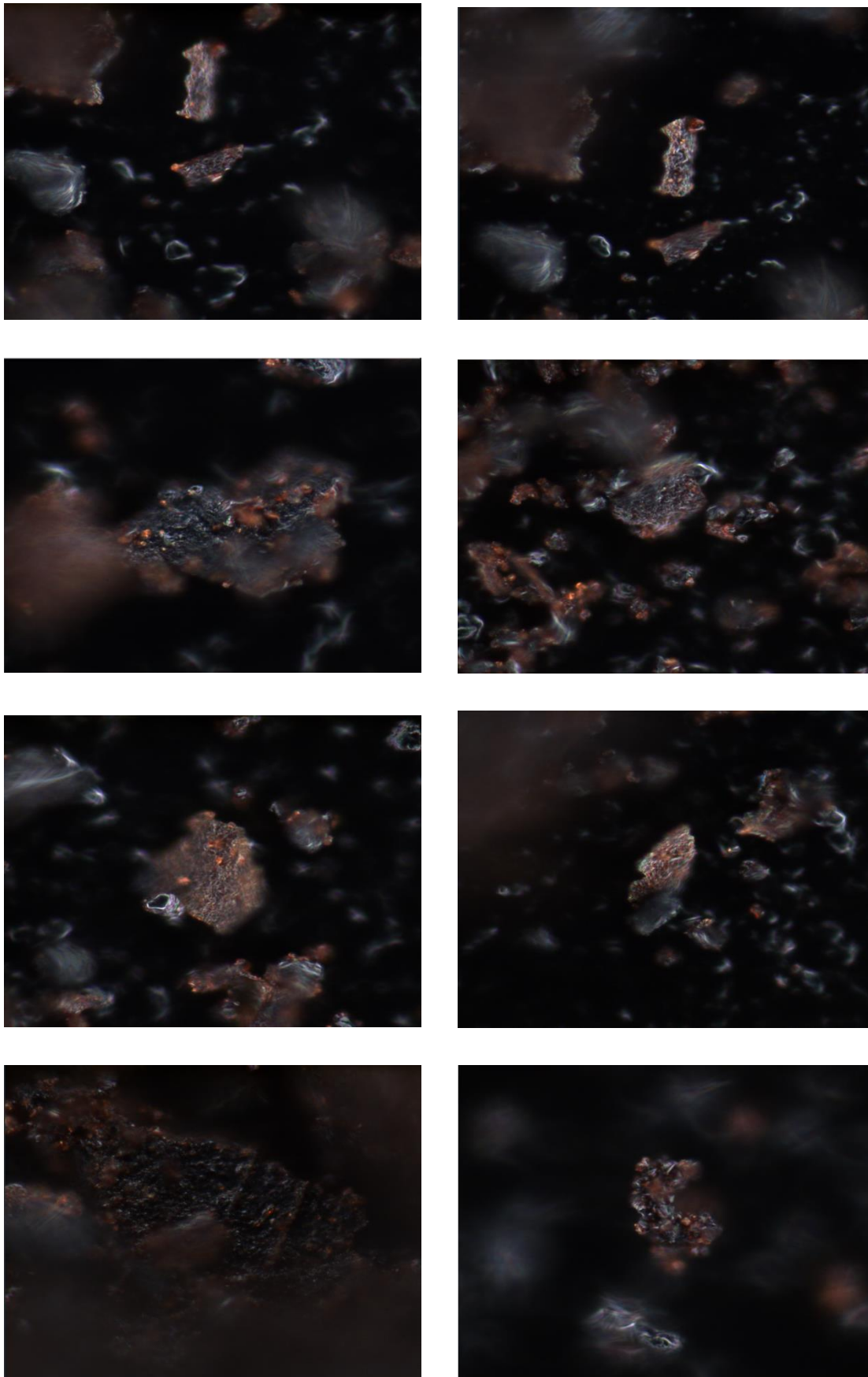
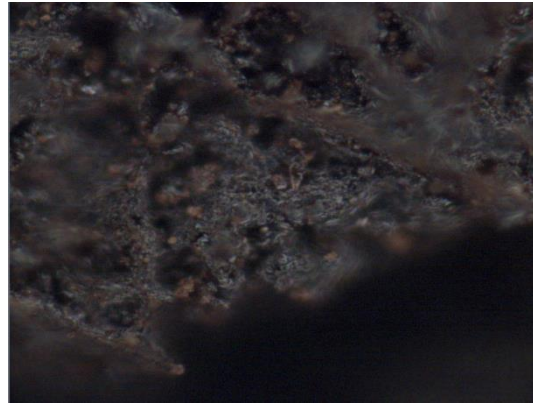
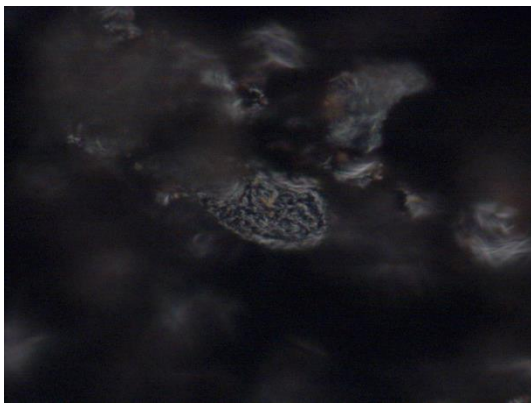
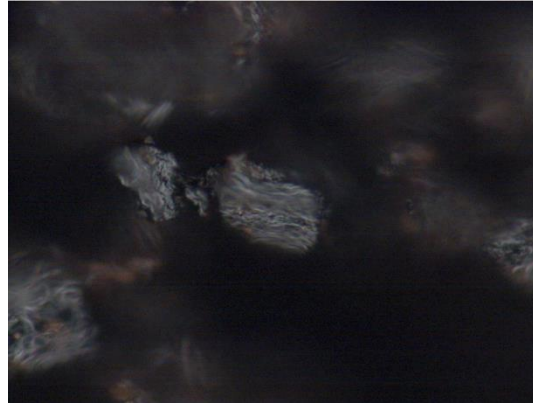
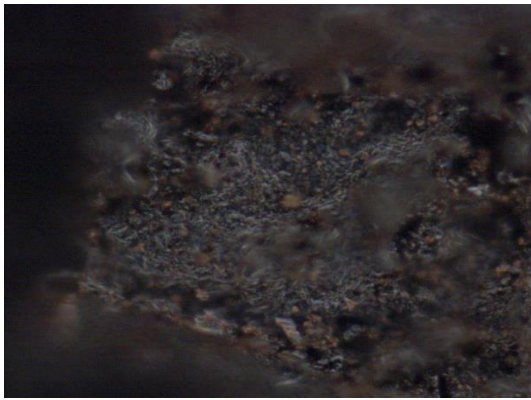
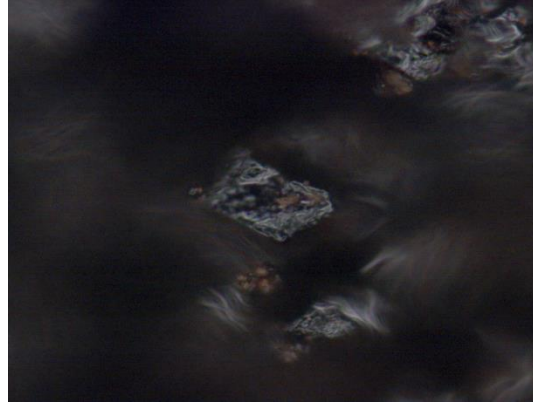
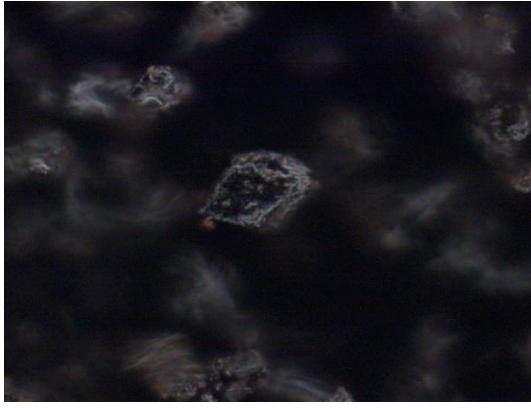


Figure 35 Microscopic images of measured areas of the spectra shown in Figure 4, Leonardite.



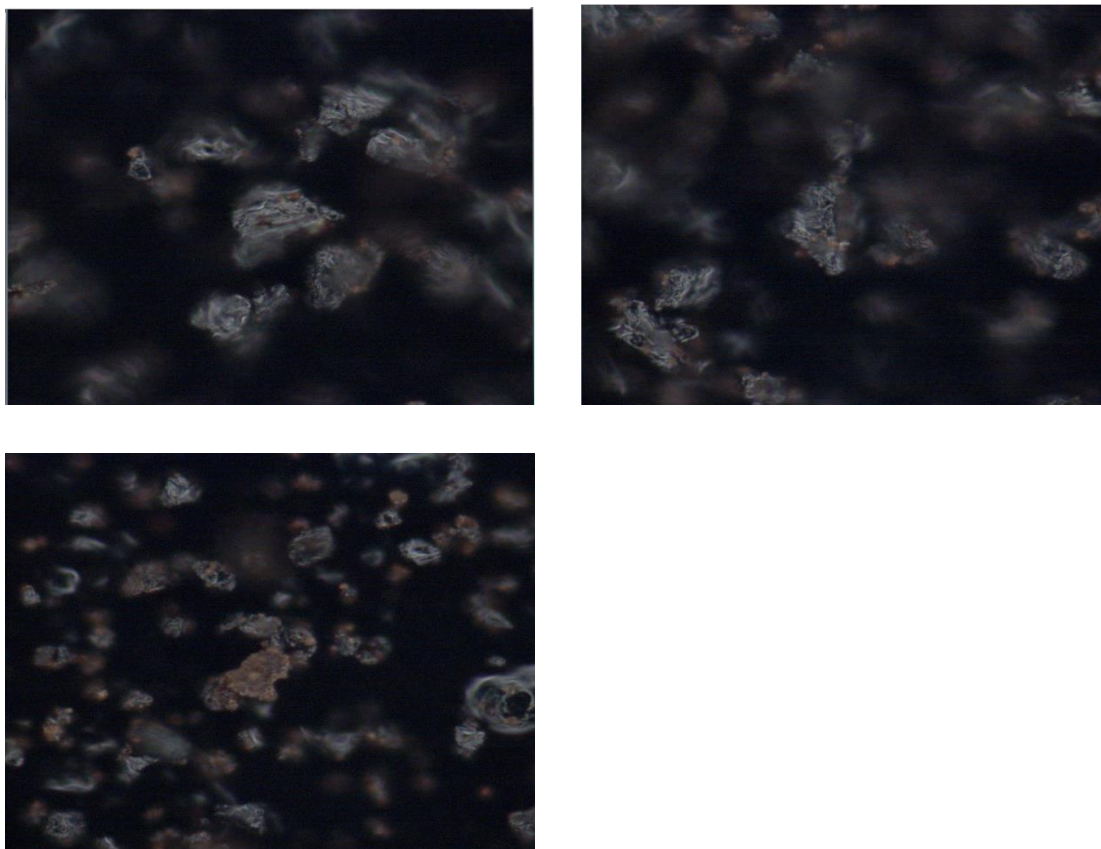


Figure 36 Microscopic images of measured areas of the spectra shown in Figure 4, Elliot soil.

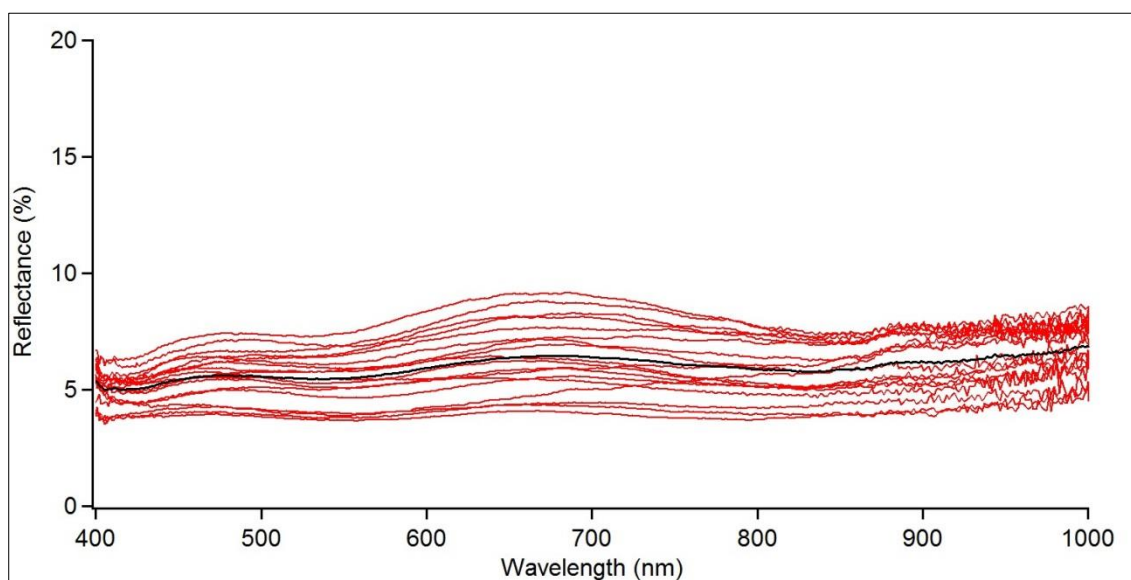
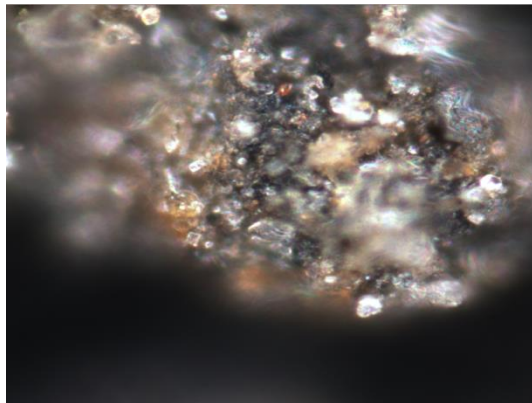
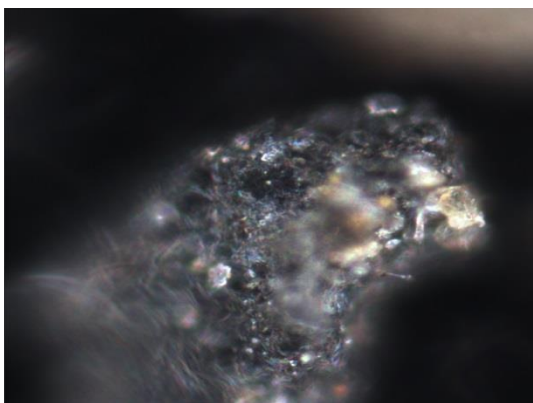
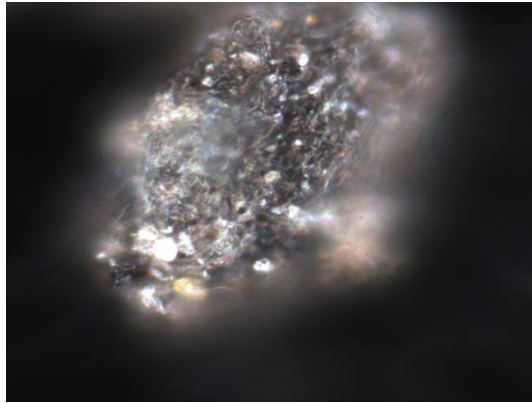
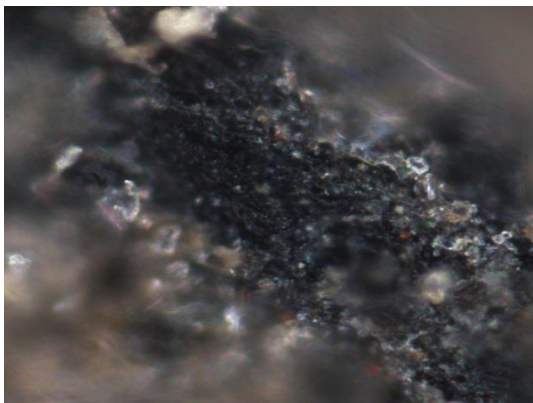
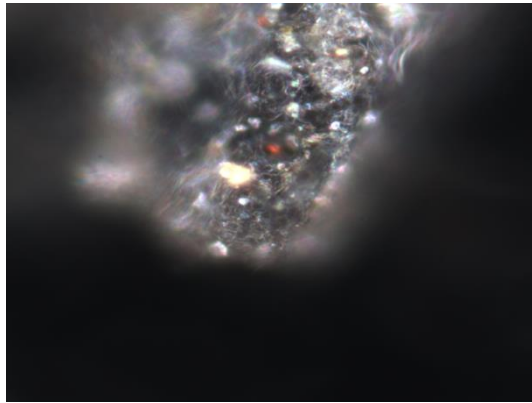
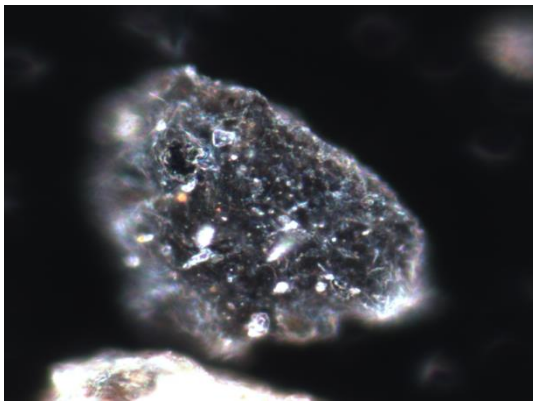
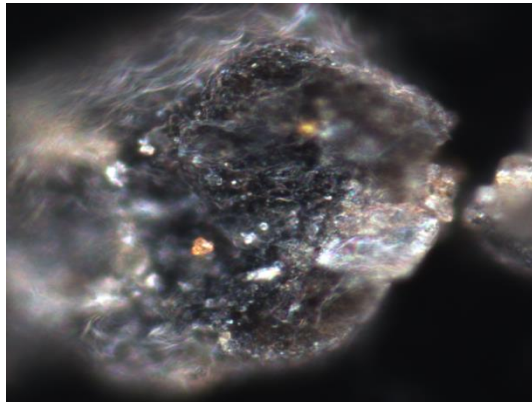
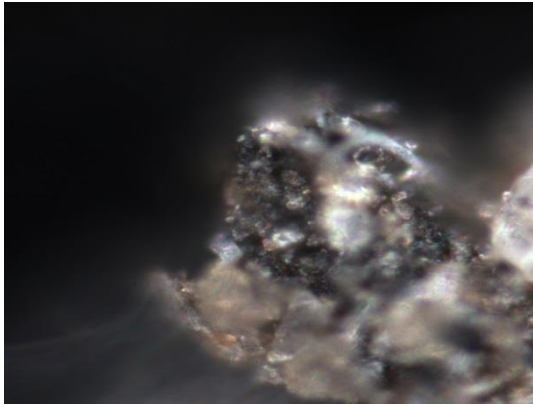


Figure 37 Reflectance spectra measured with HIMS of humic substances (red lines). The black line represents the average of 12 HIMS spectra.



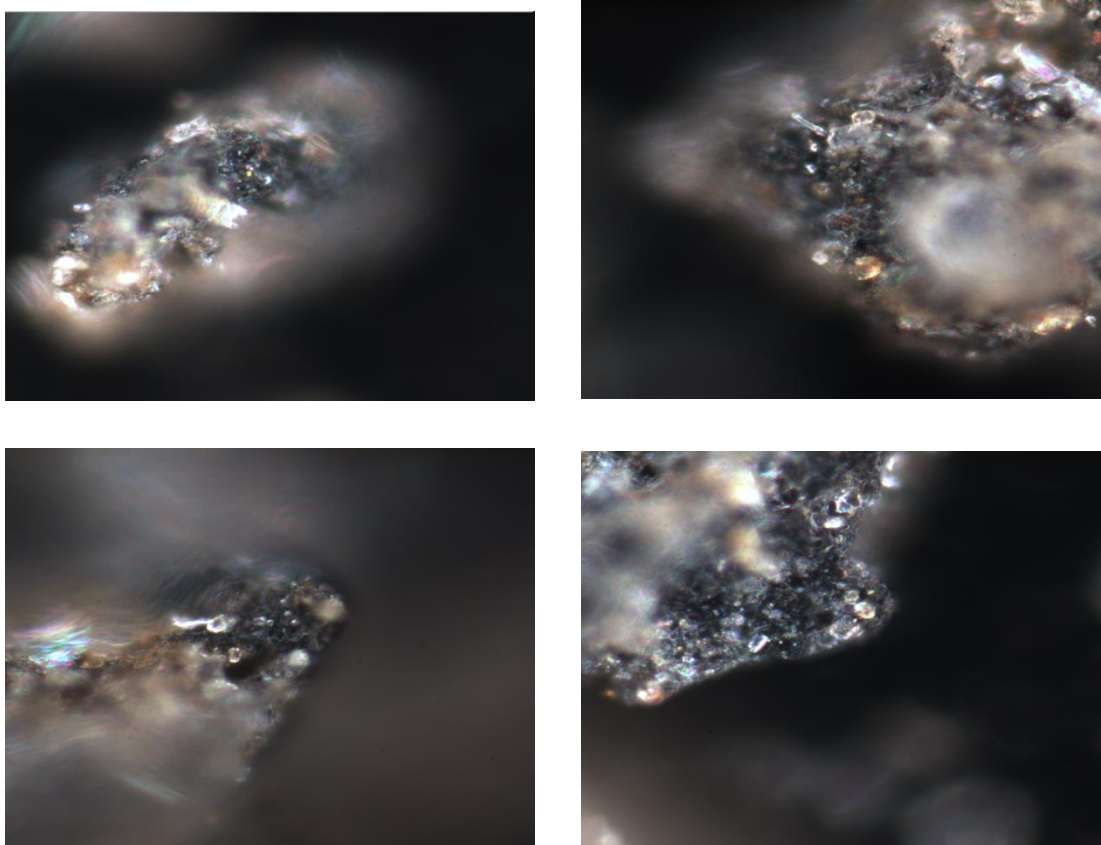


Figure 38 Microscopic images of measured areas of the spectra shown in Figure 43.

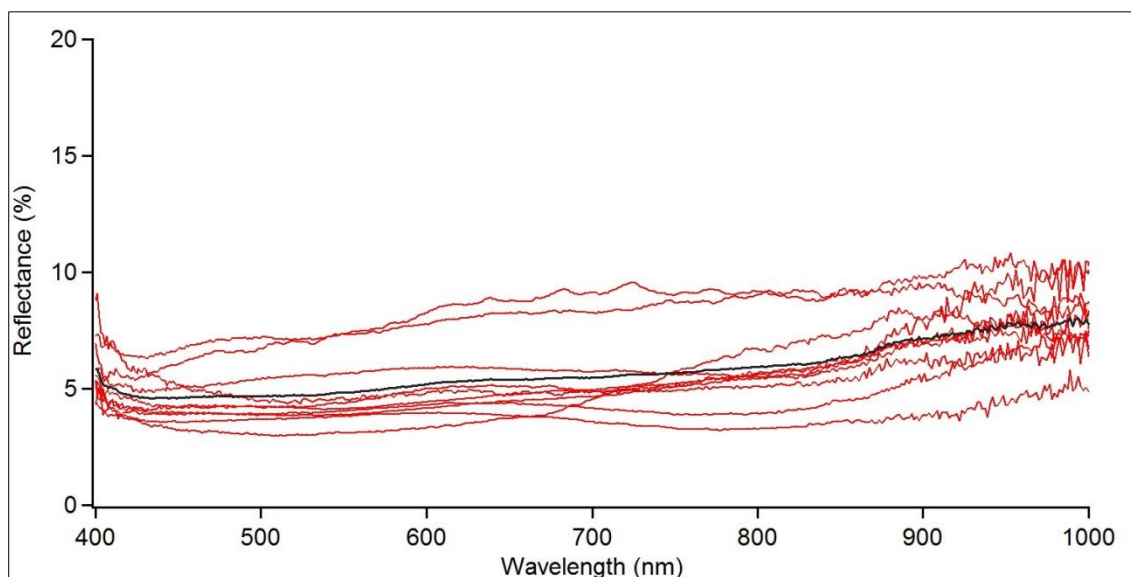
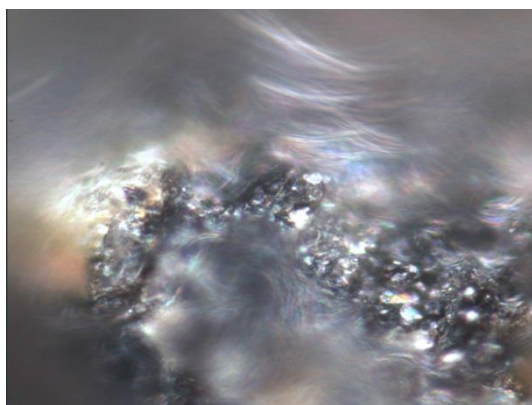
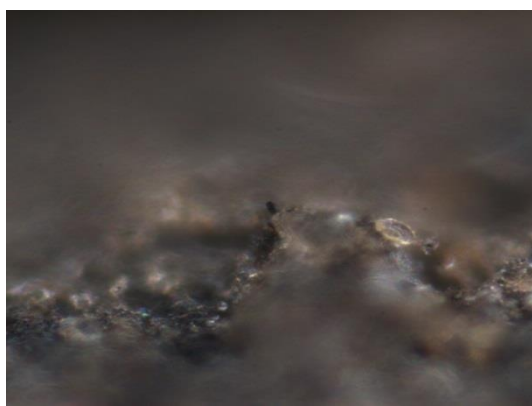
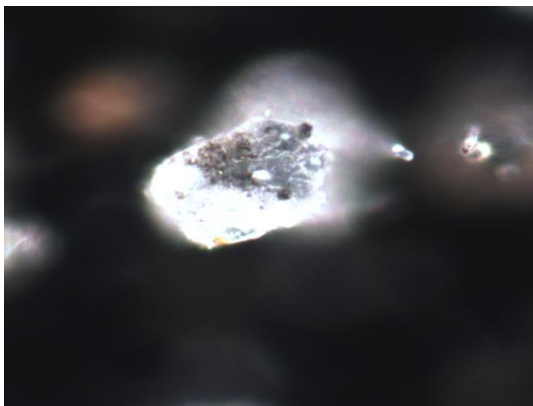
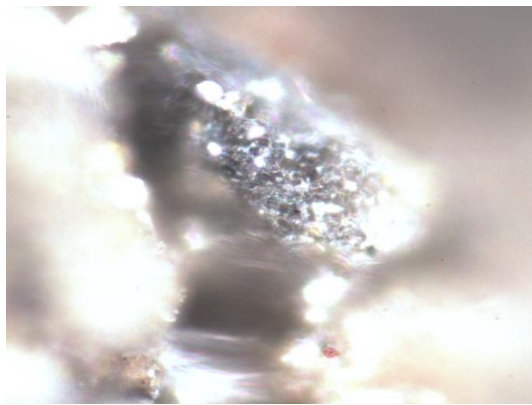
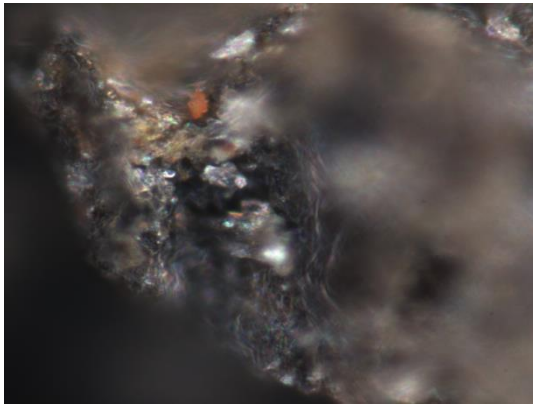
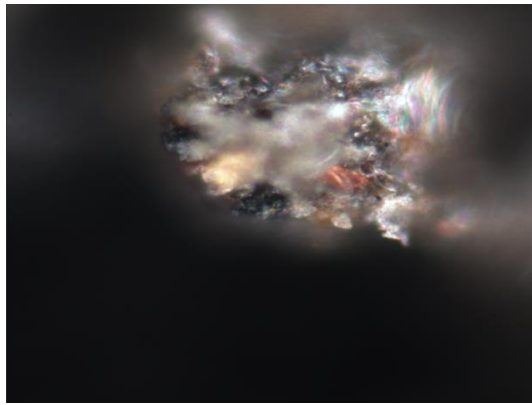
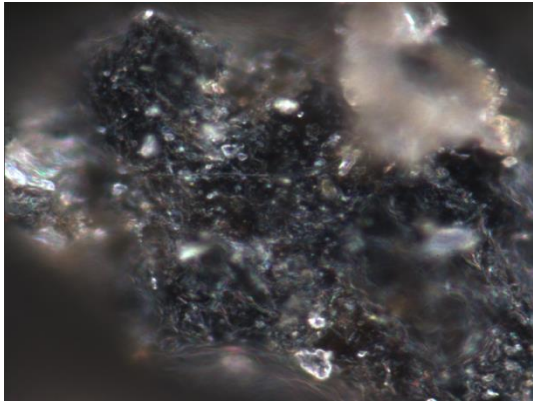


Figure 39 Reflectance spectra measured with HIMS of BC (red lines). The black line represents the average of 11 HIMS spectra.



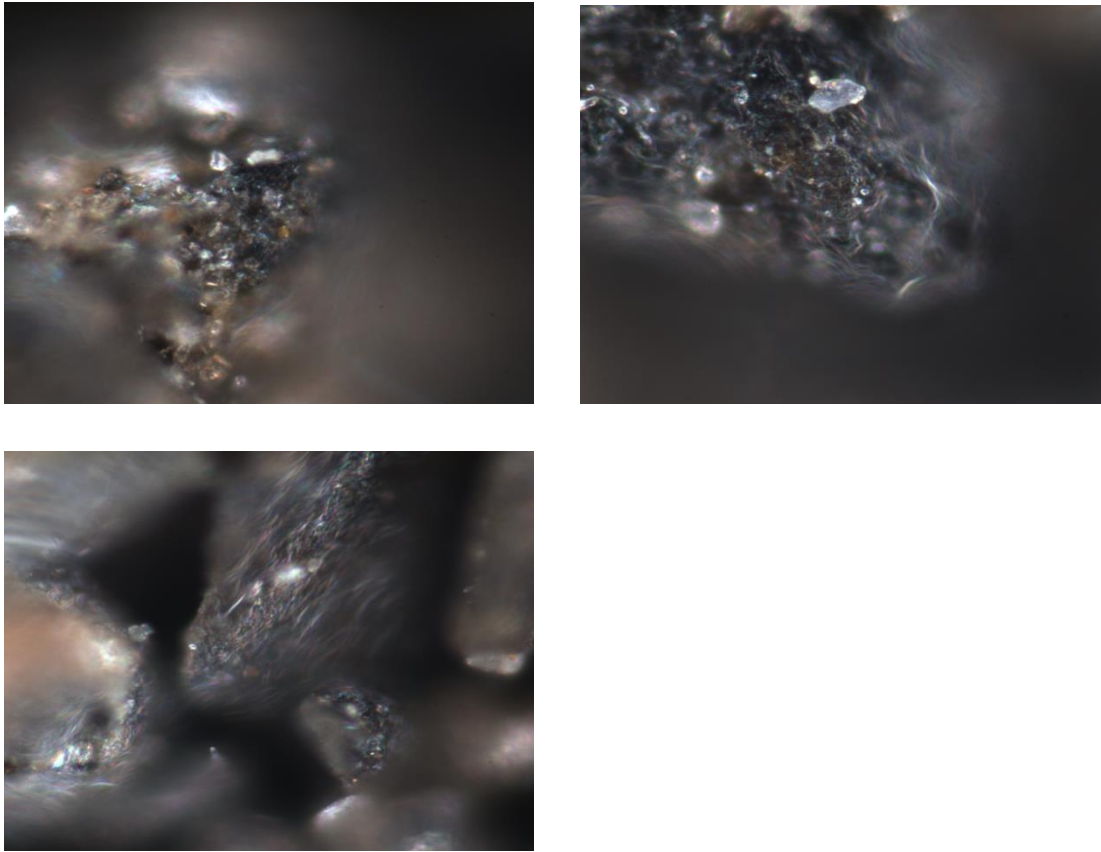


Figure 40 Microscopic images of measured areas of the spectra shown in Figure 45.

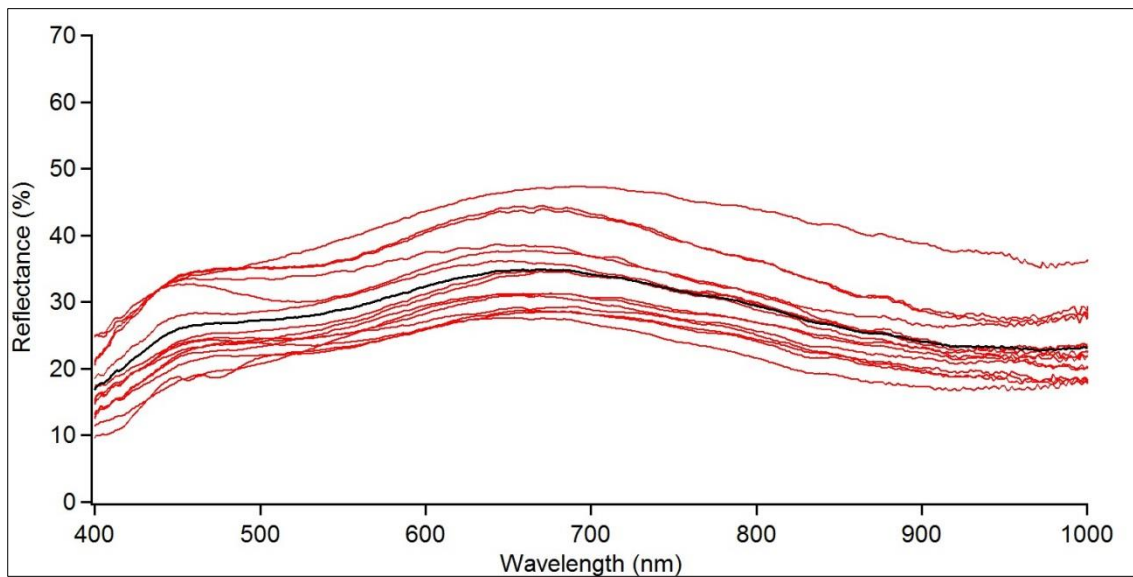
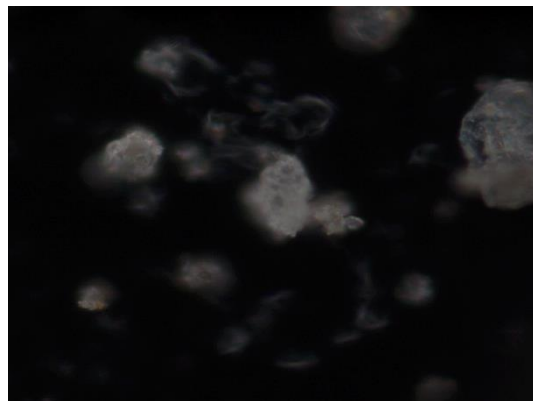
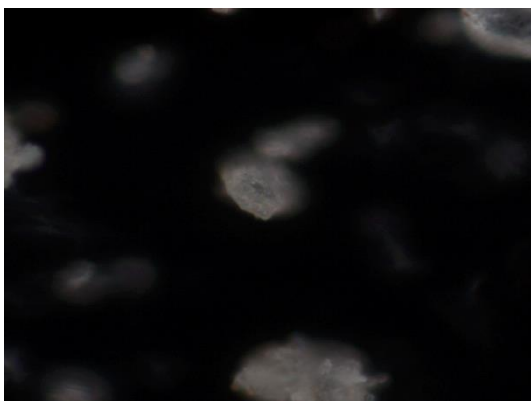
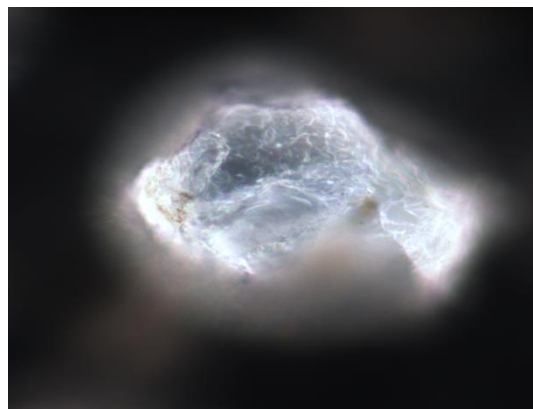
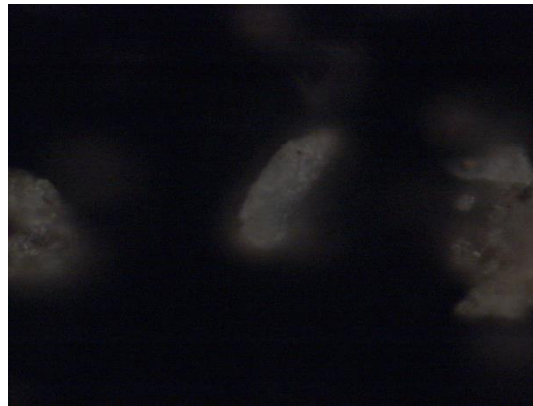
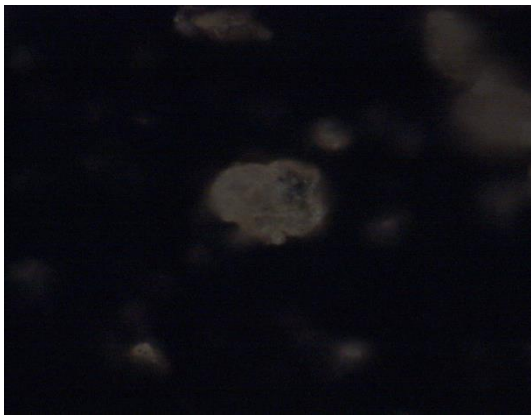
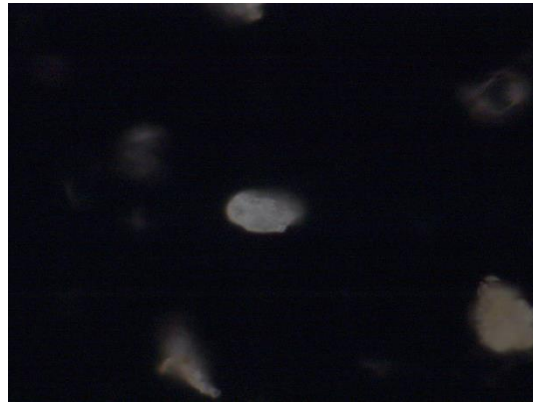


Figure 41 Reflectance spectra measured with HIMS of minerals (red lines). The black line represents the average of 15 HIMS spectra.



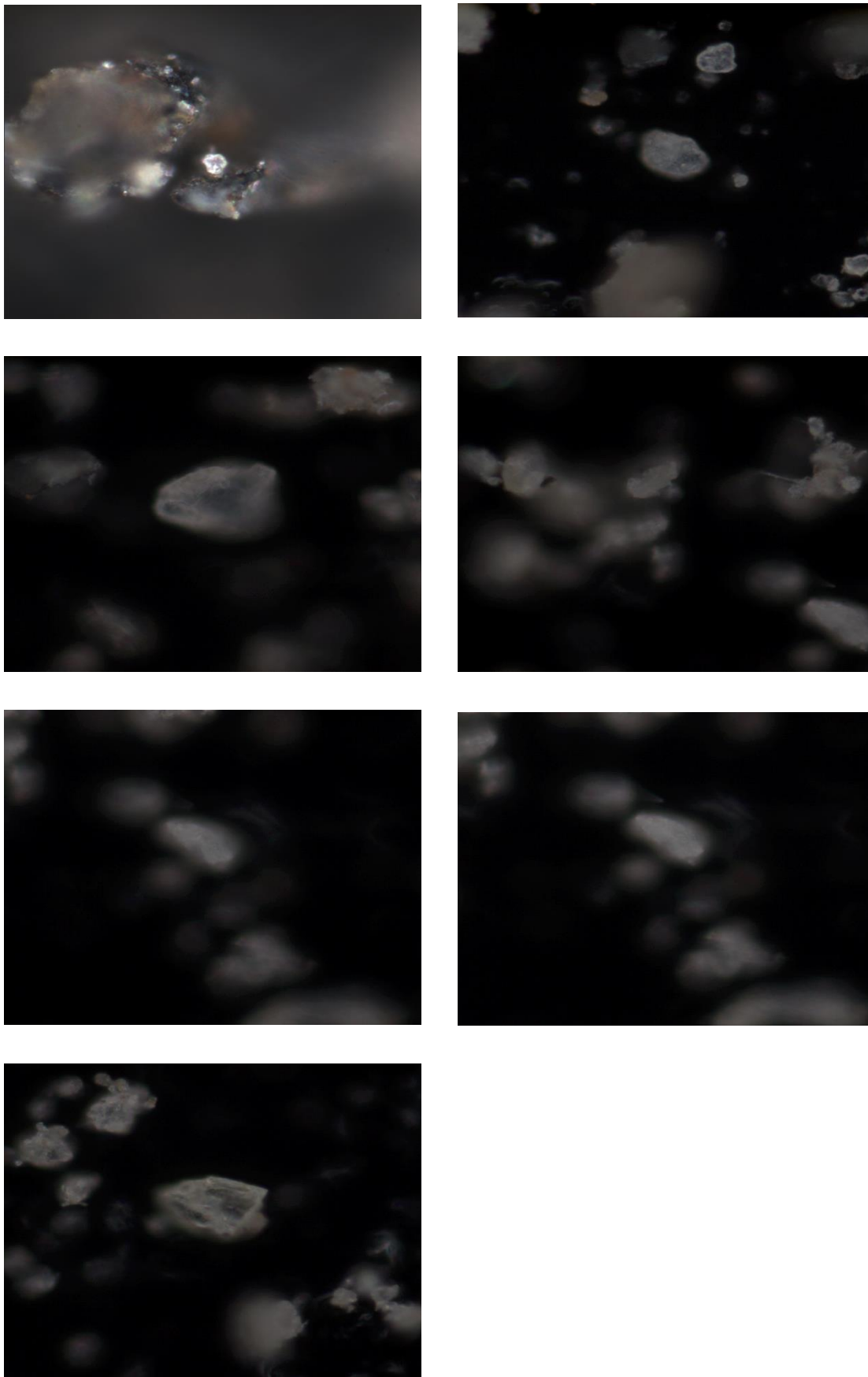


Figure 42 Microscopic images of measured areas of the spectra shown in Figure 4

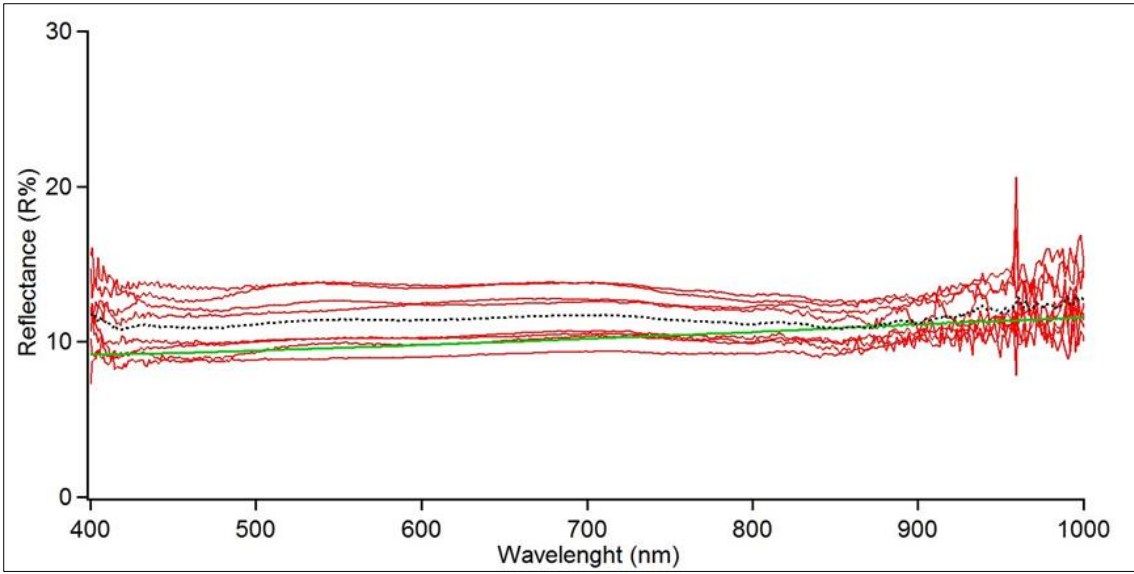


Figure 43 Reflectance spectra measured with HIMS of the 10% reflectance standard (red lines). The green line represents the average of 8 HIMS spectra and the black line is the spectrum obtained with the field spectroradiometer.

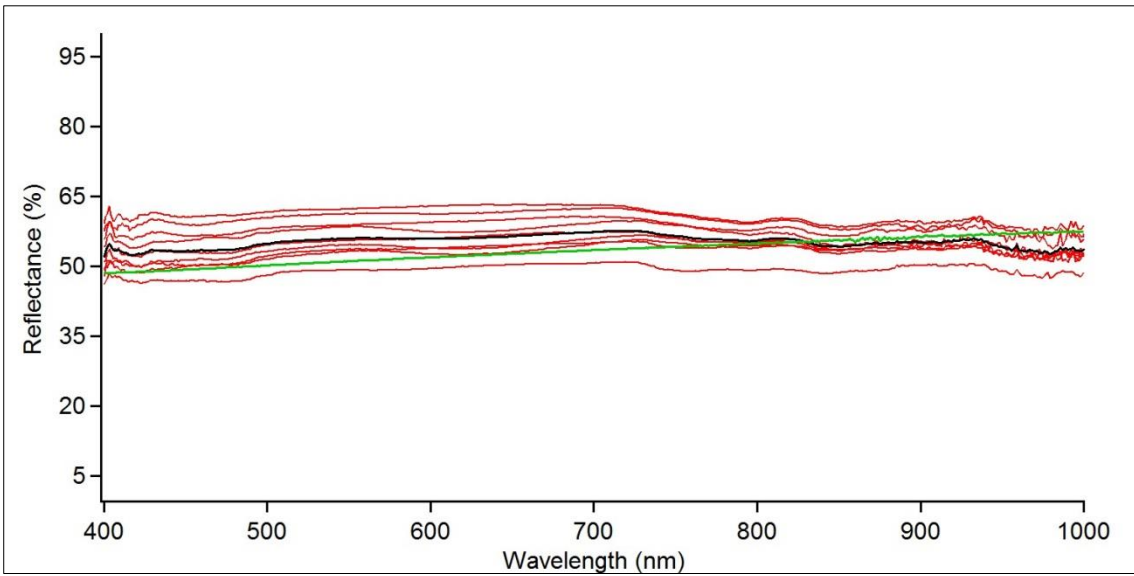


Figure 44 Reflectance spectra measured with HIMS of chlorite (red lines). The green line represents the average of 8 HIMS spectra and the black line is the spectrum obtained with the field spectroradiometer.

Acknowledgements

I would like to thank all the people who helped me more or less directly during the course of my PhD.

In primis Professor Margit Schwikowski for giving me the opportunity to work on this project as well as for allowing me to learn and grow through the many experiences I collected in these four years. I had both a lot of freedom and guidance in the direction of my work and for that I am very thankful.

I received a lot of help from Professor Susan Kaspari. During her sabbatical in Paul Scherrer Institute we started collaboration; she trusted my ideas and always provided a good prospective.

I want to thank all the people I collaborated with: Professor Michael Shaepman, for the lengthy discussions and the scientific enthusiasm, Dr. Bucheli for allowing me to freely use the HIMS and Dr. Jim Beach, for always providing technical assistance with the HIMS.

Special thanks go to Dr. Andrea Marinoni for being so proactive and enthusiastic about our collaboration since our first talk at the Earsel Conference Ice Beaker and Dr. Kathrin Naegeli, who provided her expertise to an idea we came up with at the Swiss Geo-Science Meeting Party, this undoubtedly proves that food and wine really help the creative process.

I want to thank the whole LUC group, I was really lucky to join such a successful, cohesive, and supportive group. A special thanks to all my office mates, many people came and went in the office but the atmosphere was always fun and supportive; please don't let the plants wither!

I would also like to thank the PSI volley team for being such an awesome group, as well as all the friends I made in these years.

As for my family a special thanks goes to my grandmothers, Nonna Antonia e Nonna Lidia; I was lucky to have to best grandmothers in the world, I cherish that to no end. My father Ivo and my mother Marilena as well as my sister Elisa deserve my gratitude for being always so supportive and sending "good vibrations" in times of need. I hope you are as proud of me as I am of you guys.

Most of all I would like to thank Ignasi Villacampa Rosès; a lot of wonderful things came from my time in Paul Scherrer Institute, but I didn't expect to come across the best one on my first day.

Declaration

under Art. 28 Para. 2 RSL 05

Last, first name: Dal Farra, Anna

Matriculation number: 13-141-288

Programme: Climate Sciences

Bachelor

Master

Dissertation

Thesis title: Effect of light absorbing impurities in the albedo of Alpine glaciers

.....
.....

Thesis supervisor: Professor Margit Schwikowsk

.....

I hereby declare that this submission is my own work and that, to the best of my knowledge and belief, it contains no material previously published or written by another person, except where due acknowledgement has been made in the text. In accordance with academic rules and ethical conduct, I have fully cited and referenced all material and results that are not original to this work. I am well aware of the fact that, on the basis of Article 36 Paragraph 1 Letter o of the University Law of 5 September 1996, the Senate is entitled to deny the title awarded on the basis of this work if proven otherwise.

.....
Place, date

.....
Signature

Curriculum Vitae

ANNA DAL FARRA

Date of Birth: 26/04/1987

Nationality: Italian

Address: Dorfstrasse 23, 5303 Würenlingen Switzerland

Phone: (0041) 786296156

E-mail: anna.dal-farra@psi.ch

Published Works

- DRIFTS characterization of the “Soft Stone of the Berici Hills” and first results of a fast method for the classification of its main varieties through Multivariate Analysis – A. De Lorenzi, A. Dal Farra, M. Cappellaro

(DOI: 10.7361/scicf-177)

Education

European Research Course on Atmosphere

January 2015

Université Joseph Fourier, Grenoble CNRS

University of Berne (Paul Scherrer Institut)

January 2014 - Present

Doctoral degree in Climate Science

- *Thesis: Effects of light absorbing impurities on the albedo of Alpine glaciers*

Università degli Studi di Ferrara

September 2009 – July 2013

Master Degree in Chemistry

- *Thesis: Characterization of XVI Century Pigments from the Veneto Region through Micro-Invasive Analysis*

Bachelor Degree in Chemical Science for the Preservation of Art

- *Thesis: Characterization of different types of 'Soft Stone of the Berici Hills' using DRIFT Spectroscopy (Diffuse Reflectance Infrared Fourier Transform)*

Prises and awards

SEP-NGP-Prize for young researchers for the best communication 2015 University of Bern

Graduate Symposium Prize for the excellent presentation of PhD work 2015

Languages

Italian: Mother Tongue

English: Mother Tongue

German: Intermediate (B1)

Spanish: Intermediate (B1)

French: beginner (A2)

Technical and Computer Skills

Proficient use of main instruments in Chemical Analysis: Spectroscopy, XRF, XRD, IR Spectroscopy, SEM-EDS, HPLC, GC-Mass Spectroscopy, IC, NMR Spectroscopy, Imaging Techniques

Advanced knowledge of photography and relative techniques, excellent communication abilities, expert in method development.

Basic knowledge of Hardware, of Fortran 90 and Mathematica. Knowledge of OS Windows and proficient use of Word, Excel, Igor, LaTeX and of Video and Photo Editing Tools.

Contribution to conferences and workshops

- 2017 *Poster Presentation*
- 15th Swiss Geoscience meeting, Davos, Switzerland, 17 – 18 November
- 'A study on the location and effect of light-absorbing impurities on Glacier de la Plaine Morte'*
- 2017 *Participation*
- 16th Young Researchers Meeting, Aeschi bei Spiez, Switzerland, 8 – 9 June
- 2017 *Oral Presentation*
- European Geoscience Union, Vienna, Austria, 23 -28 April
- 'Partitioning the contribution of light-absorbing impurities to albedo reductions on Glacier de la Plaine Morte, Swiss Alps using a novel Hyperspectral Microscopy method'*
- 2017 *Participation*
- EARSeL SIG Imaging Spectroscopy Workshop, Zurich, Switzerland, 19 – 21 April
- 2016 *Poster Presentation*
- 14th Swiss Geoscience meeting, Geneva, Switzerland, 18 – 19 November
- 'Effects of particulate matter on the albedo of Alpine glaciers'*
- 2016 *Participation*
- 15th Young Researchers Meeting, Aeschi bei Spiez, Switzerland, 9 – 10 June

- 2016 *Poster Presentation*
- International Partnerships in Ice Core Sciences, Hobart, Australia, 7 – 11 March
- 'Effects of particulate matter on the albedo of Alpine glaciers'*
-
- 2015 *Oral Presentation*
- 13th Swiss Geoscience meeting, Basel, Switzerland, 20 – 21 November
- 'Effects of particulate matter on the albedo of Alpine glaciers'*
-
- 2015 *Presentation*
- European Research Course on Atmospheres, Grenoble, France, 06 January – 06 February
-
- 2014 *Participation*
- 13th Young Researchers Meeting, Aeschi bei Spiez, Switzerland, 19 – 20 June
-

Contribution to scientific fieldwork

- 2014 Jungfrauojoch, surface snow sampling, snow pit sampling, testing of new drill
- 2014 First Plaine Morte Fieldwork, planning and leading a campaign for collecting samples and surface reflectance measurements
- 2015 Rhoneglacier, testing of sampling method
- 2015 Second Plaine Morte Fieldwork collecting samples and surface reflectance measurements
- 2017 Findel Glacier, Girls on ice project, porter
-

